

Morphological and functional characterization of layer 5 neurons in rat medial prefrontal cortex, their synaptic microcircuitry and serotonin modulation

Ramya Rama

Schlüsseltechnologien / Key Technologies

Band / Volume 267

ISBN 978-3-95806-688-5

Forschungszentrum Jülich GmbH
Institut für Neurowissenschaften und Medizin (INM)
JARA-Institut Brain structure-function relationships (INM-10)

Morphological and functional characterization of layer 5 neurons in rat medial prefrontal cortex, their synaptic microcircuitry and serotonin modulation

Ramya Rama

Schriften des Forschungszentrums Jülich
Reihe Schlüsseltechnologien / Key Technologies

Band / Volume 267

ISSN 1866-1807

ISBN 978-3-95806-688-5

Bibliografische Information der Deutschen Nationalbibliothek.
Die Deutsche Nationalbibliothek verzeichnet diese Publikation in der
Deutschen Nationalbibliografie; detaillierte Bibliografische Daten
sind im Internet über <http://dnb.d-nb.de> abrufbar.

Herausgeber
und Vertrieb: Forschungszentrum Jülich GmbH
 Zentralbibliothek, Verlag
 52425 Jülich
 Tel.: +49 2461 61-5368
 Fax: +49 2461 61-6103
 zb-publikation@fz-juelich.de
 www.fz-juelich.de/zb

Umschlaggestaltung: Grafische Medien, Forschungszentrum Jülich GmbH

Druck: Grafische Medien, Forschungszentrum Jülich GmbH

Copyright: Forschungszentrum Jülich 2023

Schriften des Forschungszentrums Jülich
Reihe Schlüsseltechnologien / Key Technologies, Band / Volume 267

D 82 (Diss. RWTH Aachen University, 2022)

ISSN 1866-1807
ISBN 978-3-95806-688-5

Vollständig frei verfügbar über das Publikationsportal des Forschungszentrums Jülich (JuSER)
unter www.fz-juelich.de/zb/openaccess.



This is an Open Access publication distributed under the terms of the [Creative Commons Attribution License 4.0](https://creativecommons.org/licenses/by/4.0/),
which permits unrestricted use, distribution, and reproduction in any medium, provided the original work is properly cited.

To my friends and family

Eidesstattliche Erklärung

Ich versichere hiermit an Eides statt, dass die vorliegende Dissertation von mir selbstständig und ohne unzulässige fremde Hilfe unter Beachtung der “Grundsätze zur Sicherung guter wissenschaftlicher Praxis an der Rheinisch-Westfälische Technische Hochschule (RWTH) Aachen” erstellt worden ist. Diese Dissertation wurde keiner anderen Fakultät vorgelegt und es gab bisher keine erfolglosen Promotionsversuche.

Jülich, den 10. August 2022,

Ramya Rama

Summary

Medial prefrontal cortex (*Cortex prefrontalis medialis*, mPFC) is a part of the association cortex that serves to process and integrate synaptic inputs from sensory and motor cortical areas. The mPFC plays important roles in numerous cognitive processes, such as emotional processing, executive function, decision making, spatial orientation, long-term memory and impulse control. Compared to other cortical areas, the mPFC has a particularly high density of serotonergic axons which originate from the dorsal and medial raphe nuclei; they play a crucial role in regulating the development and function of the neocortex. For this reason, a basic knowledge of the role of serotonin (5-HT) and its receptors (5-HTRs) function in the mPFC in modulating cortical activity is crucial.

In rodents, approximately 60% of pyramidal neurons (PNs) possess 5-HT_{1A}Rs or 5-HT_{1B}Rs, particular those in layer 5 (L5) of mPFC, ~80% of which express both receptor subtypes. In previous studies, L5 PNs were divided into two groups; the first group includes PNs that innervate brain areas within the telencephalon such as the cerebral cortex, the limbic system and the basal ganglia. In contrast, PNs of the second group project to brain areas outside the telencephalon such as the cerebellum, the brain stem and the spinal cord. Besides the PNs, neuronal activity of the neocortex is also under the control of the different types of inhibitory interneurons (INs); most of these IN also express 5-HTRs. PNs and INs in L5 form complex neural networks in the mPFC. In the present work, two different types of PNs and three types of INs in L5 of mPFC were identified through electrophysiological recordings with the patch-clamp technique in whole-cell mode and morphological reconstructions. PNs have been divided into adaptive-spiking (AS) and regular-spiking (RS) types, corresponding to intra- and extratelencephalic PNs. Based on the peak action potential frequency, L5 INs were classified into non-fast-spiking (nFS), regular-fast-spiking (rFS) and stuttering/intermittent burst-like fast-spiking (bFS) INs.

In this work, 5-HT showed a cell type-specific effect on electrophysiological properties of L5 PNs and INs. In AS PNs with high input resistance (R_{in}), 5-HT induced sustained depolarization through 5-HT_{2A}Rs activation and a sustained hyperpolarization in AS PNs with a low input resistance (R_{in}) that was mediated by 5-HT_{1A}Rs or 5-HT_{1B}Rs. RS PNs showed a biphasic 5-HT response with an initial transient hyperpolarization followed by a persistent depolarization. The initial transient

hyperpolarization was caused by a Ca^{2+} -dependent activation of potassium channels with low single-channel conductivity (so-called 'small-conductance' K^+ channels; SK channels).

5-HT had no effect on nFS INs, but caused a clear depolarization in rFS INs; in bFS INs, 5-HT induced either depolarization or hyperpolarization depending on the bFS IN subtypes. In INs a 5-HT induced depolarization was mediated either by 5-HT_{2A}Rs or 5-HT_{3A}Rs; a 5-HT evoked hyperpolarization was mediated by either 5-HT_{1A}Rs or 5-HT_{1B}Rs.

To investigate the effects of 5-HT on synaptic transmission between the two cell types, pair recordings of synaptically coupled pairs of neurons in L5 of mPFC were performed. By activating 5-HT_{1B}Rs, 5-HT caused a decrease in the EPSP amplitude at all synaptic connections with presynaptic L5 PNs independent of the specific type. Concomitantly, an increase in the 'paired-pulse ratio' (PPR) was observed suggesting that 5-HT reduces the presynaptic release of the neurotransmitter glutamate by activating the 5-HT_{1B}Rs on the presynaptic terminals.

In inhibitory synaptic connections, the activation of presynaptically localized 5-HT_{3A}Rs caused a potentiation of the IPSP amplitude together with a decrease in PPR suggesting a 5-HT-dependent increase in GABA release. A decrease in the IPSP amplitude observed in a different set of inhibitory connections could be attributed to presynaptic 5-HT_{1A}Rs or 5-HT_{1B}Rs.

In summary, the 5-HT induced modulation of L5 PNs and INs in the PFC investigated here causes a cell type-specific change in excitability that decisively influences the function of the neuronal network of the mPFC. The results of this work can form the basis for further investigation of 5-HT mediated neuromodulation and the underlying 5-HTRs in the various layers of the mPFC and other cortical areas.

Zusammenfassung

Der mediale präfrontale Kortex (*Cortex prefrontalis medialis*, mPFC) ist ein Teil des Assoziationskortex, der der Verarbeitung und Integration von synaptischen Eingängen aus den sensorischen und motorischen kortikalen Arealen dient. Der mPFC spielt eine wichtige Rolle bei zahlreichen kognitiven Prozessen, so der Verarbeitung von Emotionen, dem exekutiven Handeln, der Entscheidungsfindung, der räumlicher Orientierung und dem Langzeitgedächtnis sowie der Impulskontrolle. Im Vergleich zu anderen kortikalen Arealen weist der mPFC eine besonders hohe Dichte an serotonergen Axonen auf, die dem dorsalen und medialen Raphe-Kernen (*Nuclei raphes*) entspringen; sie spielen eine entscheidende Rolle in der Regulation der Entwicklung und Funktion des Neokortex. Aus diesem Grunde ist eine grundlegende Kenntnis der Rolle von Serotonin (5-HT) und der Funktion seiner Rezeptoren (5-HTRs) im mPFC bei der Modulation der kortikalen neuronalen Aktivität von entscheidender Bedeutung.

In Nagern besitzen annähernd 60% aller Pyramidenzellen 5-HT_{1A}Rs oder 5-HT_{1B}Rs, insbesondere solche in Lamina 5 (L5) des mPFCs von denen ~80% beide Rezeptorsubtypen exprimieren. In früheren Studien wurden L5 Pyramidenzellen in zwei Gruppen eingeteilt; die erste Gruppe umfasst Pyramidenzellen, die Hirnareale innerhalb des Telencephalons wie den Neokortex, das limbische System und die Basalganglien innervieren. Die Pyramidenzellen der zweiten Gruppe projizieren dagegen in Hirnareale außerhalb des Telencephalons bis hinunter ins distale Rückenmark. Neben den Pyramidenzellen unterliegt die neuronal Aktivität des Neokortex auch der Kontrolle durch die verschiedenen Typen inhibitorischer Interneurone; die meisten dieser Interneurone exprimieren ebenfalls 5-HTRs. Pyramidenzellen und Interneurone in Lamina 5 bilden komplexes neuronales Netzwerk im mPFC. In der vorliegenden Arbeit wurde mittels elektrophysiologischer Ableitungen mit der Patch-clamp Technik im Ganzzell-Modus sowie morphologischen Rekonstruktionen zwei unterschiedliche Pyramidenzell-Typen und drei Interneuron-Typen in Lamina 5 des mPFC identifiziert. Pyramidenzellen wurden in adaptiv-feuernde (adaptive-spiking, AS) und regulär-feuernde (regular-spiking, RS) Typen unterteilt, die den intra- und extratelencephalen Pyramidenzellen entsprechen. Basierend auf der maximalen Aktionspotentialfrequenz wurden L5 Interneurone in nicht-schnellfeuernde (non-fast-spiking, nFS), regulär-schnellfeuernde (regular fast-spiking, rFS) und intermittierend-schnellfeuernde (burst fast-spiking, bFS) Interneurone unterteilt.

In dieser Arbeit zeigte 5-HT einen Zelltyp-spezifischen Effekt auf die elektrophysiologischen Eigenschaften von L5 Pyramidenzellen und Interneurone. 5-HT induzierte eine anhaltende Depolarisation von AS Pyramidenzellen mit hohem Eingangswiderstand (R_{in}) jedoch eine

Hyperpolarisation in AS Pyramidenzellen mit niedrigem R_{in} . Es zeigte sich bei den L5 Interneuronen des mPFC, dass 5-HT keinen Effekt auf nFS Interneurone zeigte, dagegen aber in rFS Interneuronen eine deutliche Depolarisation hervorrief. In bFS Interneuronen bewirkte 5-HT entweder eine Depolarisation oder eine Hyperpolarisation abhängig vom bFS Interneuron-Subtyp. In Pyramidenzellen wurde die 5-HT induzierte Depolarisation von 5-HT_{2A}Rs vermittelt, in Interneuronen jedoch von 5-HT_{3A}Rs; dagegen wurde die 5-HT evozierte Hyperpolarisation entweder über 5-HT_{1A}Rs oder 5-HT_{1B}Rs vermittelt. Es konnte auch gezeigt werden, dass die in RS Pyramidenzellen beobachtete transiente Hyperpolarisation auf einer Ca²⁺-abhängigen Aktivierung von Kalium-Kanälen mit geringer Einzellkanal-Leitfähigkeit (sogenannter 'small-conductance' K⁺-Kanäle; SK-Kanäle) basierte.

Um die Effekte von 5-HT auf die synaptische Transmission zwischen verschiedenen Zelltypen zu untersuchen, wurden Paableitungen von synaptisch gekoppelten Neuronenpaaren in Lamina 5 des mPFC durchgeführt. Durch Aktivierung von 5-HT_{1B}Rs verursachte 5-HT eine Verminderung der EPSP Amplitude bei allen synaptischen Verbindungen mit präsynaptischen AS oder RS L5 Pyramidenzellen. Gleichzeitig konnte eine damit einhergehende Erhöhung des sogenannten Verhältnisses zweier konsekutiver EPSPs (die sogenannte 'paired pulse ratio', PPR) beobachtet werden. Dies läßt vermuten, dass 5-HT durch Aktivierung auf den präsynaptisch Terminalien lokalisierten 5-HT_{1B}Rs die präsynaptische Freisetzung des Neurotransmitters Glutamat vermindert.

Es konnte daneben auch gezeigt werden, dass bei einigen inhibitorischen synaptischen Verbindungen die Aktivierung präsynaptisch lokalisierter 5-HT_{3A}Rs eine Potenzierung der IPSP Amplitude bewirkten; eine Verminderung der IPSP Amplitude in inhibitorischen Verbindungen konnte dagegen auf präsynaptische 5-HT_{1A}Rs or 5-HT_{1B}Rs zurückgeführt werden.

Zusammenfassend kann gesagt werden, die hier untersuchte 5-HT induzierte Modulation der verschiedenen L5 Pyramidenzellen und Interneurone einer Zell-spezifische Veränderung der Erregbarkeit bedingt, die die Funktion des neuronalen Netzwerke des mPFC entscheidend beeinflusst. Die Resultate dieser Arbeit können die Basis für eine weitere Erforschung der 5-HT vermittelten Neuromodulation und der zugrundeliegenden 5-HTRs in den verschiedenen Laminae des mPFC und anderen kortikalen Arealen bilden.

Acknowledgements

I would like to express my sincere gratitude to my PhD supervisor and doctoral father, Prof. Dr. Dirk Feldmeyer who guided me throughout this project. I would like to thank him for allowing me to make my doctoral study in his lab. His expertise, advice and continuous help, highly inspired me and carried me through all the stages of my thesis work. I would like to give special thanks to Dr. Gabriele Radnikow who helped me equally together with my supervisor in achieving the goals of this project and finishing this work efficiently.

I would like to thank Prof. Dr. Marc Spehr for being my second supervisor and for his support and discussions in several group meetings. I would like to extend my thanks to Prof. Dr. Björn Kampa for his valuable time for being my committee member. I owe my deepest thanks to Prof. Dr. Ted Abel, Prof. Dr. Thomas Nickl-Jockschat and Prof. Dr. Ted Brodtkin, and their lab members for allowing me to work with them in their labs.

I would like to thank Dr. Guanyao Qi, Dr. Chao Ding and Dr. Danqing Yang for introducing me to the patch-clamp technique and helping me in data analysis and morphological reconstructions. They have always offered valuable suggestions and helpful discussions that helped me in progressing through this project. I thank and greatly appreciate Werner Hucko for his efficient technical help in the laboratory and excellent histological staining, without which it would be impossible to get high-quality data. I would like to extend my thanks to all of my other lab members - Dr. Vishalini Sivarajan, Dr. Manuel Marx, Dr. Claudia Barz, Irene Melati Aji, Charlotte Witt and Brinda Vaidya. A very special thanks to Dr. Vishalini Sivarajan, I miss her a lot and she will be always remembered. I would also like to thank all my friends outside the lab, especially Dr. Sreeharsha Hanumanthu, Manohar Kampili, Dr. Venkata Raveendra Nallagatla, Dr. Krithika Sahni, Aniket Sonawane and Praveen Shripad for being there for me through all of the good times, the rough times and everything in-between and I will never forget it.

I would like to thank International Research Training Group - 2150, RWTH Aachen University, German Research Foundation (DFG) and Research Center Jülich for supporting me financially during my PhD work.

Finally, I would like to thank my parents Shyam Sunder Rama and Roopa Rama, my siblings Shravya Rama and Venkat Siddhartha Rama, and my partner Dr. Sreeharsha Hanumanthu for believing in me and supporting me during the whole process of finishing this thesis. I dedicate this thesis to them.

Table of contents

Eidesstattliche Erklärung	3
Summary	4
Zusammenfassung	6
Acknowledgements	8
1. Introduction	11
1.1. Cerebral cortex	11
1.2. Prefrontal cortex	11
1.3. Neuronal classification in the neocortex	13
1.4. Serotonin and its receptors	18
1.5. 5-HT receptor function in the context of neuropsychiatric disorders	21
1.6. Aim of this doctoral thesis	24
2. Materials and Methods	25
2.1. Slice Preparation	25
2.2. Solutions	25
2.3. Identification of cortical layers and neurons in mPFC	26
2.4. Patch-clamp technique	27
2.4.1. Single-cell recordings	27
2.4.2. Paired recordings	29
2.5. Drug Application	31
2.6. Analysis of electrophysiological data	32
2.6.1. Passive membrane properties of a single neuron	32
2.6.2. Active membrane properties of a single neuron	32
2.6.3. Physiological properties of synaptically coupled neuronal pairs	35
2.7. Morphological reconstructions and analysis	36
2.7.1. Histological procedures	36
2.7.2. Morphological 3D reconstructions	37
2.8. Statistical analysis	37
3. Results	39
3.1. Neuronal classification in L5 of mPFC	39
3.2. Effect of 5-HT on PN activity in L5 of mPFC	52
3.3. Effect of 5-HT receptor agonists on the AS and RS PNs in L5 of mPFC	59
3.4. Effect of 5-HT on INs in L5 of mPFC	59

3.5. Synaptic transmission in the L5 of mPFC	59
3.5.1. Synaptic connectivity between E-E pairs in L5 of mPFC	61
3.5.2. Synaptic connectivity between E-I pairs in L5 of mPFC	62
3.5.3. Synaptic connectivity between I-E pairs in L5 of mPFC	63
3.5.4. Serotonergic suppression of E-E connections in L5 of mPFC.....	64
3.5.5. 5-HT suppresses synaptic transmission of E-E microcircuitry in L5 of mPFC through 5-HT1BRs.....	64
3.5.6. Serotonergic suppression in reciprocal E-I and I-E connections in L5 of mPFC	70
3.5.7. 5-HT suppresses synaptic transmission of E-I microcircuitry in L5 of PFC through 5-HT1BRs.....	70
3.5.8. 5-HT facilitates synaptic transmission of the I-E microcircuitry in L5 of PFC through 5-HT3ARs.....	73
4. Discussion	76
4.1. Classification of PNs in L5 of mPFC	76
4.2 Classification of INs in L5 of mPFC	78
4.3. Serotonergic effect in L5 neurons in mPFC.....	81
4.3.1. Serotonergic effect in L5 PNs in mPFC.....	81
4.3.2. Serotonergic effect on SK channels in L5 PNs in mPFC.....	84
4.3.3. Serotonergic effect in L5 INs in mPFC.....	85
4.4. Monosynaptic connections in L5 of mPFC	87
4.5. Serotonergic modulation on synaptic neurotransmission in mPFC of rats.....	91
5. Bibliography	95
Abbreviations.....	111
List of Figures.....	113
List of Tables.....	115
Curriculum Vitae.....	116

1. Introduction

1.1. Cerebral cortex

The brain together with the spinal cord constitutes the central nervous system. The brain consists of three major regions: cerebrum, cerebellum and medulla oblongata or brain stem. The cerebrum is divided into two cerebral hemispheres with the cerebral cortex being its outer region. In humans, the neocortex comprises 90% of the cerebral cortex while the remaining 10% belong to the so-called allocortex (e.g. the olfactory bulb, the perirhinal cortex and the hippocampus) which is evolutionary substantially older than the former (Strominger 2012). There are about 21-26 billion neurons in the human cerebral cortex which is subdivided into six major layers, from the outer pial surface to the inner white matter (Gilmore and Herrup 1997, Herculano-Houzel 2009, Wagstyl, Larocque et al. 2020). Layer 1 (L1) mainly contains inhibitory interneurons (INs) and extensions of apical dendritic tufts and axon collaterals of pyramidal neurons (PNs) of deeper layers. Layer 2 (L2) mostly contains small-sized PNs. Layer 3 (L3) largely contains small and medium-sized PNs. PNs of L2 and L3 project their axon collaterals to either intracortical or intercortical regions. Layer 4 (L4) contains different types of PNs. L4 is the main target of thalamocortical afferents from the thalamus and cortico-cortical afferents from contralateral hemispheres (Miller, Pinto et al. 2001, Lubke and Feldmeyer 2007, Rao and Mizuno 2021). Therefore, L4 is considered to be the primary input layer that conveys the information to other cortical layers (Feldmeyer 2012, Bopp, Holler-Rickauer et al. 2017). In the rodent prefrontal cortex (PFC), however, L4 is very thin or almost absent. Layer 5 (L5) contains large-sized PNs, while layer 6 (L6) contains many small PNs and different types of multiform excitatory neurons (Thomson 2010, Kawaguchi 2017).

1.2. Prefrontal cortex

Traditionally, each brain hemisphere has been divided into four lobes: the frontal, parietal, occipital and temporal lobes. The frontal lobe is the largest of all lobes and is covered by the frontal cortex which includes the premotor cortex and primary motor cortex. The anterior part of the frontal lobe is the PFC. The most prominent function of the PFC is to regulate working memory and executive function. The term executive function is defined as the process of higher-order cognitive control to attain a specific goal (Moriguchi 2014). PFC lesion studies directly link PFC to executive functions (Chudasama 2011, Kesner and Churchwell 2011, Yuan and Raz 2014). Cognitive control is impaired in several psychological and psychiatric disorders including autism, attention deficit

hyperactivity disorder (ADHD), schizophrenia and addiction (Nestler and Malenka 2004, Russo, Dietz et al. 2010). The PFC has been also implicated in human personality and social behavior (Frith and Dolan 1996, Roberts 1996, Sakurai and Gamo 2019). The PFC has reciprocal input-output connections to several cortical areas (motor, sensory, perirhinal and entorhinal cortices) and other brain regions (amygdala, hippocampus, thalamus, hypothalamus, striatum and brainstem). Disruptions of these input-output connections lead to an impairment in structural and functional connectivity between these brain regions and may eventually result in dysfunctional behavior (Miczek, de Almeida et al. 2007, Siever 2008, Soyka 2011, Rosell and Siever 2015).

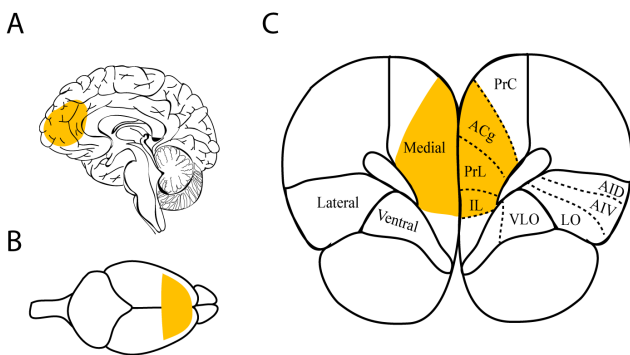


Fig. 1.1: Functional and neuroanatomical homology between human and rodent PFC. A region (shown in yellow) within dlPFC of human brain (A) shares homology with mPFC of rodent brain (B). C. Rodent brain depicting the coronal sectioning of PFC and its subdivisions: medial (PrC, ACg, PrL, IL and MO), lateral (AID, AIV), LO, VO and VLO cortices.

Although the rodent brain is about a thousand times smaller than the human brain, there is significant functional homology between rodent and human PFC (Fig. 1.1) (Kolb B. 2004, Ko 2017). Therefore, rodents and rats in particular are good animal models to study structural and functional aspects of the PFC as well as PFC-related disorders. Human PFC is divided into two major regions: the ventromedial PFC (ventral and medial) and the lateral PFC (dorsolateral (dlPFC) and dorsoventral). In rodents, the PFC is structurally divided into three major regions: medial (mPFC), lateral and ventral regions (Fig. 1, C) (Dalley, Cardinal et al. 2004). The mPFC is further sub-divided into precentral (PrC), anterior cingulate (ACg), prelimbic (PrL), infralimbic (IL) and medial orbital (MO) cortices, while the lateral PFC is sub-divided into the dorsal and ventral agranular insular (AID, AIV) and lateral orbital (LO) cortices; the ventral PFC is divided into the ventral orbital (VO) and ventral lateral orbital (VLO) cortices. A specified region in human dlPFC has been found to be directly associated with executive functions and social behavior (Steinbeis, Bernhardt et al. 2012, Barbey, Colom et al. 2013). The rodent mPFC is the functional and neuroanatomical homologue to the human dlPFC (Fig. 1.1, A, B) (Bizon, Foster et al. 2012).

Therefore, it is important to understand the basic neuroanatomy and function of the mPFC of the rat brain to correlate the respective functions in the human brain.

1.3. Neuronal classification in the neocortex

The principal neuronal cell type (80-90% of total neurons) in the neocortex are glutamatergic PNs in which glutamate is the major excitatory neurotransmitter (Elston, Benavides-Piccione et al. 2006, Meyer, Wimmer et al. 2010, Meyer, Wimmer et al. 2010). The PNs are cortical projection neurons that receive both excitatory and inhibitory synaptic inputs and provide excitatory output to intracortical, subcortical and the targets regions in contralateral brain hemispheres. PNs across different layers of the cortex differ in their molecular identity, morphological characteristics, electrophysiological properties, and synaptic connectivity (Dembrow, Chitwood et al. 2010, Kawaguchi 2017, Baker, Kalmbach et al. 2018, Collins, Anastasiades et al. 2018). The diversity of excitatory PNs in different layers of the PFC is depicted in [Fig. 1.2, A](#). The generic anatomy of a typical PN has a soma resembling a pyramid; it has a thick long apical dendrite that arises from the soma and extends towards superficial layers of the cortex sometimes terminating at the border of the pial surface. PNs have several basal dendrites which are largely confined to the ‘home’ cortical layer and a single axon that arborizes extensively and projects to distant intra- and subcortical target regions of the brain (van Aerde and Feldmeyer 2015, Radnikow and Feldmeyer 2018, Wang, Ye et al. 2018). PNs that project to the contralateral cerebral hemisphere are termed commissural/callosal/cortico-cortical or more broadly intratelencephalic (IT) neurons (neurons projecting within the telencephalic region including the cerebral cortex, the limbic forebrain structures and the basal ganglia). On the other hand, PNs that project to distal subcortical structures is termed corticopontine/long-range corticofugal/pyramidal-tract (PT) neurons all of which are extra-telencephalic (ET) neurons projecting out of the telencephalic region. Both types of PNs also project to the striatum. According to the transcriptomic and morphoelectric (morphological and electrophysiological) properties of PNs, IT, ET and corticothalamic (CT) subtypes of PNs are separated (Scala, Kobak et al. 2021). Since L5 is the primary output layer of the cortex, PNs in this layer have been studied in considerable detail (Spruston 2008, Kim, Juavinett et al. 2015). Besides the basic anatomy, PNs show a significant degree of diversity in different cortical layers (Marx and Feldmeyer 2013, van Aerde and Feldmeyer 2015, Radnikow and Feldmeyer 2018). There are two major types of PNs in L5 of PFC; broad (Bd)-tufted PNs with apical dendrites having many terminal branches and slender (Sl)-tufted PNs with only a few tuft dendrites. These two types of

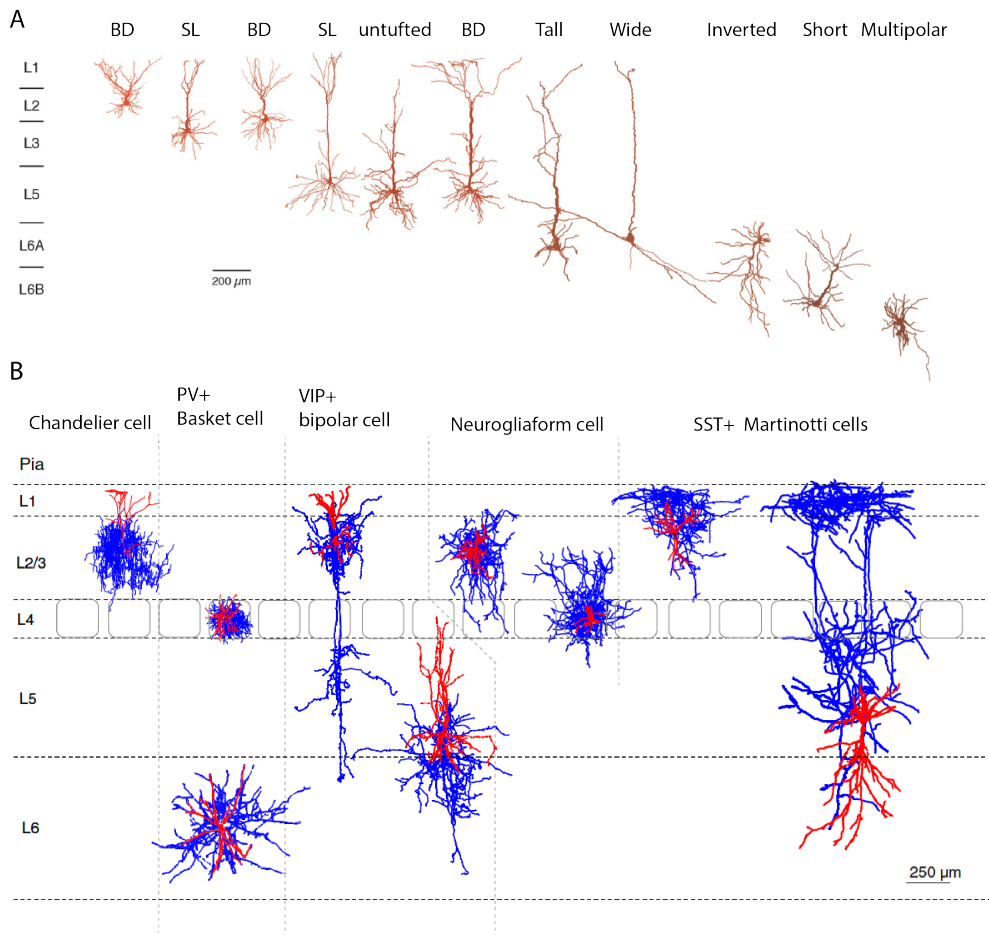


Fig. 1.2: Types of PNs and INs across different layers in rat neocortex. (A) Different PN types in L1–L6 of the PFC. Somato-dendritic compartments were shown in brown. (B) IN types in different layers of the somatosensory or barrel cortex; because no detailed description of PFC INs is so far available this neocortical region was chosen as example. Dendrites and axon are shown in red and blue, respectively. Adapted from Feldmeyer, Qi et al. 2018, Radnikow and Feldmeyer

PNs have different subcortical targets in the brain. Bd-tufted PNs send their axons to pontine nuclei, striatum, the ipsilateral thalamus and the spinal cord, whereas SI-tufted PNs project only to the ipsilateral and contralateral striatum (Kawaguchi 2017, Baker, Kalmbach et al. 2018, Collins, Anastasiades et al. 2018). The long-range axonal projection pattern of a typical PN (Economo, Clack et al. 2016) is illustrated in Fig. 1.3. SI-tufted PNs display an adaptive-spiking (AS) firing pattern while the Bd-tufted PNs display regular-spiking (RS) firing pattern in L5 of mPFC (van Aerde, Qi et al. 2015, Baker, Kalmbach et al. 2018).

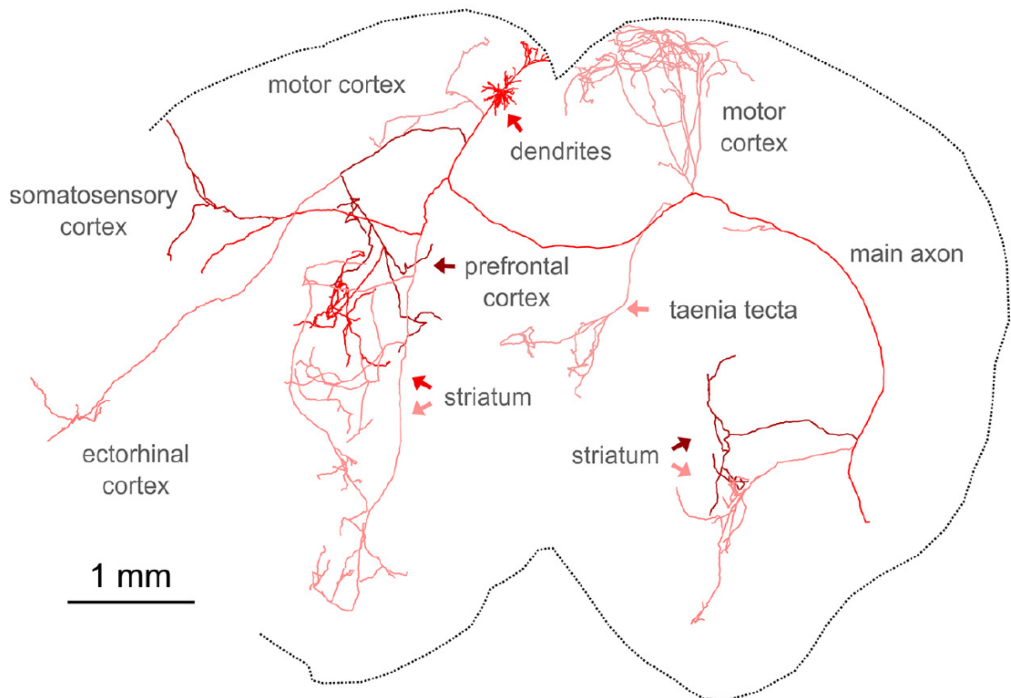


Fig. 1.3: 3D-reconstruction of a single PN spanning different regions of brain. High-speed two-photon microscopic picture of whole mouse brain at high resolution reveals the long-range, brain-wide axonal projection pattern of a single PN; note in particular the dense projections to the ipsi- and contralateral striatum. The somato-dendritic domain is shown in bright red while different axonal collaterals are depicted in shades of red. Adapted from Economo, Clack et al. 2016.

In addition to the glutamatergic excitatory projection PNs, the neocortex contains local inhibitory INs which release the inhibitory neurotransmitter GABA (γ -aminobutyric acid). INs account for about 10-20% of the total neuronal population (Lefort, Tómm et al. 2009, Wierenga, Mullner et al. 2010, Meyer, Schwarz et al. 2011, Tremblay, Lee et al. 2016, Riedemann 2019, Swanson and Maffei 2019). The diversity of inhibitory INs in different neocortical layers is depicted in Fig. 1.2, B. A typical IN most commonly has a smaller soma size compared to that of PNs, multiple dendrites and a dense axonal plexus which may span multiple layers within a brain area. GABAergic INs are enormously heterogeneous and there are more than 20 subtypes of INs in the neocortex (Porter, Johnson et al. 2001, Gonchar, Wang et al. 2007, Kelsom and Lu 2013, Beebe, Young et al. 2016, Feldmeyer, Qi et al. 2018, Riedemann 2019, Gouwens, Sorensen et al. 2020). There are several parameters by which INs have been classified and none of the classification methods is complete. Consortia on IN classification (Petilla Interneuron Nomenclature, Ascoli et al. 2008, DeFelipe,

Lopez-Cruz et al. 2013, Yuste, Hawrylycz et al. 2020) have classified INs by combining morphological (soma size and shape, dendritic arborization, axon orientation, postsynaptic target etc), molecular (transcription factors, Ca²⁺-binding proteins, ion channels, cell surface markers, etc) and electrophysiological parameters (R_{in} , rheobase, AP parameters, firing pattern, etc). For instance, based on the axonal terminal arrangement that looks like a 'chandelier' or basket around the soma of a PN, INs were termed chandelier cells or basket cells, respectively. Later, electron microscopic studies showed that the axon of chandelier cells targets the axon initial segment of PNs while basket cells innervate the perisomatic region of PNs. Based on molecular markers, INs were categorized into five different groups, namely those expressing parvalbumin (PV, chandelier and basket cells), somatostatin (STT, Martinotti cells), NPY (neuropeptide Y, multipolar cells), vasoactive intestinal peptide (VIP, double-bouquet cells) and cholecystokinin(CCK, basket cells) (Bartos and Elgueta 2012, Bartolini, Ciceri et al. 2013, DeFelipe, Lopez-Cruz et al. 2013). Based on the electrophysiological parameters like the firing pattern more than nine different types of INs (Markram, Toledo-Rodriguez et al. 2004, Ascoli, Alonso-Nanclares et al. 2008) were categorized including fast-spiking (FS, steady inter-spike interval (ISI) rapid firing), non-adapting non-fast-spiking (nFS, steady ISI non-rapid firing), adaptive nFS (increased ISI non-rapid firing), irregular spiking (irregular ISI non-rapid firing), intrinsic burst spiking (irregular ISI with a typical burst of two or more spikes) and accelerating spiking (decreased ISI non-rapid firing). More recently, INs in the neocortex has been classified into five subgroups mainly based on their transcriptomic and morphoelectric characteristics. The five IN subgroups that are differentially distributed in different layers of the neocortex are PV, STT, VIP, synuclein-gamma (SNCG) and lysosomal-associated membrane protein 5 (LAMP5) expressing (+) INs (Gouwens, Sorensen et al. 2019, Gouwens, Sorensen et al. 2020, Scala, Kobak et al. 2021). The INs and PNs classifications based on transcriptomic and morphoelectric characteristics are depicted in [Fig. 1.4](#).

INs can control the neuronal activity within a confined brain area by forming synapses onto neighboring PNs and other INs. GABAergic INs mainly mediate two types of inhibitions: feed-forward and feed-back inhibition (Mohler 2002, Isaacson and Scanziani 2011, D'Souza and Burkhalter 2017). If the excitatory afferent inputs synapses onto PNs or INs, this generates feed-forward inhibition onto PNs. When there is reciprocal connectivity between PN and IN, the firing of PNs initiates the activation of IN and as consequence inhibits the firing and activity of PN itself or neighboring PNs. This is termed feedback (lateral) inhibition. The PN can fire again only when the

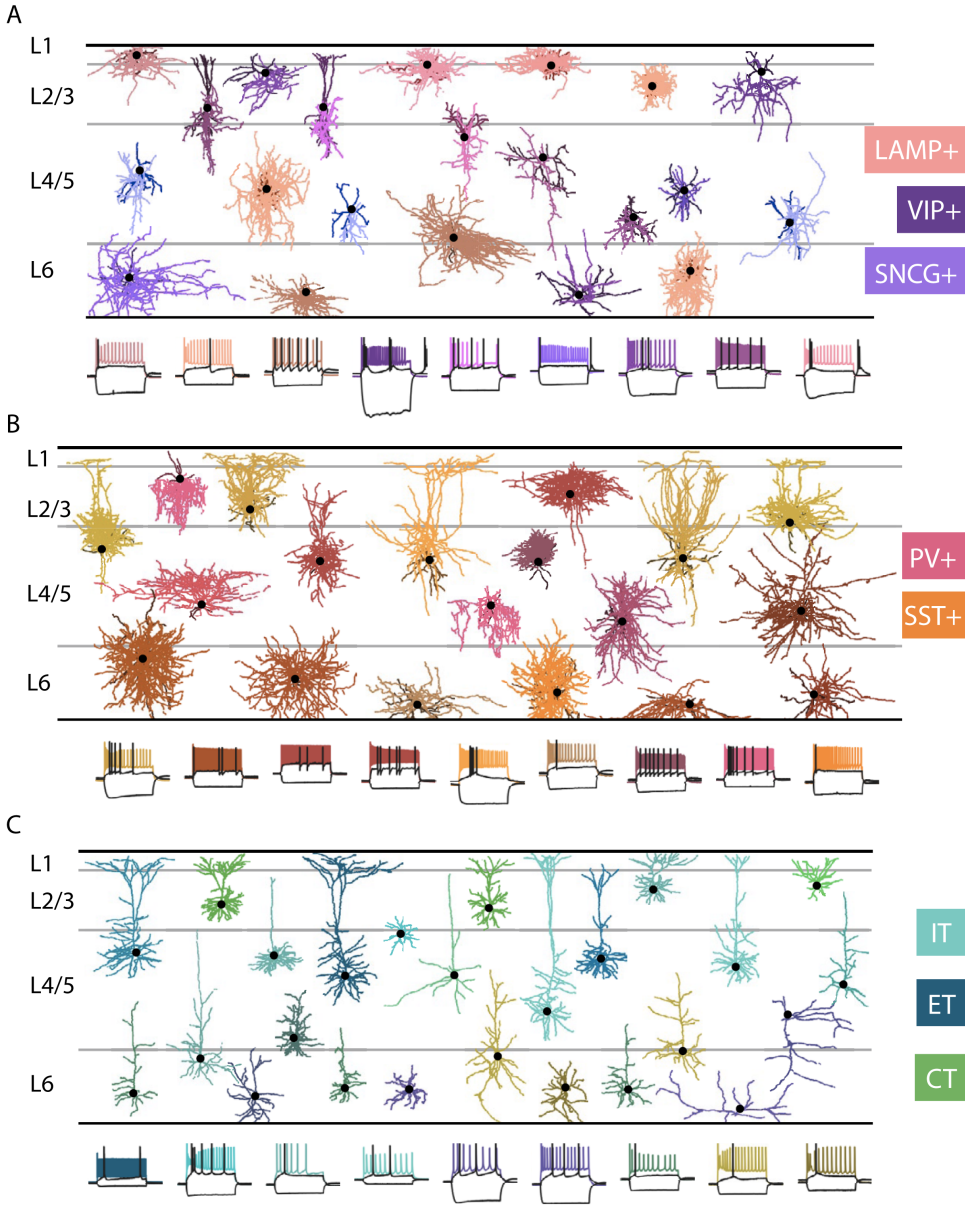


Fig. 1.4: Neuronal classification based on transcriptomic and morphoelectric characteristics. (A) Example morphologies of LAMP+, VIP+ and SNCG+ INs across different cortical layers were depicted. (B) Example morphologies of PV+ and SST+ INs across different cortical layers were depicted. (C) Example morphologies of IT, ET and CT PNs across different cortical layers were depicted. Somas were indicated with black dots. Dendrites and axons are depicted in dark and its respective light colors for INs. For PNs, only dendrites are shown. The hyperpolarization trace (from least current), the first AP (rheobase current) and the firing pattern are depicted for each of the cell shown. Adapted from Scala F et al., 2020.

feedback inhibition decays. Through these two types of GABAergic inhibitions, INs gain control of excitatory PNs. This PN-IN microcircuitry balances the excitatory to inhibitory (E/I) ratio and synchronizes neuronal activity within a brain area. Besides the aforementioned two types of inhibitions, the 3rd type of inhibition is disinhibition, i.e., this inhibitory circuit consists of an IN-IN motif of which one is connected to a PN (IN-IN-PN). Within the IN-IN motif, the first IN suppresses the inhibitory activity of the intermediate INs thus disinhibiting the PN (Pi, Hangya et al. 2013, Letzkus, Wolff et al. 2015). For instance, the IN-IN circuit motif mostly contains a VIP+ IN that targets other STT+ INs, or an STT+ or PV+ IN that specifically targets dendritic tufts (apical and basal) and somatic region of PNs respectively (Naka and Adesnik 2016, Yang, Murray et al. 2016).

Patterns of the local synaptic microcircuitry between neuronal populations vary across different brain regions (Brown and Hestrin 2009, Naka and Adesnik 2016, Baker, Kalmbach et al. 2018). In L5 of the visual and sensory-motor cortex, both AS and RS PNs form homotypic (AS-AS (18%) and RS-RS (7%)) excitatory synaptic connections. AS-RS heterotypic connections form at a fairly high rate but RS-RS and RS-AS connections are rare. Both AS and RS PNs establish synapses with PV+ INs; RS PNs form also synapses with STT+ INs. PV+ INs form homotypic inhibitory synaptic connections whereas VIP+ INs form heterotypic synapses with PV+ and STT+ INs. 5-HT_{3A}R-expressing INs in L5 are very rare (6-10%) and little data is available on these neurons (Puig and Gullledge 2011, Santana and Artigas 2017). However, these connectivity patterns differ among different cortices and are also layer-specific because the different IN types do not distribute evenly.

1.4. Serotonin and its receptors

The dorsal raphe nucleus (DRN) is the largest source of serotonin in the forebrain and is implicated in reward-seeking behavior (Nakamura 2013, Liu, Zhou et al. 2014). Several studies (Sharp, Boothman et al. 2007, Riga, Matos et al. 2014, Challis and Berton 2015, Maier 2015) provided a detailed insight into the functional connectivity between mPFC and DRN. [Fig. 1.5](#) depicts serotonergic pathways in the human and rodent brains. The DRN sends serotonergic afferents to all sub-regions of the mPFC while receiving the highest extent of cortical inputs from PrL and IL of mPFC (Maier, Amat et al. 2006, Puig and Gullledge 2011). DRN serotonergic neurons project mostly to L5 of mPFC. PNs of mPFC that project to caudal DRN form monosynaptic connections with serotonergic neurons, while the mPFC neurons that project to rostral DRN form disynaptic connections onto serotonergic neurons via intermediate GABAergic neurons. Thus, monosynaptic

mPFC-DRN connections stimulate serotonergic output while disynaptic connections inhibit serotonergic output.

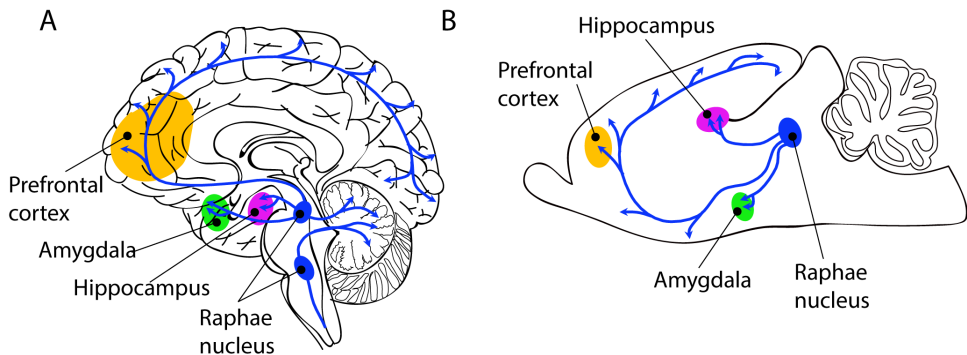


Fig. 1.5: Serotonergic pathways in human and rodent brain. The DRN sends its serotonergic inputs to PFC and other brain regions including amygdala and hippocampus in human (A) and rodent (B) brains.

5-HT is released from serotonergic neurons of DRN onto glutamatergic PNs and GABAergic INs of the forebrain and subcortical regions. There are about 14 different 5-HT receptor subtypes that are widely distributed across several brain regions and throughout the body. In the PFC, the most abundantly expressed receptors are 5-HT_{1A}R, 5-HT_{1B}R, 5-HT_{2A}R and 5-HT_{3A}R. About 50-60% of PNs express 5-HT_{1A}Rs and 5-HT_{2A}Rs in their somatodendritic compartments, whereas 5-HT_{1B}Rs are expressed at axon terminals in L5 of mPFC. 5-HT receptor expression pattern in INs is complex and not very well known. About 25% of INs are known to express either 5-HT_{1A}Rs or 5-HT_{2A}Rs (Celada, Puig et al. 2013, Santana and Artigas 2017). A subset of FS-type INs were shown to express only 5-HT_{1A}Rs and another subset expresses 5-HT_{2A}Rs (Puig, Celada et al. 2004, Puig, Watakabe et al. 2010). 5-HT_{3A}Rs are abundantly expressed in L2/3 VIP+ INs of PFC and very rarely (6-10% expression) in L5 INs of mPFC (Naka and Adesnik 2016, Posluszny 2019).

All 5-HT receptors are G protein-coupled receptors (GPCRs), except for the 5-HT_{3A}R which is a cation channel that is permeable to Na⁺, K⁺ and Ca²⁺ ions and is hence an excitatory ligand-gated receptor channel (Fig. 1.6) (Millan, Marin et al. 2008, Nichols and Nichols 2008, McCorvy and Roth 2015, Ohno, Shimizu et al. 2015). GPCRs are heterotrimeric G-protein receptor complexes containing a G_α and G_{βγ} complex. The G_α subunit remains associated with either guanosine diphosphate in the inactive state or guanosine triphosphate in the activated state. In the PFC as in other cortices, 5-HT_{3A}Rs are selectively expressed in subsets of GABAergic INs (Lee, Hjerling-

Leffler et al. 2010, Tremblay, Lee et al. 2016). Activation of 5-HT_{3A}R channels induces GABA release onto PFC PNs, thereby inhibiting neuronal activity.

There are three different types of GPCRs namely G_{q/11}, G_{i/o}, and G_s-proteins. The G_β and G_γ subunits always form an inseparable G_{βγ} complex. In the absence of GPCR activation, the G_α subunit binds to guanosine diphosphate (GDP) together with the G_{βγ} subunit complex. Activation of GPCR by a ligand induces coupling of the heterotrimer. Subsequently, GDP is exchanged for GTP on the G_α subunit and the GTP-bound G_α dissociates from the G_{βγ} complex. This dissociated G_{βγ} complex from the activated GPCR now stimulates many downstream intracellular second

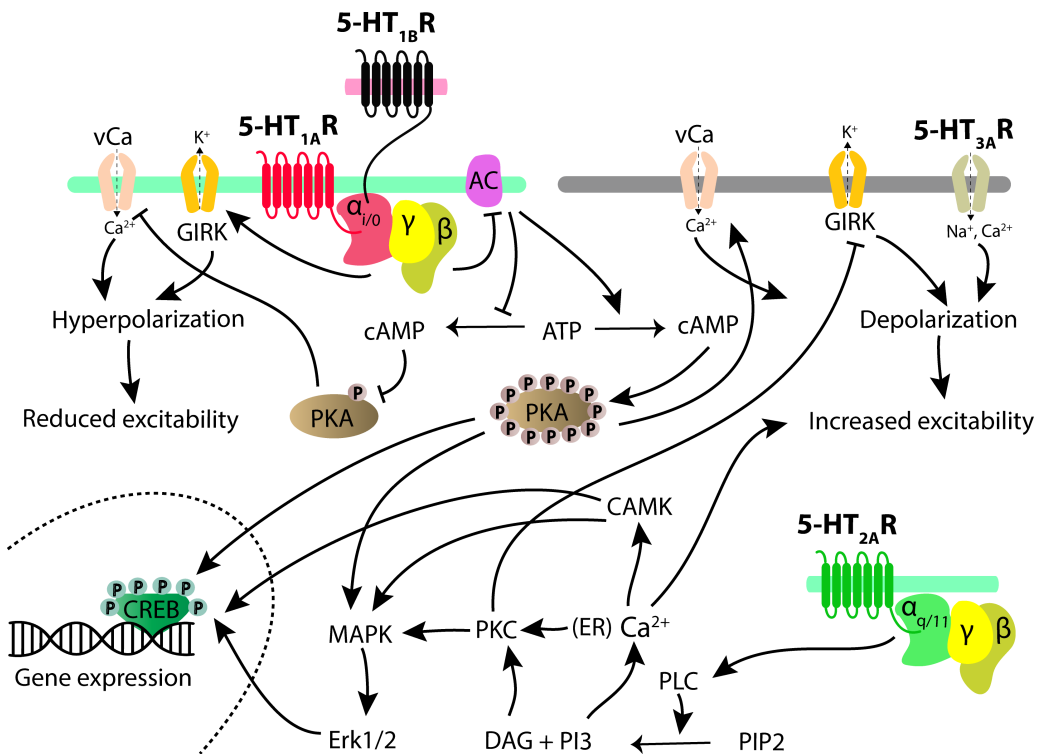


Fig. 1.6: Signaling mechanisms associated with 5-HTRs in mPFC. 5-HT_{1A}R and 5-HT_{1B}R are coupled to a G_{i/o} protein to mediate downstream signaling cascades that reduce neuronal excitability. 5-HT_{2A}R are coupled to G_{q/11} proteins the activation of which enhances neuronal excitability. 5-HT_{3A}R are cation-selective ligand-gated ion channels; influx of Na⁺ and Ca²⁺ through these channels depolarizes V_m thereby increasing neuronal excitability and synaptic release probability. Specific kinases (PKA, PKC, MAPK, CAMK and Erk1/2) are involved in several downstream signaling cascades, for e.g. phosphorylation of transcription factors like CREB to mediate gene expression or Ca²⁺ release from the endoplasmic reticulum via inositol trisphosphate signaling.

messenger cascades, protein expression, immediate early genes etc., which in turn trigger excitatory or inhibitory responses (Hilger, Masureel et al. 2018). The activation of $G_{q/11}$ -coupled receptors stimulates the activity of phospholipase C (PLC) leading to hydrolysis of membrane phosphoinositides, thereby elevating the intracellular inositol trisphosphate (IP_3) and diacyl-glycerol (DAG). DAG activates protein kinase C (PKC) which inhibits inwardly-rectifying K^+ channels (K_{ir} channels, also called G-protein-coupled inwardly-rectifying K^+ channels, short GIRK channels) contributing to membrane depolarization (Hibino, Inanobe et al. 2010, Yaman and Bal 2020). The binding of IP_3 to its receptors in the membrane of the endoplasmic reticulum leads to the opening of these endoplasmatic Ca^{2+} channels thereby elevating intracellular Ca^{2+} (Ryglewski, Pflueger et al. 2007). Activation of G_s -coupled receptors stimulates adenylate cyclase (AC) activity, resulting in an enhanced conversion of ATP to cyclic adenosine monophosphate (cAMP). cAMP acts as a second messenger that phosphorylates protein kinase A (PKA) which then regulates membrane excitability by opening voltage-gated Ca^{2+} (Ca_v) channels. Increased cytosolic Ca^{2+} either via release from intracellular stores or via Ca^{2+} influx through Ca_v channels contributes to membrane depolarization; Ca^{2+} serves also as a second messenger that enhances neurotransmitter release, kinase activity and gene expression by activating transcription factors like cAMP response element binding protein (CREB) (Millan, Marin et al. 2008, Brini, Cali et al. 2014). Activation of $G_{i/o}$ -coupled receptors inhibits the activity of AC and PKA-dependent pathways with simultaneous inhibition of Ca_v channels and activation of K_{ir} channels. In addition to the PKA-mediated opening of Ca_v channels by GPCRs, direct binding of $G_{\beta\gamma}$ to the $\alpha 1$ subunit of N-type ($Ca_v2.2$) and P/Q-type ($Ca_v2.1$) channels can inhibit these Ca_v2 channels thus regulating membrane excitability and synaptic transmission (Currie 2010, Zamponi and Currie 2013). 5-HT binding to 5-HT_{1A}Rs causes inhibition of PKA-mediated phosphorylation and an opening of K_{ir} channels, resulting in a neuronal hyperpolarization and hence a reduced firing rate (Nichols DE et al., 2008, Albert PR et al., 2011, Masson J et al., 2012, Huang X et al., 2017). Similar to 5-HT_{1A}Rs, 5-HT_{1B}Rs are also coupled to the $G_{ai/o}$ proteins; the binding of 5-HT to these receptors has similar effects on PKA-activity and K_{ir} channels (Sharp, Boothman et al. 2007, Masson and Darmon 2012, McCorvy and Roth 2015).

1.5. 5-HT receptor function in the context of neuropsychiatric disorders

5-HT signaling and function are critically involved in the regulation of cortical neuronal activity. Abnormalities in 5-HT signaling are strongly associated with cognition, anxiety, mood, depression,

aggression, impulsivity and motor functions (Apter, van Praag et al. 1990, Celada, Puig et al. 2013, Wang and Wong-Lin 2013, Garcia-Garcia, Meng et al. 2017). Since 5-HT receptors are differentially expressed in different neuronal populations in PFC, 5-HT can directly modulate their neuronal activity by modulating the release of other neurotransmitters like glutamate, GABA and dopamine as well.

Serenics are anti-aggressive drugs that enhance the activity of both 5-HT_{1A}Rs and 5-HT_{1B}Rs in PFC to profoundly reduce aggression and enhance sympathy or empathy (Olivier, Mos et al. 1985, Olivier and van Oorschot 2005). Both selective 5-HT_{1A}R and 5-HT_{1B}R agonists are crucial in mitigating aggressive behavior. The mixed 5-HT_{1A/1B} agonist, eltoprazine and the more specific 5-HT_{1B}R agonists, CP-94,253 are successful in reducing excessive levels of aggressive behavior in aggressive resident mice (Mos, Olivier et al. 1992, Fish, Faccidomo et al. 1999). Upregulation of 5-HT_{2A}R availability and function in PFC is a characteristic feature observed in several aggressive patients (Dean 2003, Soloff, Price et al. 2007, Rosell, Thompson et al. 2010). Therefore, blocking the 5-HT_{2A}R function could be a possible option to reduce aggressive behavior. Risperidone – a potent inverse agonist of 5-HT_{2A}Rs and a partial dopamine 2 receptor antagonist, significantly reduced isolation-induced aggressive behavior in mice (Rodriguez-Arias, Minarro et al. 1998). Therefore, risperidone is considered a second-generation atypical antipsychotic and is used in the treatment of aggressive and violent behaviors of patients with neuropsychiatric disorders (Burns 2006, Ostinelli, Hussein et al. 2018). Activation of 5-HT_{1A/1B}Rs and inhibition of 5-HT_{2A}Rs results in a reduction of offensive aggression, whereas activation of 5-HT_{2A}Rs alone can reduce defensive aggression (Muehlenkamp, Lucion et al. 1995, Sakaue, Ago et al. 2002, de Boer and Koolhaas 2005, Olivier and van Oorschot 2005).

Several studies in rodents have shown that 5-HT_{2A}R modulation is often associated with stress and steroid-induced pathology (Lopez, Vazquez et al. 1997, Vazquez, Eskandari et al. 2002, Pitychoutis, Dalla et al. 2012). Rodents often develop a social hierarchy within their habitats. Stronger animals become dominant, while weaker ones are subordinate. Being subordinate results in chronic stress leading to profound behavioral, physiological, and endocrine changes. These animals show intense weight loss due to reduced feeding, reduced aggressiveness, copulation and activity, increased weight of adrenal glands resulting in elevated basal corticosterone levels, and exhibit earlier mortality compared to dominant animals and wild-type normal animals (Blanchard, Blanchard et al.

1985, Blanchard, Flannelly et al. 1988, Blanchard and Blanchard 1990, Blanchard, Yudko et al. 1993). Chronic stress conditions in subordinate animals induced a profound increase in the density of cortical 5-HT_{2A}Rs, as a consequence of the activation of the hypothalamic-pituitary-adrenal (HPA) axis (McKittrick, Blanchard et al. 1995). In humans, functional changes associated with an altered 5-HT_{2A}R density could be a mechanism underlying stress-associated neuropsychiatric disorders. For instance, an increased 5-HT_{2A}R density was found in post-mortem brains especially in PN in L5 of PFC of suicide victims that showed a pronounced lifetime aggressive behavior (Pandey, Dwivedi et al. 2002, Oquendo, Russo et al. 2006). However, reduced 5-HT_{2A}R density in PFC was observed in subjects with an enhanced risk for schizophrenia (Burnet, Eastwood et al. 1996, Hurlmann, Boy et al. 2005).

Schizophrenia is a well-studied psychiatric disorder characterized by abnormal neuronal activity and disturbed functional connectivity in the cortico-limbic and cortico-striatal circuitry (Begre and Koenig 2008, White, Schmidt et al. 2009, Butler, Weisholtz et al. 2012, Eack, Wojtalik et al. 2016, Cadena, White et al. 2018, Lin, Wang et al. 2018). Schizophrenia is associated with positive (delusions and hallucinations), negative (apathy, poor motivation, emotional and social deprivation) and cognitive symptoms (impaired attention, learning and problem solving; Stahl 2008). Projections from different brain regions innervating glutamatergic neurons in PFC can modulate glutamatergic signaling. Serotonergic neurons of the DRN innervate the neocortex and receive glutamatergic input in return. In accordance with the so-called 5-HT hypothesis of schizophrenia, increased 5-HT_{2A}R activity in PFC overdrives glutamatergic signaling in schizophrenia (Aghajanian and Marek 1999). Unmedicated naïve patients did not show any difference in the cortical expression of 5-HT_{2A}Rs, while schizophrenic patients on medication showed a significant reduction in cortical 5-HT_{2A}R levels (Meltzer, Li et al. 2003, Hurlmann, Matusch et al. 2008). This indicates that antipsychotics used to treat schizophrenia were specifically acting on cortical 5-HT_{2A}R to ameliorate the symptoms. Furthermore, increased 5-HT_{1A}R density in PFC was observed in medicated schizophrenia patients which were thought to improve negative symptoms (Bantick, Deakin et al. 2001). Therefore, 5-HT_{2A}R antagonists and/or 5-HT_{1A}R agonists can be used to reduce the excitability of glutamatergic neurons to treat patients suffering from schizophrenia and other psychiatric disorders.

1.6. Aim of this doctoral thesis

The primary aim of this thesis is to understand how 5-HT signaling can regulate neuronal activity in L5 of mPFC. The diversity of the PNs in L5 of mPFC is well documented but how the 5-HT function differs between the different PN types is less well known. Many studies have classified PNs and INs based either on their electrophysiological or their morphological properties and in some cases by the synaptic inputs (thalamus or striatum) they receive. Here, in this work, I set out to investigate the nature of PNs based on electrophysiological and morphological properties. The 5-HT effect depends on the different 5-HTR's expression and function in the PNs. 5-HT_{1A}R, 5-HT_{1B}R and 5-HT_{2A}R are the three major G-protein coupled 5-HT receptors present in PNs of PFC. It has been established already that 5-HT_{1A}R and 5-HT_{2A}R largely (60-70%) co-express in rat and mice PFC, however the functional significance of this co-expression is not clearly known. In addition to PNs, there are INs in L5 that expresses 5-HT receptors. To date, the structural and functional properties of INs in L5 are not well studied. Therefore, the diversity of INs and the effect of 5-HT on the different IN subtypes in L5 of mPFC were also studied in the framework of this thesis.

PNs and INs form local synaptic connections in L5 of mPFC. 5-HT has been shown to regulate excitatory and inhibitory connections differentially. For instance, 5-HT suppressed excitatory neurotransmission in the human PFC and rat entorhinal cortex, while 5-HT did not induce any synaptic changes in GABAergic output in both species (Schmitz, Gloveli et al. 1998, Komlosi, Molnar et al. 2012). Therefore, the second aim of this study was to investigate how 5-HT affects excitatory and inhibitory connections in L5 of rat mPFC. Synaptic connections based on pre- and postsynaptic neurons in the L5 microcircuitry of the mPFC were intended to study. In addition, the effect of 5-HT and its receptors on the synaptic activity and synaptic connection of L5 neurons were investigated. In order to achieve these aims, whole-cell patch-clamp recordings in single and synaptically coupled neurons were performed. Patch-clamp electrophysiology and morphological analysis were combined with pharmacology, including 5-HT and its receptor agonists and antagonists to investigate mechanisms of serotonergic neuromodulation in L5 of mPFC.

2. Materials and Methods

2.1. Slice Preparation

Following the guidelines of the Federation of European Laboratory Animal Science Association (FELASA) and the German Animal Welfare Act, coronal sections were made from the Wistar rats (Charles River Laboratories, Inc, either sex) aged 17-19 postnatal days (P17-P19). Rats were anaesthetized with isoflurane, decapitated and the brains quickly transferred into an ice-cold extracellular solution containing 4 mM MgCl₂ and 1mM CaCl₂ and bubbled with 95% O₂ and 5% CO₂ to maintain adequate levels of oxygenation. The extracellular solution helps to reduce the synaptic activity within these brains. Rat brains were glued with the frontal part (the cut surface) on the cooled metal stage of a vibration microtome (Leica Biosystems) and were cut with a blade at the position shown in Fig. 2.1. This glued brain tissue was fully immersed in the ice-cold extracellular solution and 4-5 coronal slices were cut with a thickness of 350 μm. These slices of tissue were then incubated in the same solution to recover, for at least 1 hour at room temperature (21-24 °C).

2.2. Solutions

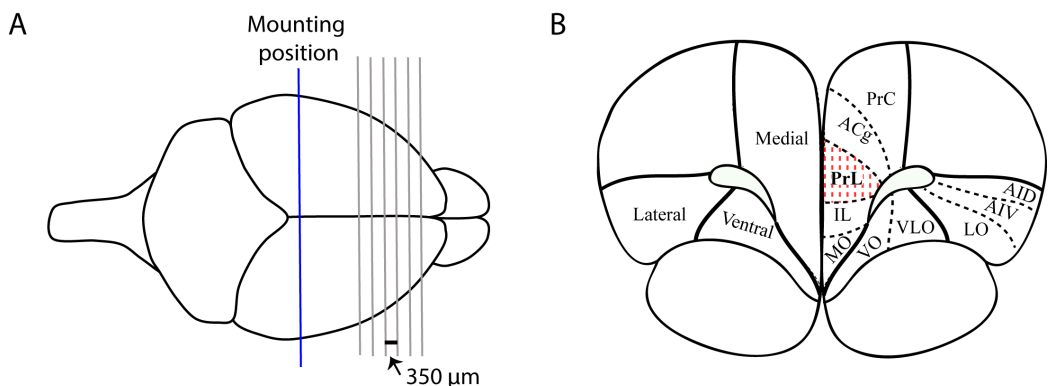


Fig. 2.1: Preparation of coronal brain sections in rat prelimbic region of mPFC. (A) Dorsal view of whole rat brain, the blue line representing the mounting position at which the brain was cut and glued on to the metal stage of vibratome stage and gray lines representing consecutive sections of 350 μm each. (B) Example of the rostral surface of coronal rat brain slice showing lateral, ventral, and mPFC in one hemisphere; their subregions are depicted in other hemispheres. All recordings were done in the prelimbic (PrL: red dashed lines) region of mPFC on both right and left hemispheres.

Individual slices were then transferred to the recording chamber of the patch-clamp setup. Here the slice was continuously perfused (~5 ml/min) with artificial cerebrospinal fluid (ACSF) containing (in mM): 125 NaCl, 2.5 KCl, 25 glucose, 2 CaCl₂, 1 MgCl₂, 1.25 NaH₂PO₄ and 25 NaHCO₃. In all

experiments, the perfusion solution was bubbled with 95% O₂ and 5% CO₂, and the temperature of this solution in the recording chamber was maintained in the range of 30.5-31.5 °C using a bath heater.

The recording pipette was filled with intracellular solution containing (in mM): 135 K-Gluconate, 4 KCl, 10 HEPES, 10 Phosphocreatine, 4 Mg-ATP, and 0.3 GTP (PH 7.4, ~300 mOsm). To stain neurons during the electrophysiological recording, Biocytin (5 mg/ml, Sigma, Munich, Germany) was added to the intracellular solution. A different solution containing (in mM) 105 Na-gluconate, 30 NaCl, 10 HEPES, 10 Phosphocreatine, 4 Mg-ATP, and 0.3 GTP was used for searching pipettes during the paired recordings.

2.3. Identification of cortical layers and neurons in mPFC

With the pial surface pointing forward, the slice was placed in the recording chamber under an upright microscope (fitted with 4×/0.13 numerical aperture (NA) and 40×, water immersion/0.80 NA objective, Olympus, Tokyo, Japan). To visualize the layer borders, bright-field illumination was used at low magnification. L2 was easily identified as a thin dark band between L1 and L3 due to the high density of neuron somata. L1 and L3 have a similar width and are located above and beneath L2, respectively. There is no L4 in rodent mPFC, therefore L5 borders directly next to L3. Under high magnification (40× objective), L5 has a large soma size of excitatory neurons with their thick, long apical dendrites, this makes L5 discriminated from L3 and L6. Depending on the age of the animal, the total distance from pia to WM is about 1100-1400 μm. The area of mPFC increases from the first slice to the next one and shows higher proportions in the 4th or 5th slice. L1 to L3 share one-third of the prelimbic cortex, whereas L5 and L6 equally separate the rest (Fig. 2.2). In this study, all the neurons were recorded in L5 of the prelimbic cortex that ranges between 600-850 μm from pia. Under high magnification, excitatory neurons and INs were differentiated by their soma appearances and their AP firing patterns. Further, 3D reconstructions of neuronal axon and dendritic projections aid post hoc identification. During patching, excitatory neurons with the thick apical dendrites were clearly visible; they showed either an AS or RS firing pattern. On the other hand, INs that lack apical dendrites displayed a higher AP firing frequency than PNs.

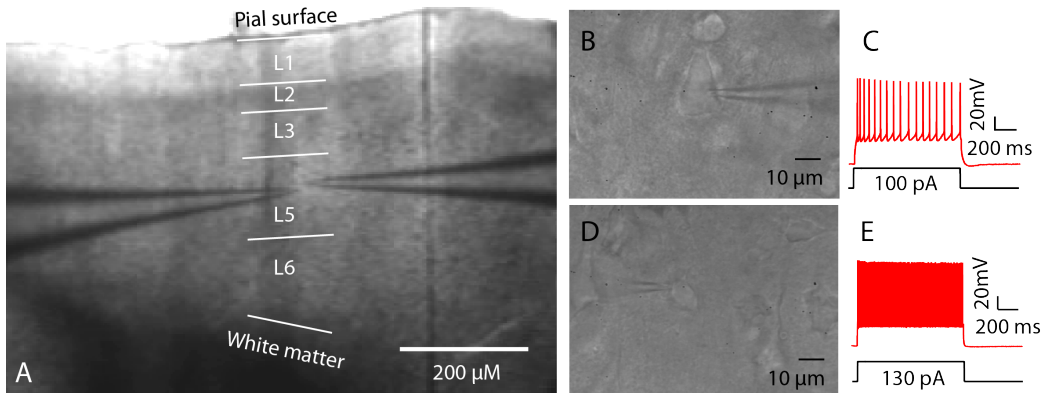


Fig. 2.2: Representation of cortical layers and identification of neurons in rat mPFC. (A) Cortical layers were depicted in an infrared differential interface contrast (IR-DIC) image of the mPFC acute rat brain section. Left and right pipettes indicate the position of pre- and postsynaptic neurons in the L5 of the PrL region of mPFC. Due to the high density of neuron somas in L2 appears as a thin dark band between L1 and L3. L1 and L3 have similar width and are located above and below L2, respectively. There is no L4 in the mPFC of rodents, therefore L5 borders directly on L3. Under higher magnification, somas of excitatory PNs in L5 appear large with thick and long apical dendrites (B); these features allow a discrimination between L5 PNs and those in L3 and L6. (C) Firing pattern of the L5 PN shown in (B). (D) High-magnification image of a L5 IN and its corresponding firing pattern (E).

2.4. Patch-clamp technique

2.4.1. Single-cell recordings

Whole-cell patch-clamp recordings in neurons of the L5 mPFC were performed at 30.5-31.5 °C. The patch pipettes of 4-9 MΩ resistance were pulled from thick borosilicate glass capillaries (outer diameter, 2.0 mm; inner diameter, 1.0 mm). Recording pipettes that were filled with intracellular solution and biocytin (5 mg/ml) were used to label the patched neurons. To visualize individual neurons in the mPFC, infrared differential interference contrast (IR-DIC) video microscopy was used. A HEKA EPC10 amplifier (Lambrecht, Germany) was used to record the voltage and current signals. "Patch Master" software (HEKA, Lambrecht, Germany) was used to program the stimulation protocol. An Ag/AgCl bath electrode was used as a reference electrode. All components of the setup were grounded to reduce interference and electrical noise. To move the pipette in three dimensions with micrometre-resolution with reference to the neuron under investigation, high-precision micro-manipulators (SM-5, Luigs & Neumann, Ratingen, Germany) were used. To avoid blockage in the pipette while moving into the slice toward a neuron, a weak positive pressure was

applied that blows away the tissue. When the pipette comes into close contact with a neuron, a dimple on the cell membrane appears. Releasing positive pressure and applying suction results in the formation of a tight seal between the recording pipette and cell membrane. A tight seal has a resistance of $\geq 1 \text{ G}\Omega$, - therefore termed ‘gigaseal’ - and ensures a good electrical signal-to-noise ratio. In addition, the application of more suction leads to a break-through of the cell membrane attached to the pipette thus forming a direct connection between the neuronal cytoplasm and the patch pipette (Fig. 2.3). Neurons with a resting membrane potential are more depolarized than -50 mV and/or a whole-cell series resistance (R_s) exceeding $50 \text{ M}\Omega$ at the beginning of the experiment

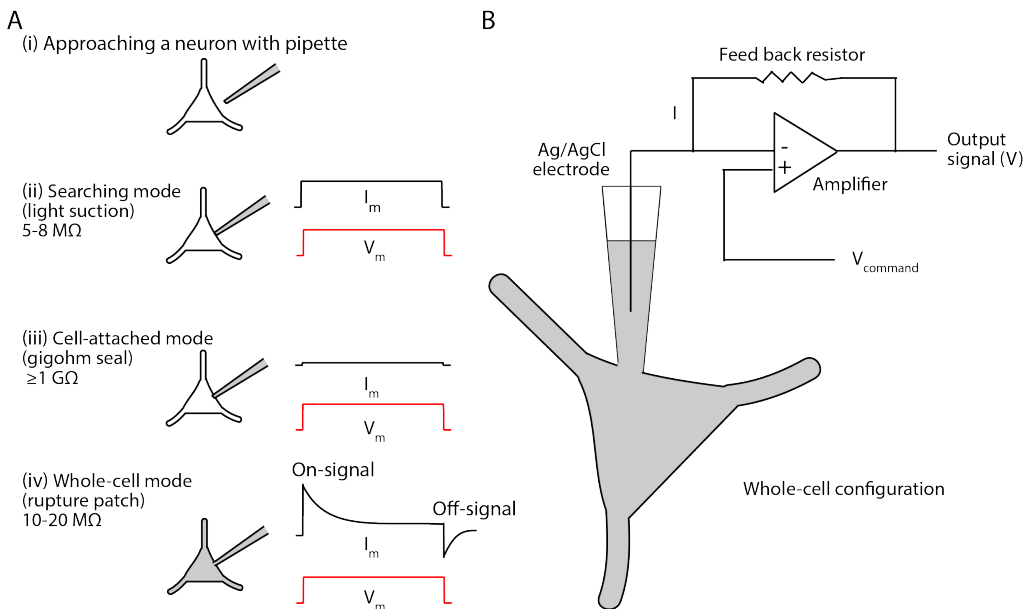


Fig. 2.3: Whole-cell patch-clamp technique. (A) Whole-cell configuration is attained in four steps. (i) In voltage-clamp mode, a patch pipette containing internal solution is brought into perfusion solution in the recording chamber by applying positive pressure. (ii) Pipettes of resistance $5\text{-}8 \text{ M}\Omega$ were used for searching neurons (iii) Once the pipette touches the cell membrane (cell-attached mode), pipette resistance increases and forms a giga seal ($\geq 1 \text{ G}\Omega$) between the pipette and membrane which is visible as a decrease in membrane current (iii, black trace, I_m). (iv) Further application of suction results in rupturing of the cell membrane and thus establishes whole-cell configuration. (B) The patch pipette containing the electrode measures the membrane potential (red trace, V_m). The electrode is connected to an amplifier which compares V_m to the command voltage (V_{command}). If V_m is different from V_c , a current is injected (I_m) into the neuron via a negative feedback loop to compensate for the difference in the membrane potential. Here, open neuron represents an intact PN for which whole-cell mode has not yet been attained while the gray filled neuron is a PN in whole cell mode. On- and the Off-signal refers to the transient capacitive current measured when (de-)charging the membrane capacitance of the neuron.

or changing by more than 25% during the entire experiment were excluded from the analysis. All active and passive electrophysiological properties of the recorded neurons were assessed by an initial hyperpolarizing current, followed by depolarizing current steps.

After attaining the whole-cell configuration, the resting membrane potential (V_m) was measured immediately. The R_s of the patched neuron was compensated by 80%. In the current-clamp mode, to elicit the first AP, current steps of 1s duration were applied starting at -100 pA at a step size of 10 pA. By using this 10 pA step size protocol, the first super-threshold AP was identified. Later, single AP characteristics were analyzed. Further, to analyze the active properties of AP firing, current steps of 1s duration were applied starting at -20 pA at a step size of 25 pA. This 25 pA step size protocol was used to generate the first AP train with a minimum of ten spikes. Continuous recordings of changes in membrane potential were performed in a current-clamp mode without current injection. To prevent the generation of APs in the recorded neurons tetrodotoxin (TTX, 0.5 μ M) was applied.

2.4.2. Paired recordings

Three different methods were performed to find synaptically coupled neurons. Direct dual patch-clamp recording (method 1) was performed when the connectivity ratio is high between synaptically coupled neurons. To check if two neurons were synaptically coupled, first the whole-cell configuration in a potential postsynaptic neuron was established and later a putative presynaptic neuron was patched. If the connectivity ratio is low the method is not very effective.

When the connectivity ratio is low, a modified paired-recording technique (method 2) with a searching protocol (Qi et al. 2015; Feldmeyer and Radnikow 2016) was performed. To avoid depolarization of the searched neurons, a searching pipette of 8-11 M Ω resistance was used in which K⁺ ions were replaced by Na⁺ ions in the internal solution. This high resistance pipette with relatively high Na⁺ ions maintains the searched neurons in a healthy condition by preventing accidental break-through of the neuronal membrane, which induced a prolonged AP firing of neurons and cytotoxic Ca²⁺ influx.

In the modified pair recording method (Fig. 2.4), a postsynaptic neuron was patched first in whole-cell current-clamp mode. Using a searching pipette, surrounding neurons were then tested for a synaptic connection. After attaining a so-called 'loose-seal' cell-attached patching in the potential

presynaptic neuron with a seal resistance of 30-300 M Ω , large current pulses (0.2-2 nA) were applied briefly (5 ms) to elicit APs. This AP is normally visible as a small spikelet on the voltage response. If the two neurons were synaptically coupled, the postsynaptic neuron would respond to the stimulation of the presynaptic neuron with a postsynaptic potential (PSP). Frequently, more than 20 potential presynaptic neurons had to be tested to find a synaptic connection. Sometimes, when the pipette tip was contaminated (>30 M Ω), the searching pipette had to be replaced.

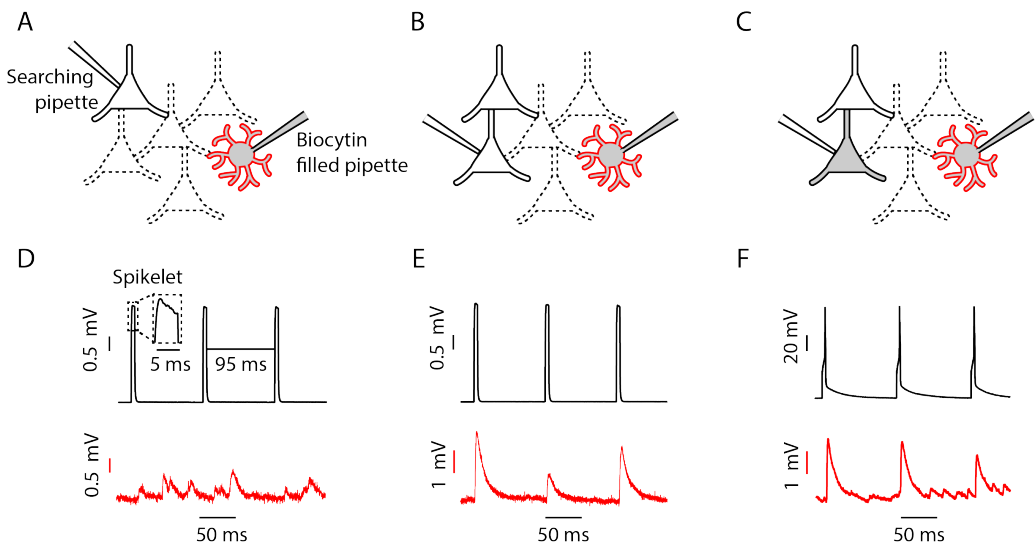


Fig. 2.4: Patch-clamp recording from and biocytin labeling of a synaptically coupled neuron pair. (A) Initially, a postsynaptic neuron (red neuron) is patched with a biocytin (gray)-filled pipette in whole-cell mode and a putative presynaptic neuron (black unfilled neuron) is patched in cell-attached current-clamp mode (loose-seal, 30-300 M Ω) with a searching pipette (no biocytin). Then large current pulses ranging between 0.2-2 nA are applied briefly (5 ms) to a potential presynaptic neuron to elicit three consecutive APs (D, black trace, visible as a small spikelet riding on the depolarizing voltage pulse) at a stimulation frequency of 10 Hz that would evoke voltage responses in postsynaptic neuron if synaptically connected (D, red trace). If there is no response in the postsynaptic neuron, a new presynaptic neuron (B, another black unfilled neuron) is patched in 'loose' cell-attached mode and tested again until a connection is found (E). Approximately 30 potential presynaptic neurons (dashed neurons in A, B, C) can be tested in the range of 50-100 μ m radial distance from the postsynaptic neuron. Here, the excitatory neurons were represented in black while inhibitory neurons are red in color. Whenever a postsynaptic neuron evokes a PSP with a latency of less than 5 ms, the searching pipette is replaced carefully with a biocytin-filled pipette (C) and the presynaptic neuron is patched in whole-cell current-clamp mode. APs (F, black) elicited from excitatory neuron induced EPSPs (F, red) in inhibitory neuron.

Once a postsynaptic response was observed, the searching pipette was slowly removed without damaging the presynaptic neuron and replaced by a biocytin-filled patch pipette. The presynaptic neuron was then re-patched and recorded in whole-cell mode. In the presynaptic neuron, action potentials (APs) were elicited by injecting short (5 ms) depolarizing current pulses and the postsynaptic responses (EPSPs or IPSPs) were recorded in current-clamp mode. Importantly, during EPSP recordings, the postsynaptic neurons were held at resting membrane potential (-70 mV). On the other hand, during IPSP recordings, the postsynaptic neurons were clamped at -55 mV by injecting a constant positive current. This is because the reversal potential of IPSPs was calculated to be -85 mV (Koelbl et al. 2015); thus depolarizing the postsynaptic neuron to -55 mV, increases the driving force of $\text{Cl}^-/\text{HCO}_2^-$ ions thereby facilitating the detection of inhibitory connections. Signals were amplified using an EPC10-triple patch-clamp amplifier (HEKA Elektronik, Lambrecht, Germany), sampled at 10 kHz, and filtered at 2.9 kHz.

When the connectivity ratio is extremely low, the presynaptic neuron was maintained in the 'loose-seal' configuration (method 3) to record PSPs in the postsynaptic neuron. At the end of the recording, the searching pipette was replaced with a biocytin-filled pipette to re-patch the presynaptic neuron and record the active and passive electrophysiological properties. In addition to the recorded electrophysiological properties of pre- and postsynaptic neurons, the morphology of these patched neurons were correlated with the recorded firing patterns. Occasionally, the re-patched neuron was in a poor condition so that the electrophysiological properties could not be determined. In such cases, the morphology of the presynaptic neuron was instead identified by the biocytin staining of the neuron recorded.

2.5. Drug Application

All drugs used in this study were purchased either from Sigma-Aldrich (Steinheim, Germany) or Tocris (Bristol, UK). The following drugs were bath applied through the perfusion system:

1. Tetrodotoxin (TTX, 0.5 μM : a sodium channel blocker)
2. Serotonin (5-HT, 10 μM : a neurotransmitter)
3. CGS-12066 maleate salt (CGS, 5 μM , an agonist of 5-HT_{1B}R)
4. SB-216641 (SB, 5 μM : an antagonist of 5-HT_{1B}R)
5. (R)-(+)-8-Hydroxy-DPAT hydrobromide (DPAT, 5 μM : an agonist of 5-HT_{1A}R)
6. Three Ca²⁺ and lipid Binding domains-2 (TCB-2: 3 μM an agonist of 5-HT_{2A}R)

7. meta-ChloroPhenylbiGuanide (mCPG, 30 μ M: an agonist of 5-HT_{3A}R)

All the single-cell recordings were made in presence of TTX (perfusion solution with TTX). Control or baseline was set with 20-30 sweeps, followed by a 'drug phase' consisting of 20-30 sweeps. After the drug phase, 30-60 sweeps of the 'wash out' phase were recorded. All paired recordings were made in the absence of TTX. A perfusion solution with either 5-HT and/or 'agonist/antagonist' was used during paired recordings.

2.6. Analysis of electrophysiological data

2.6.1. Passive membrane properties of a single neuron

Igor Pro 6 (WaveMetrics, Lake Oswego, USA) software with custom-written macros was used to analyze the electrophysiological signals recorded during experiments. After attaining the whole-cell configuration of the single neuron, initial resting membrane potential (RMP, mV) and series resistance (R_s , $M\Omega$) were measured and recorded. The input resistance (R_{in} , $M\Omega$) of the neuronal membrane was calculated as a change in the voltage recorded divided by the flow of current which is in accordance with Ohm's law ($R=V/I$). R_{in} is calculated from a linear fit to the I-V curve in the range between -50 and +50 pA (0 pA was excluded). The membrane time constant (τ_{Mem} , ms) is defined as the time required for the membrane potential to rise from the RMP to 63% (1/e) or to fall from its maximum value to reach 37% (1-1/e) in the fitting of the ON- and OFF-phase of the current pulse. Due to the delayed activation of a hyperpolarization-activated, cyclic-nucleotide gated (HCN) channel after the onset of the hyperpolarizing voltage steps, a sag in the voltage response (V_{sag} , mV) was observed. It was measured as the difference between the most hyperpolarized voltage (transient) and the steady voltage (stable) deflection (Fig. 2.5).

2.6.2. Active membrane properties of a single neuron

The excitability of any neuron was determined by its active properties. Injection of current pulses depolarizes the neuron and once V_m reaches a threshold, elicits APs. To determine the characteristics of the first elicited AP, a 1s pulse with a step size of 10pA was injected into the neuron. The rheobase current (pA) is the minimum amount of current required for eliciting the first one or two APs in a patched neuron was measured. AP threshold (mV) is defined as the point of start of acceleration of the membrane potential using the second derivative of the somatic membrane potential (d^2V/dt^2). AP time or the delay until 1st AP was described as the minimum time required

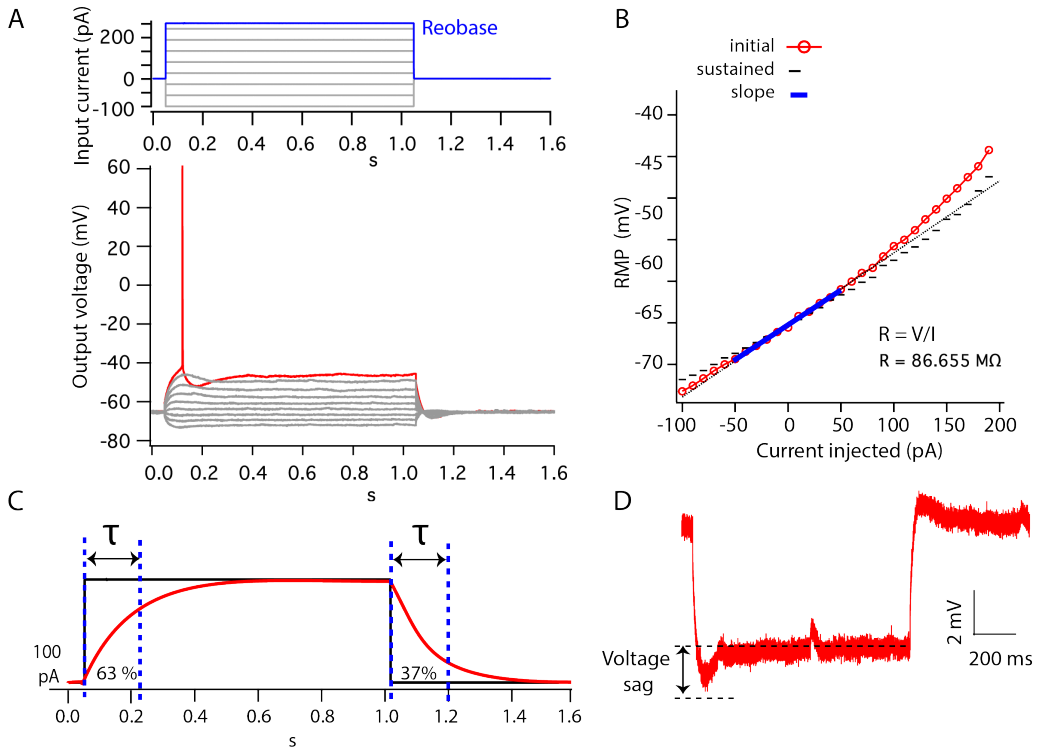


Fig. 2.5: Analysis of passive properties of L5 neurons in mPFC. (A) A series of hyperpolarizing and depolarizing currents (A, top) of increasing step size (10 pA) was injected until an AP was initiated (A, bottom). Rheobase (A, top, blue) is the minimum current required to elicit an AP. (B) The R_{in} of the membrane was measured as the linear slope that fits the I-V curve with the current injection between -50 to 50 pA. (C) The membrane time constant, τ_{Mem} , is measured as the time for the membrane potential to rise (67%) from the resting membrane potential or fall (37%) from its maximum membrane potential. (D) V_{sag} measured in response to hyperpolarizing currents.

to elicit the first AP in rheobase current stimulus. The AP amplitude (mV) is defined as the difference between AP peak and threshold voltages. The AP half-width (ms) is defined as the time duration of the width of the AP spike at its half amplitude (time between rising phase and decaying phase of AP). The amplitude of the after-hyperpolarization (AHP, mV) was measured as the difference between the AP threshold and the minimum voltage during the hyperpolarization phase of AP (Fig. 2.6, A, B).

To determine the characteristics of the AP firing pattern of a neuron, AP trains of ~10 spikes were used for analysis. The ISI (ms) is defined as the time between two neighboring AP spikes (Fig. 2.5 B). The firing frequency was calculated by plotting the number of spikes against the amplitude of

the injected current pulse. The firing frequency per 100 pA current injection was measured as the slope of the linear fit that corresponds to the number of spikes per sweep to the injected current pulse. The adaptation ratio was determined as the ratio of the third ISI divided by the tenth ISI (ISI_3/ISI_{10}) from the ten-spike train which was defined as the first super-threshold response with a minimum of 10 spikes in the AP-spike train. (Fig. 2.6, C, D).

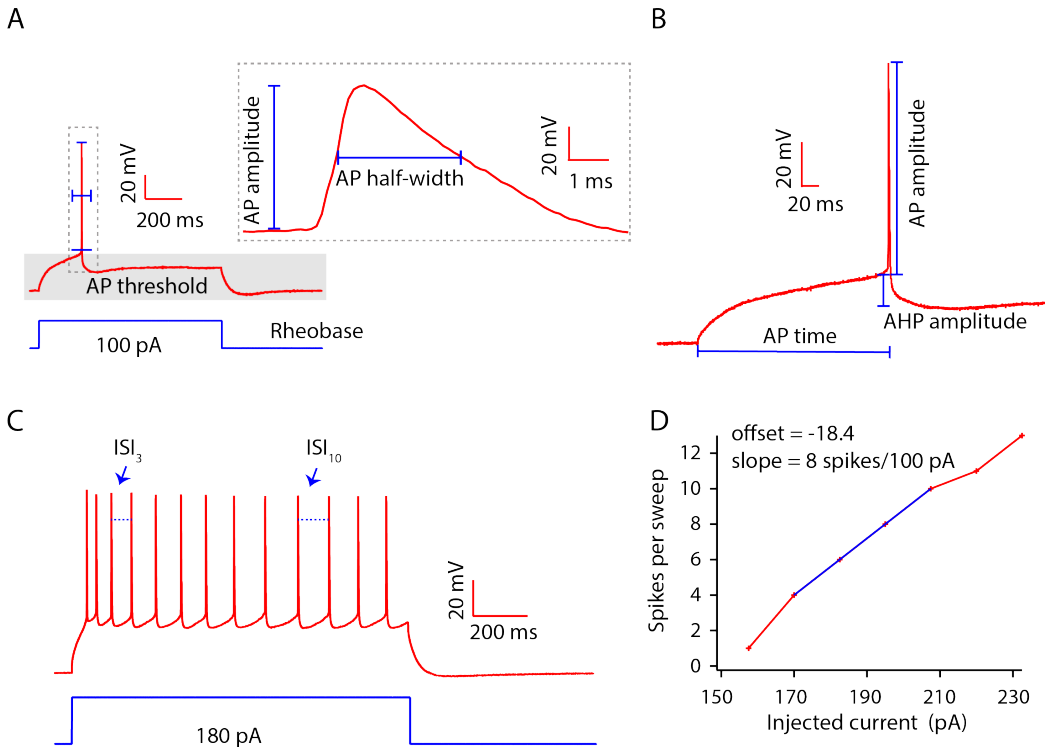


Fig. 2.6: Analysis of active properties of L5 neurons in mPFC. (A) The rheobase (bottom, blue) is the minimum current required to elicit an AP (red trace within the gray box). The AP threshold (A, gray area) is the membrane voltage to be reached by a neuron before it generates the first AP. The inset shows a representative waveform of an AP at a higher magnification showing AP amplitude and half-width. The AP amplitude is the voltage difference between the threshold and peak membrane potential; the AP half-width is the time difference between rising and decaying phase of AP at half maximum amplitude (B) The AP amplitude, AP time or delay until 1st AP and AHP amplitude are shown. AP time or the delay until 1st AP is the minimum time required to elicit the first AP spike in rheobase current stimulus; AHP amplitude is the amplitude of the after-hyperpolarization. (C) The ISI was measured as the time between individual spikes and the adaptation ratio is determined as the ratio of the 3rd ISI and 10th ISI. (D) The firing frequency per 100 pA was determined from the slope of the linear fit to the plot of the spike number vs. the injected current (red trace).

2.6.3. Physiological properties of synaptically coupled neuronal pairs

The synaptic properties of excitatory and inhibitory connections were analyzed offline using custom-written algorithms in Igor Pro software (WaveMetrics, Lake Oswego, OR) as described previously (Feldmeyer et al. 1999; Feldmeyer et al. 2002). Initially, sweeps with high spontaneous activity were excluded, then all the rest sweeps were aligned to the presynaptic AP peaks and an average of all the EPSP or IPSP sweeps was generated (Fig. 2.7, A). The PSP peak amplitude (V_{peak}) was measured by calculating the difference between the mean baseline amplitude (B1) and maximum voltage (A1) of the postsynaptic PSP. A 'peak search window' of 5 ms after the

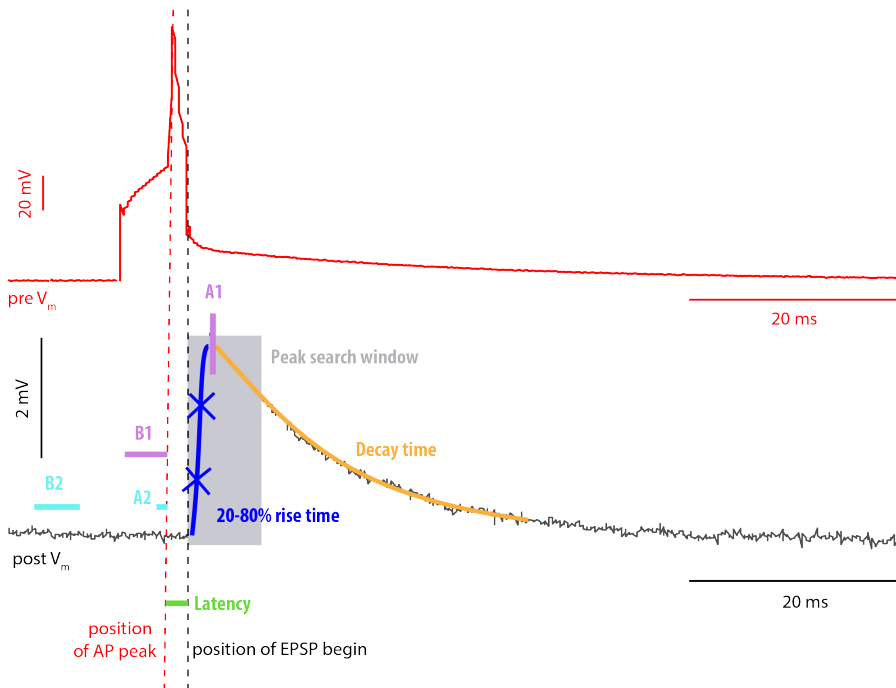


Fig. 2.7: Analysis of synaptic properties of synaptically coupled L5 neurons in mPFC. Injection of a current pulse into the presynaptic neuron initiates APs (red trace) that travels towards the synaptic terminal and induce neurotransmitter release. Current flow through postsynaptic receptor channels results in a depolarization of the postsynaptic spine or dendritic shaft. The resulting change in membrane potential is recorded as EPSP (black trace). A single presynaptic AP (red) in a PN and the EPSP (black) in another PN are recorded in a PN-to-PN connection (V_m , membrane potential). The EPSP amplitude is defined as the difference between A1 (maximum voltage of the EPSP) and (mean baseline amplitude). The baseline noise is measured as the difference between B2 and A2. The rise time was measured as the time from 20% to 80% (blue crosses) of the peak EPSP amplitude. The latency (green line) is determined as the time interval between the time of the presynaptic AP peak and the time of the EPSP initiation and the EPSP decay from a fit of a single exponential function to the decay phase of the EPSP (orange line).

presynaptic AP was selected to evaluate individual peak amplitude and averaged over 1 ms. The mean baseline amplitude (within the baseline region) was set to 5 ms (A1) preceding the PSP. The rise time was calculated as the mean time taken by a voltage signal to change from 20% to 80% of the peak amplitude which was determined from the linear fit. The latency of PSP was calculated as the time interval between the presynaptic AP amplitude peak and the onset of the PSP. The decay time constant is a measure of the rate of decline in the PSP determined from a single exponential fit to the decay phase of both individual and averaged responses. The paired-pulse ratio (PPR) is a (surrogate) measure of the neurotransmitter release probability of the presynaptic neuron and was measured as the ratio of the amplitude of the second PSP divided by the first PSP elicited by a train of 2-3 presynaptic APs at a stimulation frequency of 10 Hz. The coefficient of variation (CV) was determined as the standard deviation (SD) of the EPSP amplitude corrected for the background noise (V_{noise}) divided by the mean EPSP amplitude ($SD_{\text{EPSP}} / \text{Mean}_{\text{EPSP}}$). Failure events were defined as events with amplitudes that are smaller than 1.5 times the SD of the V_{noise} . The failure rate was calculated as the number of failure events divided by the number of sweeps recorded.

2.7. Morphological reconstructions and analysis

2.7.1. Histological procedures

After the end of single-cell or paired recordings, brain slices were processed as described previously (Marx et al. 2012). Slices containing biocytin-filled neurons were fixed using 4% paraformaldehyde (PFA) in 100 mM phosphate buffer (PB, pH 7.4) at 4 °C for at least 24 hours. PFA fixation quenches the endogenous activity of the neurons within the brain slices. Subsequently, slices were incubated in 0.1% Triton X-100 solution containing avidin-biotinylated horseradish peroxidase (Vector ABC staining kit, Vector Lab. Inc., Burlingame, USA) for about 20 minutes. 3,3'-diaminobenzidine (Sigma-Aldrich, St. Louis, MO, USA) was added as a chromogen that resulted in a dark precipitate in the biocytin-filled neuron so that its axonal and dendritic branches were clearly visible. Slices were then subjected to slow dehydration using ethanol and xylene and later rinsed several times using 100 mM PB solution and mounted on gelatinized slides and embedded in Eukitt medium (Otto Kindler GmbH, Freiburg, Germany).

2.7.2. Morphological 3D reconstructions

To reconstruct the entire morphology of excitatory and inhibitory neurons filled with biocytin in three dimensions (3D), NeuroLucida system (MicroBrightField, USA), and Olympus BX61 microscopy at 1000 X magnification (100 X objective and 10 X eyepiece) were employed. Slices were selected for 3D reconstruction when the neuron was clearly labeled and the background staining was low. After reconstructing neurons in 3D, the cortical layers, WM, and pial surface were marked. Later, reconstructions were rotated so that the pial surface was aligned at the horizontal plane. Fig. 2.8 depicts an example reconstruction of a PN in L5 of the mPFC. Correction for slice tissue shrinkage was adjusted in all spatial dimensions (correction factor 1.1 in the x and y axes, factor 2.1 in the z axes) as measured previously in Marx et al. 2012. The morphological properties were then analyzed using Neuroexplorer software (MicroBrightField, Colchester, USA).

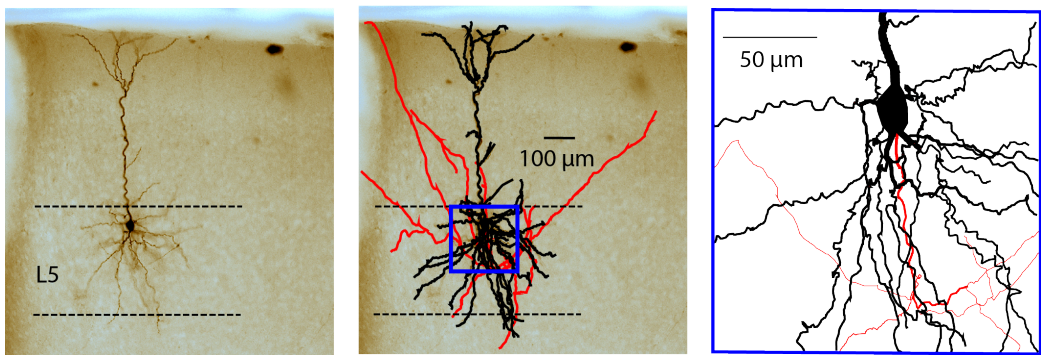


Fig. 2.8: Reconstruction of an excitatory L5 PN in mPFC. (A) Photomicrograph of a biocytin-filled PN. (B) Three-dimensional (3D) reconstruction of the somatodendritic compartment (black) and axon (red) of the neuron. (C) Higher magnification of 3D reconstruction marked in the blue boxed area in (B), shows the original thickness of somatodendritic and axonal compartments.

2.8. Statistical analysis

When the number of data points were larger than 10, data were represented as box plots. A box plot (Fig. 2.9) displays the summary of a set of data that includes interquartile range (IQR) represented as a box (50% of data points), minimum whisker (lower 25% of data points excluding outliers) and maximum whiskers (upper 25% of data points excluding outliers), first quartile (Q1: median of data points to the left of the median), median marks the midpoint of the data represented by a horizontal line within the box and third quartile (Q3: median of data points to the right of the median). An outlier is defined as the data points that are numerically distant from the rest of the data and

therefore lie outside of the minimum and maximum whiskers of the box plot. When the number of data points were lower than 10, bar graphs with mean \pm SD were used. Paired student t-test or Wilcoxon signed-rank test was used for statistical comparisons between the two groups. Tukey's test was used when the sample size is different between the two groups.

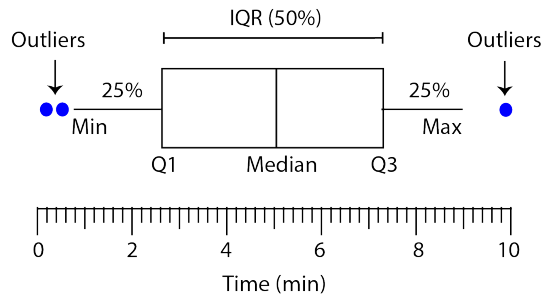


Fig. 2.9 Schematic representation of a box-plot. A box plot displays a summary of a set of data. IQR: 50% of data points, Min: minimum whisker depicting lower 25% of data points excluding the outliers; Q1: first quartile is the median of data points to the left of the median; Median: median value in the data set; Q3: third quartile is median of data points to the right of the median; Max: maximum whisker depicting upper 25% of data points excluding the outliers; Blue circles: outliers are the data points distant from the rest of the data.

3. Results

3.1. Neuronal classification in L5 of mPFC

The balance of excitation and inhibition (E/I) in cortical microcircuits is crucial to maintaining normal function and efficiency of information processing. Cortical microcircuits are established by both excitatory PNs and inhibitory INs. Several studies have investigated the neuronal diversity and function in rodent mPFC (van Aerde and Feldmeyer 2015, Meunier, Cancela et al. 2017, Ding, Emmenegger et al. 2021, Nakajima 2021). A previous study from our lab (van Aerde and Feldmeyer 2015) suggests that three major types of excitatory PNs exist in L5 of mPFC: broad (Bd)-tufted RS PNs, slender (Sl)-tufted low R_{in} AS PNs and Sl-tufted high R_{in} AS PNs. Based on the AP firing pattern, the existence of at least two major classes of inhibitory INs has been proposed (Kawaguchi and Kondo 2002). Inhibitory neurons displaying a high frequency AP firing pattern and with almost no adaptation are classified as FS INs while inhibitory neurons with a relatively low frequency firing pattern and AP frequency adaptation are classified as nFS INs. PNs and INs form synaptic connections with each other and among themselves. To study the functional and structural properties of these neurons, whole-cell patch clamp recordings with simultaneous biocytin fillings were performed during the experiment. PNs were identified by the triangular or pyramidal shape of their soma and the presence of a thick apical dendrite. L5 INs were identified by their oval soma shape; the IN soma was considerably smaller than that of PNs. After electrophysiological recordings, histochemical processing was performed to identify the morphology of the patched neurons.

3.1.1. Classification of PNs in L5 of mPFC based on AP firing pattern.

Based on the adaptation ratio of the AP firing pattern, PNs in L5 of PFC were classified into two different groups (Fig. 3.1): adaptive-spiking (AS) PNs and regular-spiking (RS) PNs. In AS PNs, the ISI during a spike train increases, resulting in an adaptation ratio (ISI_3/ISI_{10}) smaller than 0.8. In RS PNs, the ISI during a spike train remained constant after the 3rd AP, resulting in an adaptation ratio larger than 0.8. To understand how distinct these two groups are from each other, the passive membrane properties, single AP properties and firing properties between these two groups were compared (Fig. 3.2). Of the neurons included in this work, 108 were in the AS and 93 in the RS group. AS PNs had a more negative RMP than RS PNs (-69.1 ± 4.8 vs -67.7 ± 5.1 mV). In addition, in AS PNs, R_{in} (176.9 ± 74.9 vs 125.8 ± 71.4 M Ω), τ_{Mem} (23.6 ± 13.3 vs 15.2 ± 8.0 ms), AP half-

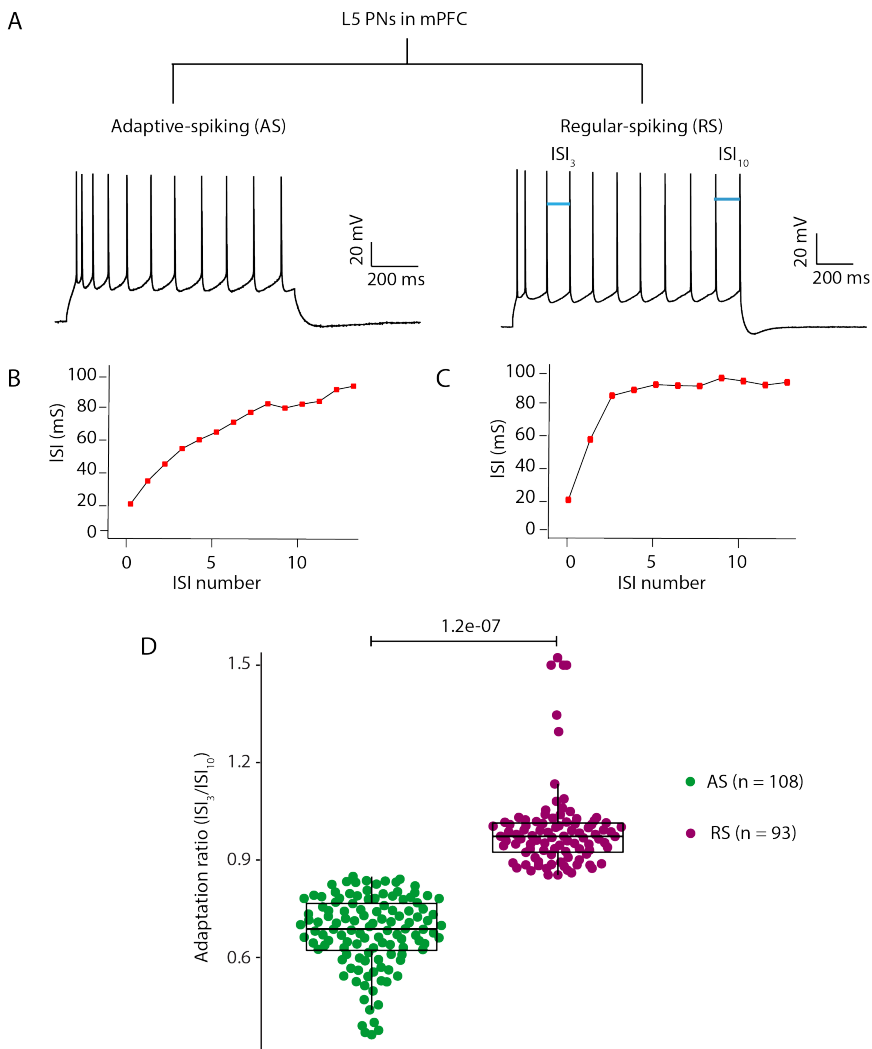


Fig. 3.1: Electrophysiological classification of L5 PNs in mPFC. (A) Based on the adaptation ratio of the AP firing patterns evoked in response to depolarizing current pulses, L5 PNs were classified into AS and RS PNs. (B, C) Changes in the ISI (blue bars in A) of a single AS (B) and a single RS (C) PN, respectively were shown. (D) The adaptation ratio was significantly different between the two PN groups. AS and RS PNs are color-coded in green and purple, respectively. Tukey's test was performed to determine differences between the two neuronal types. Absolute P-values are given above the box plots.

width (0.9 ± 0.2 vs 0.8 ± 0.2 ms) and ISI SD (31.4 ± 23.2 vs 19.8 ± 21.5 ms) were larger in comparison to the RS PNs. AS PNs had a lower rheobase for the generation of the first AP (114.1 ± 56.9 vs 181.7 ± 74.0 pA), displayed a lower V_{sag} (-0.7 ± 0.5 vs. -0.8 ± 0.3 mV) upon hyperpolarization and a lower AP amplitude (88.7 ± 6.1 vs. 93.9 ± 8.9 mV) and a lower firing

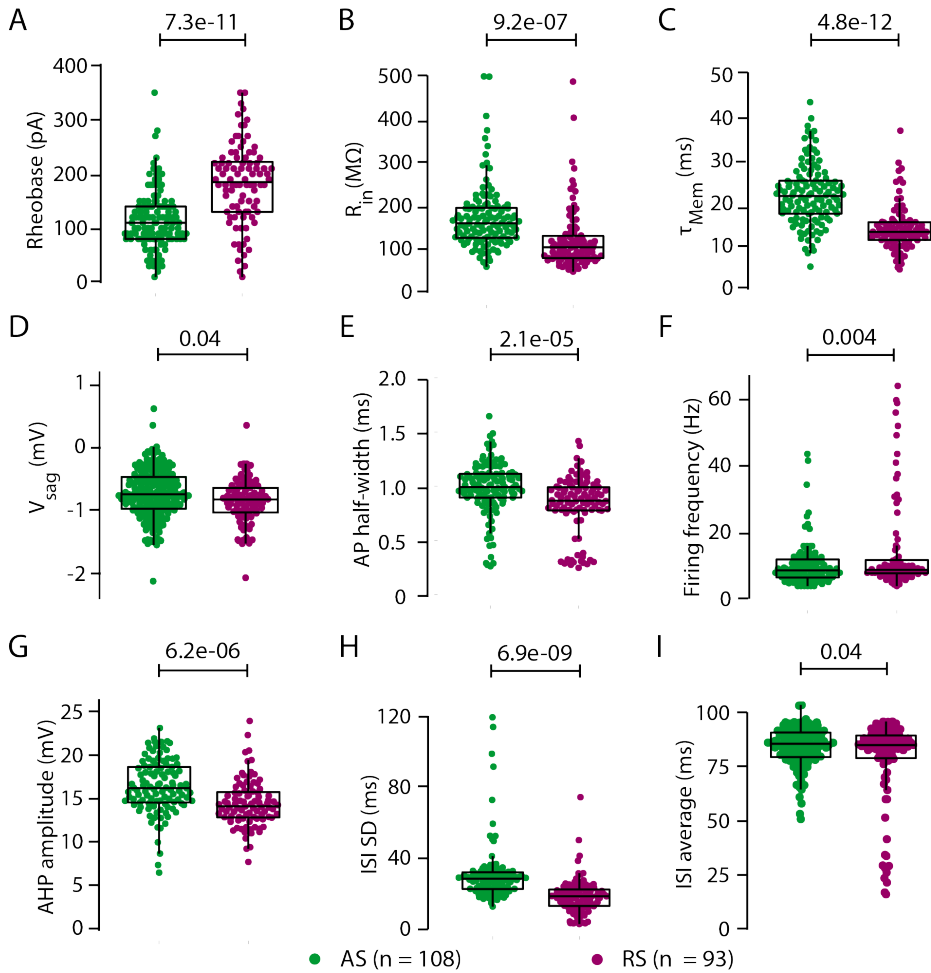


Fig. 3.2: Quantification of electrophysiological properties of L5 PNs in mPFC. Comparison of passive and active electrophysiological properties of AS PNs and RS PNs showed differences in rheobase, R_{in} , τ_{Mem} , V_{sag} , AP half-width, firing frequency AHP amplitude, standard deviation (SD) of inter-spike-interval (ISI) and ISI average. AS PNs and RS PNs are given in green and purple, respectively. Tukey’s test was performed to determine differences between the two neuronal types. Absolute P-values are given above the box plots.

frequency (11.8 ± 14.3 vs 16.6 ± 20.9 Hz) compared to RS PNs. The electrophysiological parameters of the two types of PNs and their statistical differences are summarized in [Table 1](#).

Of all recorded L5 PNs, 47 neurons were reconstructed. Based on their adaptation ratio, 22 neurons were identified as AS PNs and 25 as RS PNs. In AS PNs, the apical dendrite ended in SI-tufted branches; that of RS PNs ended in a broad, profusely branching dendritic tuft in L1 ([Fig. 3.3](#)). SI-

PARAMETERS	AS (n = 108)	RS (n = 93)	P-values
Passive properties			
R_{in} (MΩ)	176.9 ± 74.9	125.8 ± 71.4	***9.25e-07
RMP (mV)	69.1 ± 4.8	67.7 ± 5.1	*0.03
V_{sag} (mV)	-0.7 ± 0.5	-0.8 ± 0.3	*0.04
τ_{Mem} (ms)	23.6 ± 13.3	15.2 ± 8.0	***4.8e-12
AP properties			
Rheobase (pA)	114.1 ± 56.9	181.7 ± 74.0	***7.3e-11
AP threshold (mV)	35.6 ± 4.0	36.3 ± 5.2	0.2
AP amplitude (mV)	88.7 ± 6.1	93.9 ± 8.9	***1.e-06
AP half-width (ms)	0.9 ± 0.2	0.8 ± 0.2	***2.1e-05
Delay until 1st AP (ms)	252.0 ± 105.8	245.6 ± 178.7	0.7
AHP amplitude (mV)	16.5 ± 3.0	14.5 ± 2.7	***6.2e-06
Firing properties			
Adaptation ratio (ISI₃/ISI₁₀)	0.6 ± 0.1	1.0 ± 0.2	***0.0
Firing frequency (Hz/100 pA)	11.8 ± 16.6	14.3 ± 20.9	**0.004
ISI average (ms)	84.7 ± 8.9	80.5 ± 20.4	*0.04
ISI SD (ms)	31.4 ± 23.2	19.8 ± 21.5	***6.9e-09

Table 1: Statistical comparison of the electrophysiological parameters between L5 AS and RS PNs. All electrophysiological properties are given as average ± SD. *P < 0.05, **P < 0.01, ***P < 0.001, when P value is extremely small i.e., less than e-20, 0.0 is used. Tukey's test.

tufted PNs showed relatively strong axonal projections to superficial layers and would reach up to the pial surface while the axons of Bd-tufted PNs projected deep into the white matter. In acute brain slices, dendrites were almost intact but the axon suffers from major truncation due to their wide range of projections (Narayanan, Egger et al. 2015). Therefore, axonal properties were not analyzed for these PNs. In AS PNs, the total length of the apical dendrite (4.0 ± 1.1 vs 6.9 ± 2.9 mm) was larger and the number of bifurcations (15.5 ± 3.9 vs 30 ± 10.3) was higher in comparison to AS PNs. In RS PNs, the mean length of basal dendrites (5.2 ± 1.5 vs 4.4 ± 1.2 mm) was larger in comparison to AS PNs. In RS PNs, the dendritic vertical (1.0 ± 0.1 vs 1.1 ± 0.1 mm) and horizontal field span (0.4 ± 0.04 vs 0.5 ± 0.08 mm) was larger in comparison to AS PNs. The morphological parameters of the two L5 PN types and their statistical differences are summarized in [Fig. 3.4](#) and [Table 2](#).

To understand the relationship between the three major parameters of PNs, a 3D scatter plot with adaptation ratio, R_{in} and horizontal field span of the apical dendrites was constructed (Fig. 3.5). The plot illustrates the difference between AS PNs (dark green triangles) and RS PNs (purple triangles). Very little overlap between the parameters for the two groups was observed.

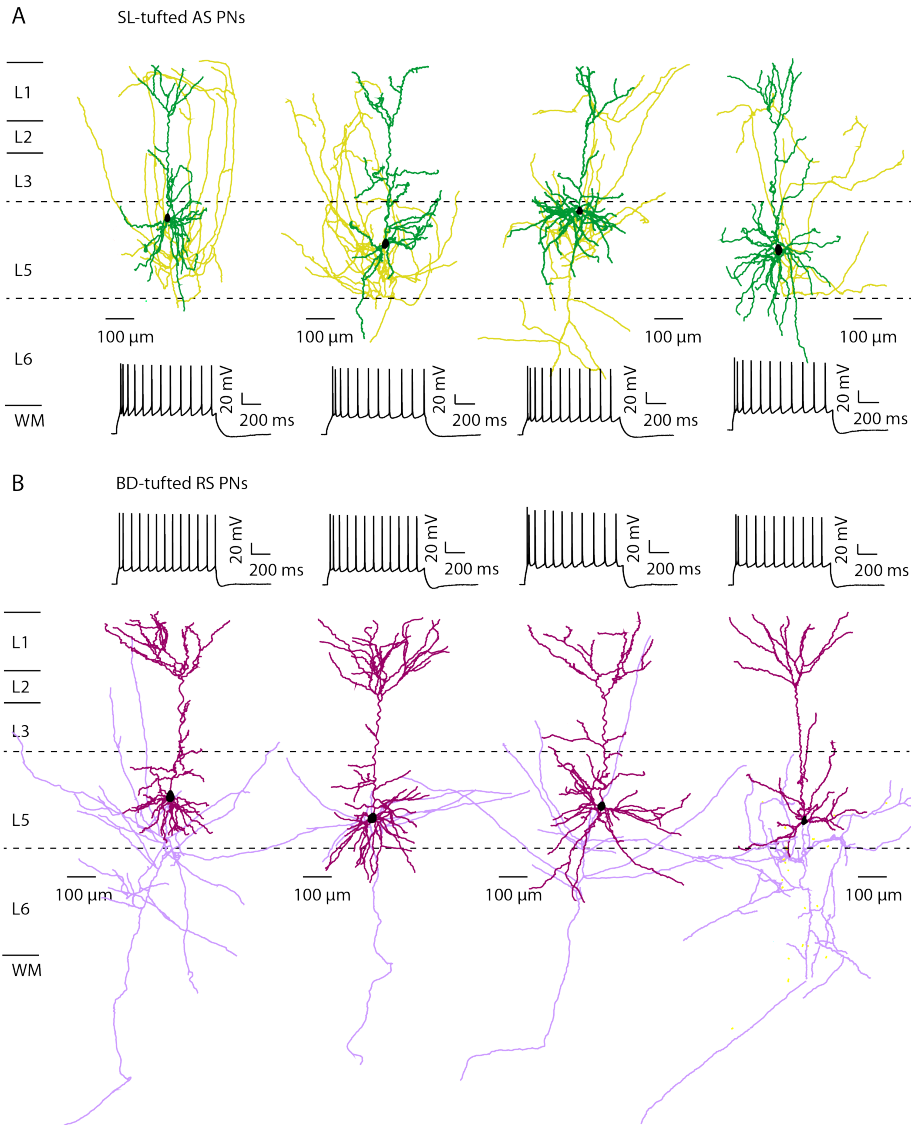
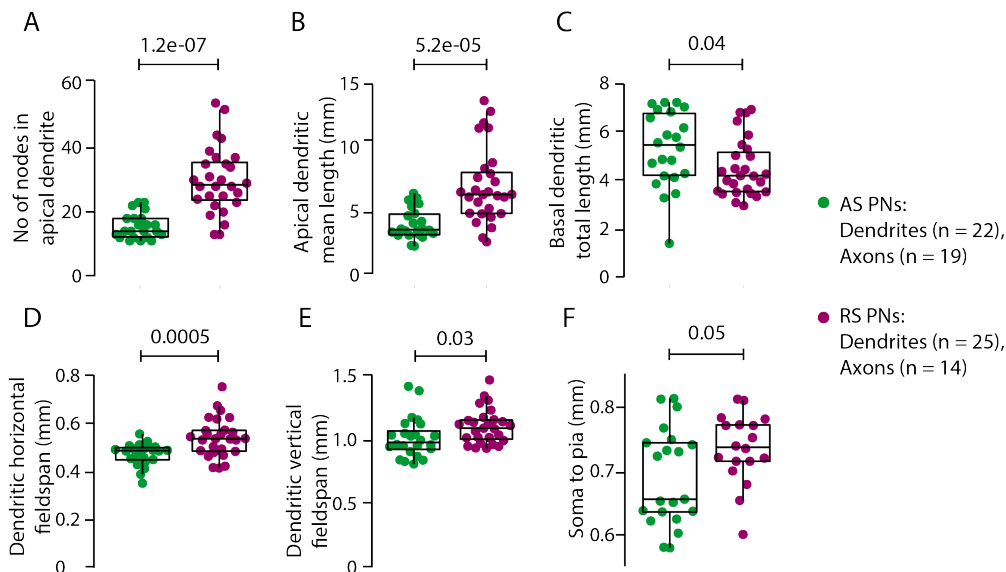


Fig. 3.3: Morphological reconstructions of L5 PNs in mPFC. Example reconstructions of four neurons in (A) AS and (B) RS groups are shown, respectively. The corresponding firing patterns of the both neuronal types are given in the lower/upper panel of A and B. AS PNs showed SL-tufted apical dendrite, while RS PNs showed Bd-tufted apical dendrite at the distal end. The cell bodies of all neurons are in black while dendrites and axon are color-coded green and yellow, respectively for AS PNs, and purple and violet, respectively for RS PNs.



3.4: Quantification of morphological properties of L5 PN in mPFC. Comparison of the morphological properties among AS PNs and RS PNs. AS PNs and RS PNs are represented in dark green and purple, respectively. In acute brain slices, dendrites are mostly intact but the long range axon collaterals suffer from major truncations (>90% (Narayanan, Egger et al. 2015)). Therefore, axonal parameters were not included in analysis. Layers are identified as mentioned in Fig. 2.2. Tukey’s test was performed to test for differences between the two neuronal types. Absolute P-values are given above the box plots.

PARAMETERS	AS (Dendrites:n = 22) (Axon:n = 19)	RS (Dendrites:n = 25) (Axon:n = 14)	P-values
Number of nodes in apical dendrite	15.5 ± 3.9	30 ± 10.3	***1.2e-07
Total length of apical dendrite (mm)	4.0 ± 1.1	6.9 ± 2.9	***5.2e-05
Horizontal field span of apical dendrites (mm)	0.5 ± 0.04	0.6 ± 0.07	***1.6e-05
Number of basal dendrites	8.0 ± 2.5	7.7 ± 1.9	0.6
Mean length of basal dendrites (mm)	0.7 ± 0.2	0.6 ± 0.1	0.1
Total length of basal dendrites (mm)	5.2 ± 1.5	4.4 ± 1.2	*0.04
Horizontal field span of dendrites (mm)	0.4 ± 0.04	0.5 ± 0.08	***0.0005
Vertical field span of dendrites (mm)	1.0 ± 0.1	1.1 ± 1.3	*0.03
Soma to pia (mm)	0.6 ± 0.07	0.7 ± 0.05	*0.05

Table 2: Statistical comparison of morphological parameters between L5 AS and RS PNs. All the electrophysiological properties are given as average ± SD. *P < 0.05, **P < 0.01, ***P < 0.001, Tukey’s test.

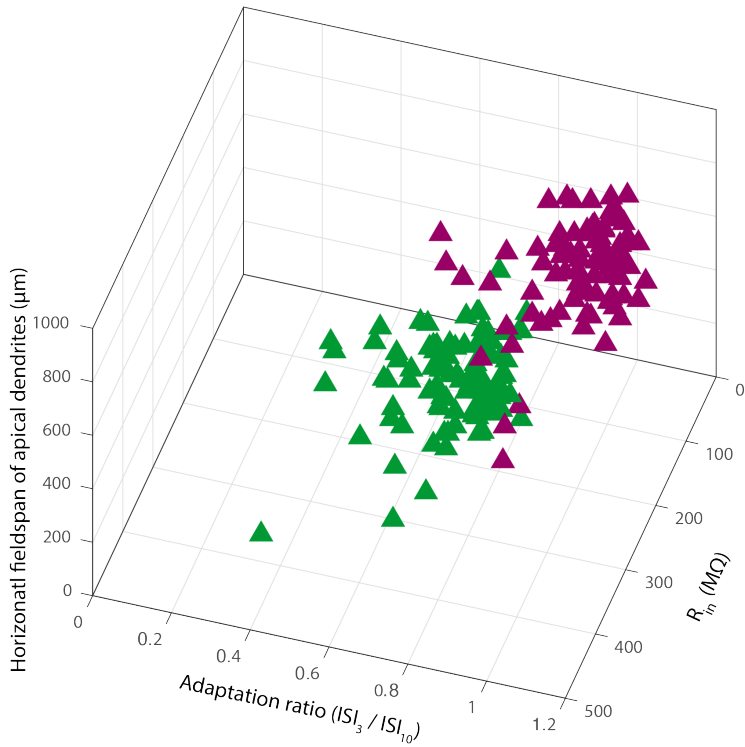


Fig. 3.5: 3D scatter plot of the adaptation ratio, R_{in} and horizontal field-span of apical dendrites of AS PNs and RS PNs. In the scatter plot, each point represents one neuron. Dark green triangles represent AS PNs while the purple triangles represent RS PNs. Note that there is little overlap between the parameters for the two PN types.

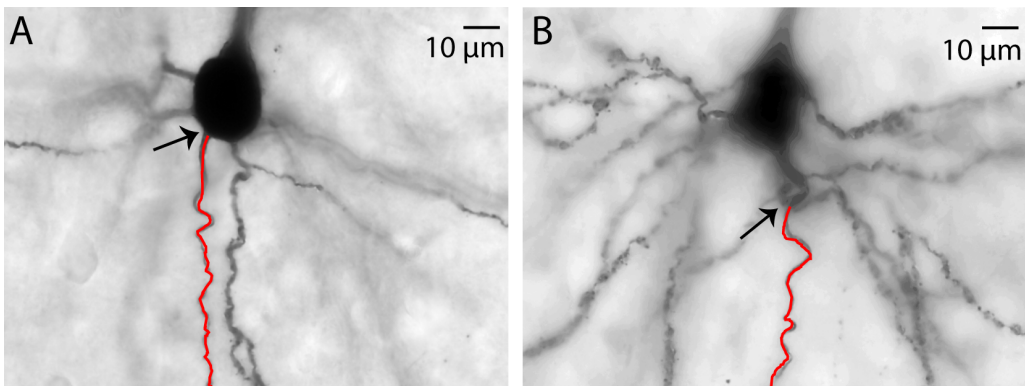


Fig. 3.6: Dendritic origin of the axon in few of the Bd-tufted RS PNs in L5 of mPFC. (A) Biocytin filled Bd-tufted L5 PN of the mPFC, whose axon (reconstructed axon shown in red) originated from the soma. (B) In a fraction of Bd-tufted PNs, the axon (reconstructed axon shown in red) originated from a basal dendrite. In eight of the Bd-tufted PNs, the axon originated from basal dendrite and in 20 of the Bd-tufted PNs axon originated from soma.

One of the axonal features observed during reconstructions was, that in 8 RS PNs the axon originated from one of the basal dendrites while in the rest of the 20 RS PNs, the axon originated from the soma (Fig. 3.6). The functional significance of this feature is not yet understood. In AS PNs, however, the axon originated always from the soma.

3.1.2. Classification of INs in L5 of mPFC based on the AP firing frequency

INs were classified into non-fast-spiking (nFS) and fast-spiking (FS) INs based on the adaptation ratio of the AP firing patterns evoked in response to depolarizing current pulses. INs whose adaptation ratio was less than 0.8 were categorized as nFS INs (0.5 ± 0.1) and those having more than 0.8 were categorized as FS INs (1.0 ± 0.2) (Fig. 3.7). There were 30 neurons in the nFS and 66 neurons in the FS group. A subset of neurons in FS neurons showed variations in the firing continuity. Therefore, based on firing frequency per 100 pA, FS type INs were further classified into regular-FS (rFS) (80.2 ± 52.0 Hz, $n = 43$, 59.7 %) and intermittent/burst-like FS (bFS) ($49.1 \pm$

PARAMETERS	nFS (n = 30)	rFS (n = 43)	bFS (n = 23)	nFS vs rFS	nFS vs bFS	rFS vs bFS
Passive properties						
R_{in} (MΩ)	377 ± 145	203 ± 88.2	214 ± 72.5	***1.9e-09	***1.3e-07	0.9
RMP (mV)	61.8 ± 9.1	70.4 ± 4.8	72.3 ± 6.8	***2.9e-06	***2.6e-07	0.5
τ_{Mem} (ms)	24.2 ± 8.7	9.5 ± 5.6	10.9 ± 13.3	***8.8e-09	***1.2e-06	0.8
AP properties						
Rheobase (pA)	37.3 ± 21.3	161 ± 85.8	204 ± 67.5	***1.0e-9	***1.21e-9	*0.03
AP threshold (mV)	38.9 ± 4.6	32.8 ± 5.1	30.7 ± 5.9	***3.5e-10	***1.2e-05	0.1
AP half-width (ms)	0.6 ± 0.1	0.3 ± 0.1	0.3 ± 0.08	***8.8e-13	***3.0e-13	0.9
Delay until 1st AP (ms)	218 ± 136	286 ± 221	467 ± 338	0.46	***0.0004	**0.006
AHP amplitude (mV)	16.8 ± 3.8	22.8 ± 3.8	22.6 ± 2.8	***2.01e-09	***5.5e-08	0.9
Firing properties						
Adaptation ratio (ISI₃/ISI₁₀)	0.5 ± 0.1	1.0 ± 0.1	1.0 ± 0.3	***3.05e-10	***2.79e-10	0.6
Firing frequency (Hz/100 pA)	22.5 ± 10.4	49.1 ± 23.2	80.2 ± 52.0	**0.002	***2.2e-09	***0.0003
ISI average (ms)	67.6 ± 18.4	38.5 ± 19.1	43.7 ± 20.5	***2.4e-08	***2.5e-05	0.5
ISI SD (ms)	29.5 ± 26.7	21.1 ± 30.8	66.9 ± 52.2	0.6	***0.0006	***4.6e-06

Table 3: Statistical comparison of the electrophysiological parameters among L5 nFS, rFS and bFS INs in mPFC. All the electrophysiological properties are shown as average ± SD. *P < 0.05, **P < 0.01, ***P < 0.001, Tukey's test.

23.2 Hz, $n = 29$, 40.2 %) type INs. Here, data from nFS, rFS and bFS INs are color-coded black, blue and red respectively. rFS (-70.8 ± 4.3 mV) and bFS INs (-69.3 ± 5.0 mV) had a more negative RMP than nFS INs (-61.8 ± 9.1 mV). Other passive electrophysiological parameters like R_{in} ($[196.9 \pm 76.0$ M Ω and 215.9 ± 78.6 M Ω] vs 377.2 ± 145.9 M Ω) and τ_{Mem} ($[9.5 \pm 5.6$ ms and 8.4 ± 2.8 ms]

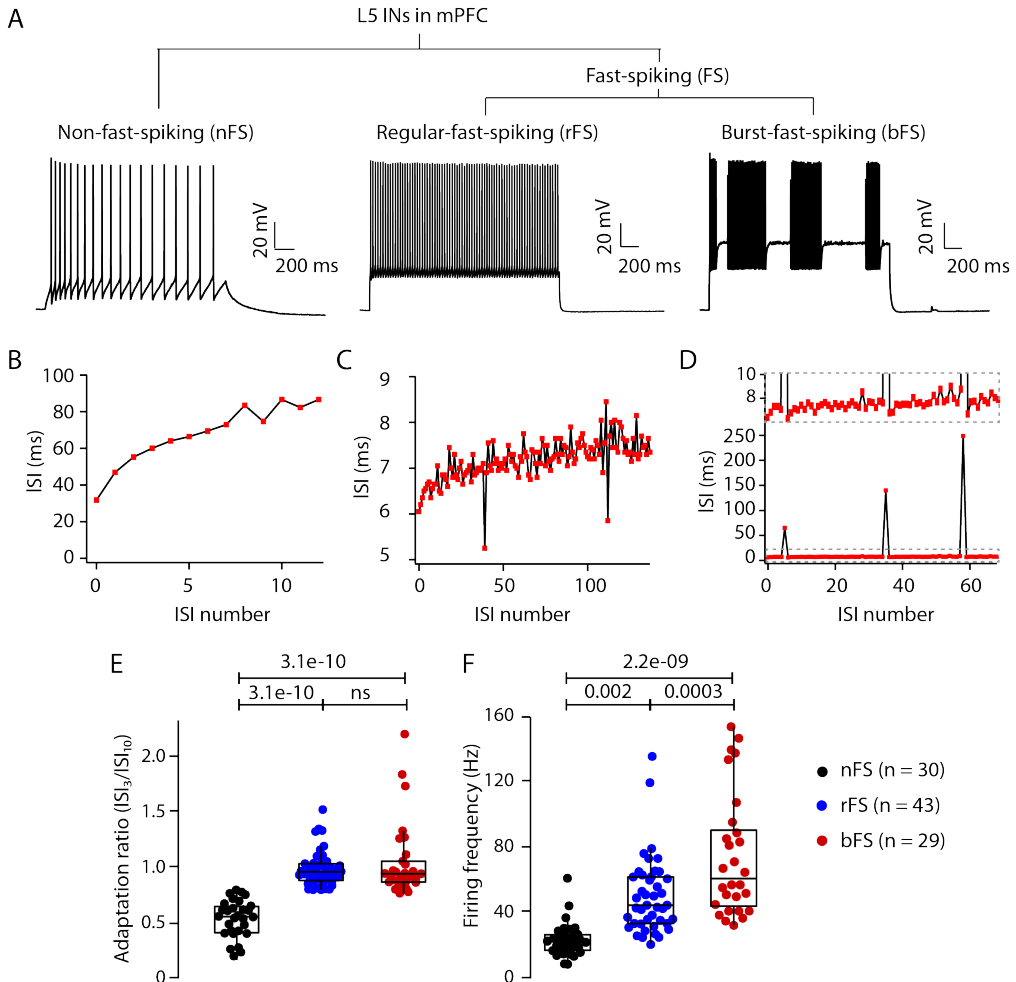


Fig. 3.7: Electrophysiological classification of L5 INs in mPFC. (A) Based on the adaptation ratio of the AP firing patterns evoked in response to depolarizing current pulses, L5 INs were classified into nFS and FS. Based on the firing frequency, FS neurons were further subdivided into rFS and bFS neurons. ISI of nFS, rFS and bFS INs are shown in panels B-D, respectively. In case of bFS, higher magnification of ISIs are given in an inset in panel D. Adaptation ratios and firing frequencies of FS and nFS INs are shown in E and F respectively. nFS INs are color-coded in black, while rFS and bFS INs are color-coded in blue and red, respectively. Tukey's test was performed to explore differences between the three neuronal types. Absolute P-values are given above the box plots.

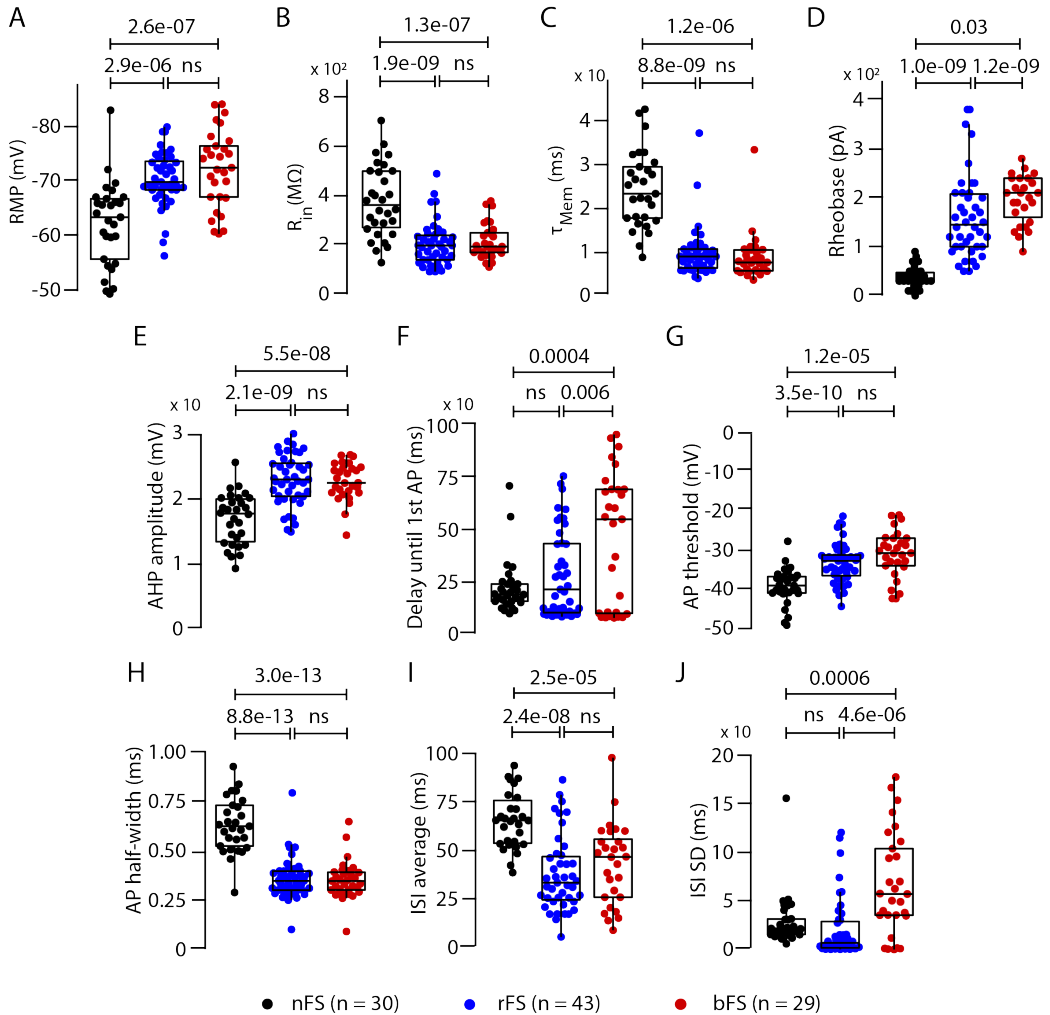


Fig. 3.8: Quantification of electrophysiological properties of L5 INs in mPFC. (A-J) Comparison of the passive and active electrophysiological properties among nFS, rFS and bFS IN types. nFS INs are color-coded in black, while rFS and bFS INs are color-coded in blue and red, respectively. Tukey's test was performed to explore differences between the three neuronal types. Absolute P-values are given above the box plots.

vs 24.2 ± 8.7 ms) were lower in rFS and bFS INs in comparison to nFS INs. nFS INs fired at a lower threshold (-38.9 ± 4.61 mV vs $[-32.8 \pm 5.1$ mV and -30.7 ± 5.9 mV]), displayed a least delay until 1st AP (218.2 ± 136.52 ms vs $[286.1 \pm 221.1$ ms and 186.7 ± 64.3 ms]) and a lower AHP amplitude (16.86 ± 3.88 mV vs $[22.8 \pm 3.8$ mV and 22.6 ± 2.8 mV]) but had a larger AP half-width (0.64 ± 0.15 mV vs $[0.3 \pm 0.1$ mV and 0.3 ± 0.1 mV]) compared to rFS and bFS INs. The primary difference between the two types of FS INs was the rheobase and ISI SD. bFS INs needed a higher

injection of current (204.4 ± 67.5 pA) to generate the first AP than rFS (161.1 ± 85.8 pA) and nFS (37.33 ± 21.32 pA) INs. The ISI SD of bFS INs was larger (44.1 ± 26.6 ms) than that of rFS (21.1 ± 30.8 ms) and nFS (24.7 ± 12.8 ms) INs. The electrophysiological parameters of the three L5 IN

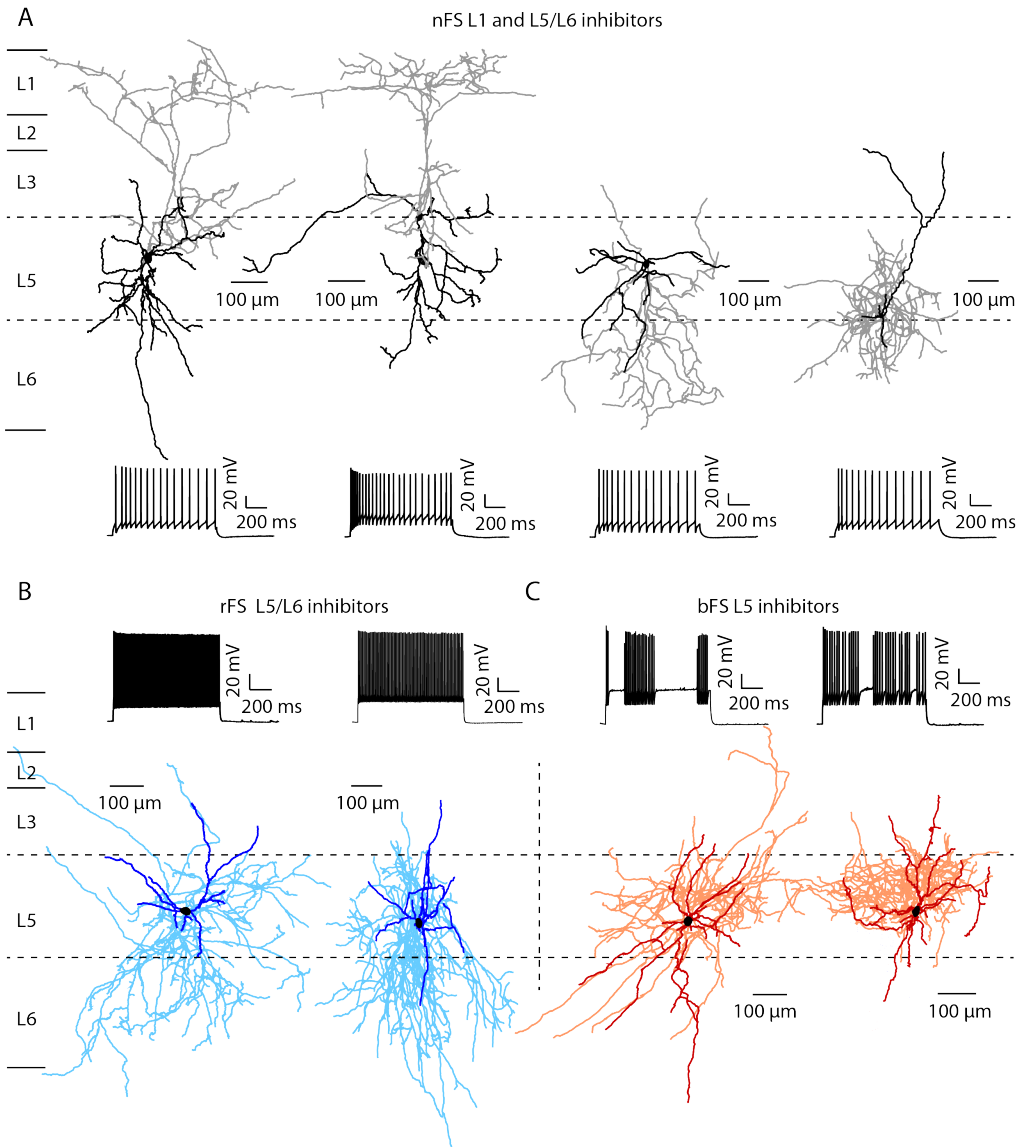


Fig. 3.9: Morphological reconstructions of L5 INs in mPFC. Example reconstructions of two (A) nFS L1 projecting INs and two nFS L5/L6 projecting INs, (B) two rFS and (C) two bFS IN types. The corresponding firing patterns of the all neuronal types are given in the lower/upper panel of A, B and C. The cell bodies of all neurons are in black, while dendrites and axons are color-coded in black and gray for the nFS INs, dark blue and light blue respectively for rFS INs and dark red and light red for bFS type INs, respectively.

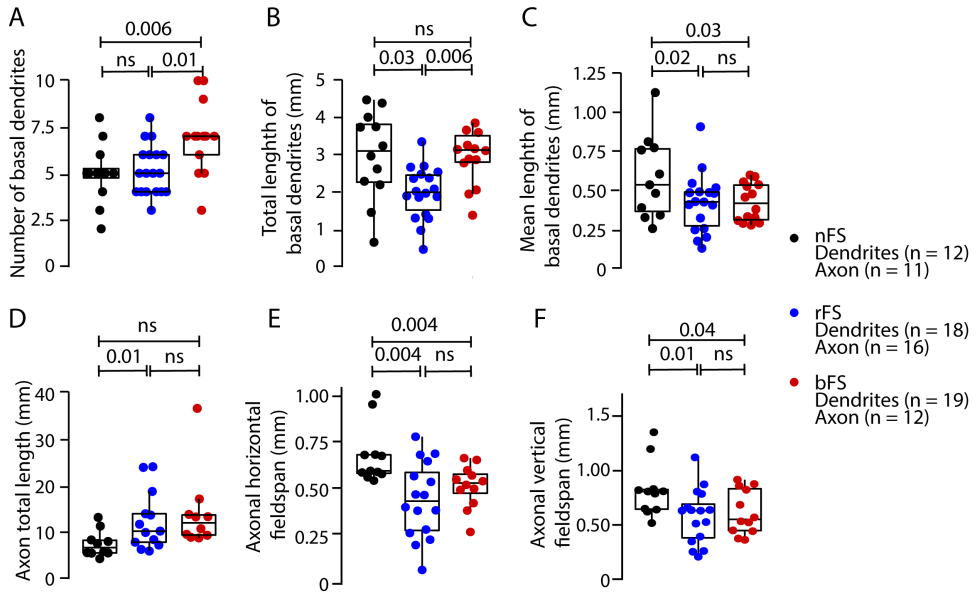


Fig. 3.10: Quantification of morphological properties of L5 INs in mPFC. Dendritic (A-C) and axonal (D-F) properties of nFS, FS and bFS IN types in L5 of mPFC. nFS INs are color-coded in black, while rFS and bFS INs are color-coded in blue and red, respectively. Tukey's test was performed to explore differences between the three neuronal types. Absolute P-values are given above the box plots.

PARAMETERS	nFS	rFS	bFS	nFS vs rFS	nFS vs bFS	rFS vs bFS
Number of basal dendrites	5.0 ± 1.5	5.1 ± 1.3	6.9 ± 1.9	0.9	**0.006	*0.01
Mean length of basal dendrites (mm)	0.6 ± 0.2	0.4 ± 0.1	0.4 ± 0.1	*0.02	*0.03	0.9
Total length of basal dendrites (mm)	2.9 ± 1.1	1.9 ± 0.7	3.2 ± 1.2	*0.03	0.8	**0.006
Total length of axon (mm)	7.2 ± 3.5	12.4 ± 6.2	14.0 ± 8.3	*0.01	0.06	0.8
Horizontal field span of dendrite (mm)	0.5 ± 0.2	0.5 ± 0.2	0.6 ± 0.2	0.4	0.5	0.9
Vertical field span of dendrite (mm)	0.4 ± 0.2	0.3 ± 0.1	0.4 ± 0.1	0.5	0.7	0.1
Vertical field span of axon (mm)	0.8 ± 0.3	0.6 ± 0.3	0.6 ± 0.2	*0.01	*0.04	0.6
Horizontal field span of axon (mm)	0.7 ± 0.2	0.5 ± 0.2	0.5 ± 0.2	**0.004	*0.04	0.6

Table 4: Statistical comparison of the morphological parameters among L5 nFS, rFS and bFS INs. All the axonal and somatodendritic properties are shown as average ± SD. *P < 0.05, **P < 0.01, ***P < 0.001, Tukey's test. nFS (dendrites: n = 12, axon: n = 11); rFS (dendrites: n = 18, axon: n = 16); bFS (dendrites: n = 19, axon: n = 12);

types and their statistical differences (Fig. 3.8) are summarized in Table 3. Of all the mPFC L5 INs recorded, 49 neurons were reconstructed; 12 were identified as nFS, 18 as rFS and 19 as bFS INs (Fig. 3.9). The axon collaterals of PFC L5 INs were found to be much denser than those of PNs because most PN axon collaterals innervate other regions of the cortical and subcortical structures and therefore undergo extreme truncation during the slice preparation. However, *in vivo* recordings in L5 of the somatosensory cortex showed densely and elaborated axon collaterals that measured about 86 mm (Oberlaender, Boudewijns et al. 2011). Neuronal reconstructions of INs with severe axonal truncation (< 40% of average axonal length) were excluded from the analysis of the axonal properties (Fig. 3.10). The average axonal length of nFS INs was ~8 mm, so reconstructions with an axonal length < 3.2 mm were excluded from the final analysis. The average axonal length of rFS and bFS INs was ~13 mm, therefore reconstructions with an axonal length < 5.2 mm were excluded from the final analysis. Based on their axonal projection pattern, two types of nFS neurons were identified. The first type had axons projecting to L1 and was hence termed nFS-L1 inhibitor, the

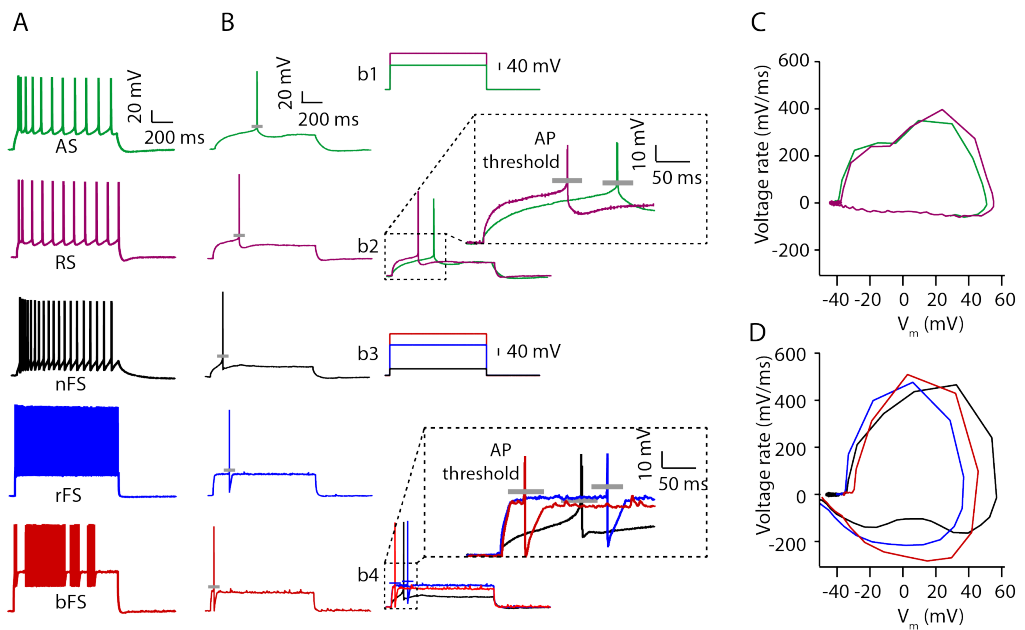


Fig. 3.11: Comparison of AP properties among L5 PNs and INs in mPFC. (A) The AP firing patterns of different PNs and INs are represented in respectively. (B) The first elicited AP of a representative PNs and INs in response to rheobase current injection (b1 and b3); b2 and b4, the first AP in higher magnification that illustrates the differences in AP threshold (gray bars) and latency. Phase plots of first AP elicited in PNs (C) and INs (D) evoked by rheobase current injection. The color codes of different neurons is as follows: AS (green), RS (purple), nFS (black), rFS (blue) and bFS (red) neurons.

second had axons projecting to L5 and L6, and was therefore termed nFS-L5/L6 inhibitors. rFS and bFS neurons had distinct axonal projection patterns: rFS neurons whose axons spanned L5 and L6 were termed rFS-L5/L6 inhibitors and bFS neurons whose axons remained in L5 were termed bFS-L5 inhibitors. The other dendritic and axonal parameters of the three IN types and their statistical differences are summarized in [Table 4](#).

Comparison of the first AP and AP firing train of PNs and INs showed characteristic differences in firing patterns as shown in [Fig. 3.11](#). Further, to differentiate different subtypes of INs, rheobase, firing frequency and AP half-width were plotted in a 3D scatter plot ([Fig. 3.12](#)). The scatter plot illustrates the separation of nFS, rFS and bFS INs, with only little overlap between all types.

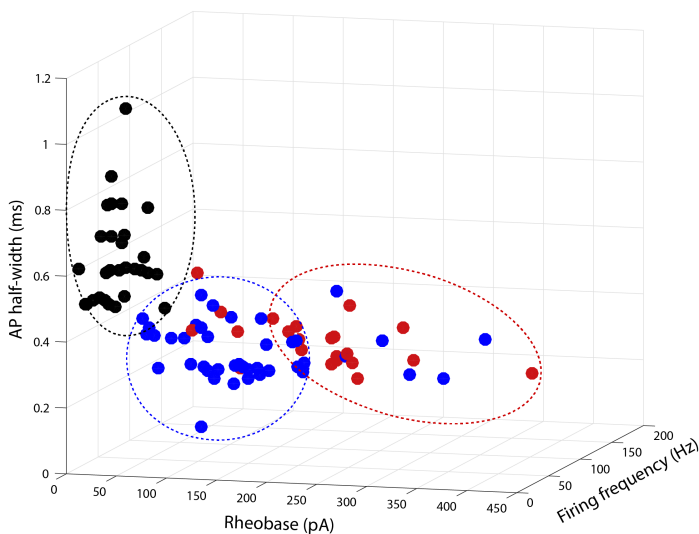


Fig. 3.12: 3D scatter plot using intrinsic properties of L5 INs in mPFC. Scatter plot showing different groups of INs. In the scatter plot, each point represents one neuron. Black circles within black dashed line represents nFS, while blue and red circles within blue and red dashed lines represents rFS and bFS INs respectively. Note that there is little overlap between the parameters for the three IN types.

3.2. Effect of 5-HT on PN activity in L5 of mPFC

To investigate the effect of 5-HT on the activity of a single neuron, L5 PNs of the PFC were recorded in whole-cell mode and 5-HT, its specific agonists and antagonists were bath-applied. PNs with a series resistance $< 40 \text{ M}\Omega$ that did not change by more than 25% during the experiment were used for analysis. After attaining the whole-cell configuration, passive and active membrane properties of single neurons were measured. Later, TTX was applied through the perfusion system to prevent the generation of APs during recordings. The TTX-containing perfusion solution serves as a control in all phases of experiments. 5-HT at a concentration of $10 \text{ }\mu\text{M}$ was applied to all the

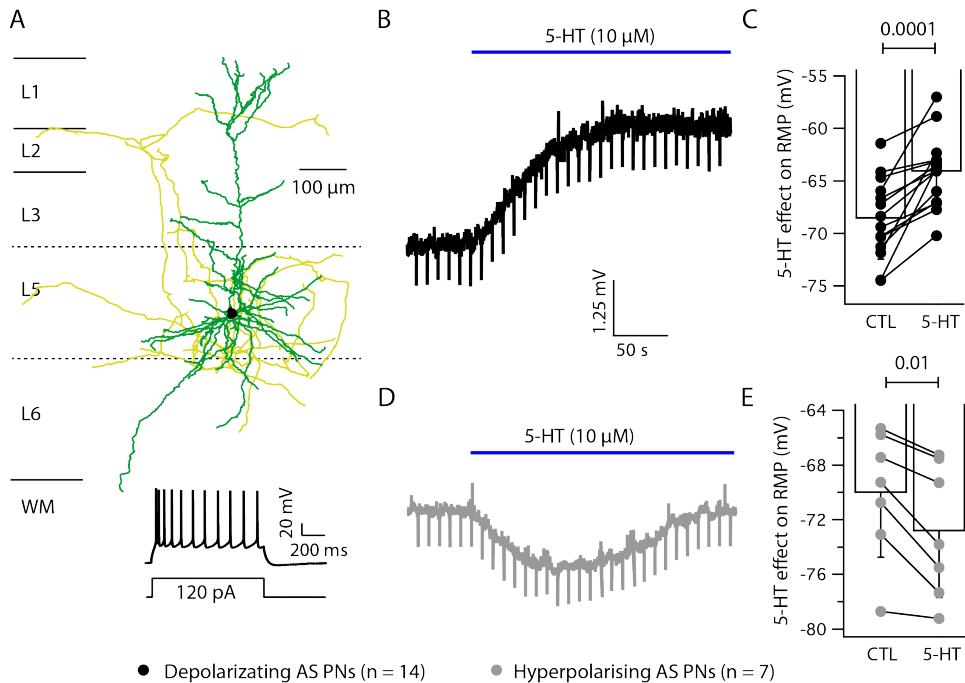


Fig. 3.13: Effect of 5-HT on L5 AS PNs in mPFC. Example reconstruction of a L5 AS PN (A). Bottom, the corresponding firing pattern and the rheobase current are shown. 5-HT induced a depolarization of the RMP (black, B, C). A minor fraction of neurons showed a hyperpolarization of the RMP following 5-HT application (gray, D, E). The blue bar marks the duration of 5-HT application. In case of hyperpolarizing AS PNs, a desensitization of the response was observed in presence of 5-HT. The soma, dendrites and axon are color-coded black, green and yellow, respectively, for AS PNs. Black circles represent depolarizing PNs while gray circles represent hyperpolarizing PNs. A Wilcoxon signed-rank test was performed to explore significant effect of 5-HT. Absolute P-values are given above the bar graphs.

PNs in bath application mode. The RMP was measured before, during and after the 5-HT application. In RS PNs (Fig. 3.13), 5-HT induced an initial transient hyperpolarization (-64.3 ± 2.8 vs -65.9 ± 2.6 mV) followed by a depolarization (-64.3 ± 2.8 vs -62.7 ± 2.5 mV). A similar transient hyperpolarization has also been observed in L2/3 and L5 PNs following acetylcholine application and was found to be mediated by SK channels (Gulledge and Stuart 2005, Eggermann and Feldmeyer 2009). In the majority (66.7%) of AS PNs (Fig. 3.14, B, C), 5-HT induced depolarization of the RMP (3.71 ± 2.40 mV). In a minor fraction (33.3%) of AS PNs (Fig. 3.14, D, E), 5-HT induced hyperpolarization of the RMP (-1.9 ± 1.2 mV). In the case of hyperpolarizing AS PNs, a decrease in the 5-HT response was observed during application which is probably due to receptor

desensitization. Compared to AS PNs, RS PNs showed a significantly smaller 5-HT induced depolarization (2.6 ± 1.3 vs 4.3 ± 2.7 mV; Fig. 3.15).

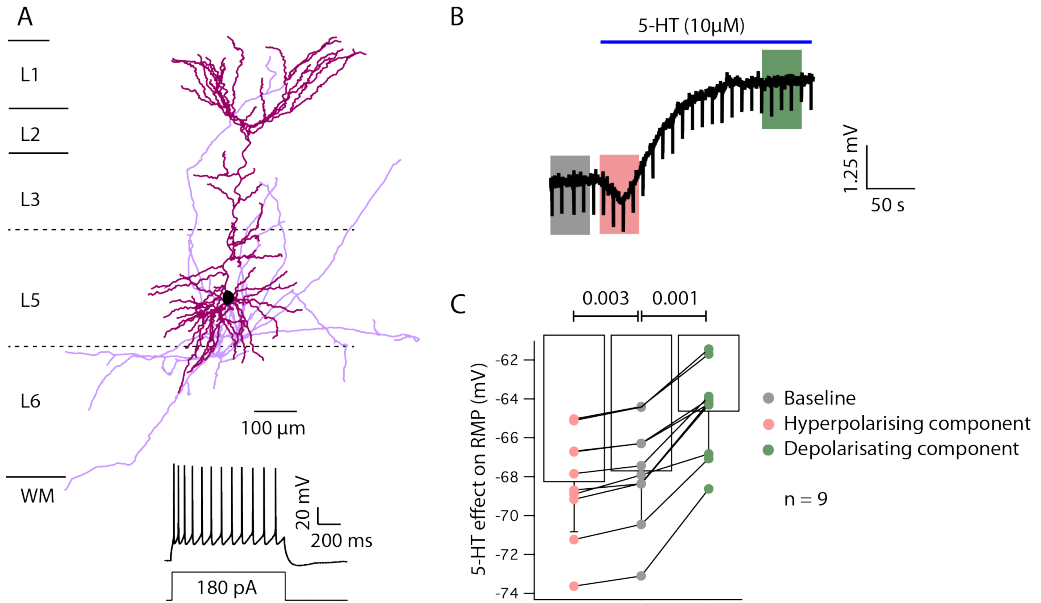


Fig. 3.14: Effect of 5-HT on L5 RS PNs in mPFC. Example reconstruction of a L5 RS PN (A). Bottom, the corresponding firing pattern and the rheobase current were given. (B) 5-HT induced transient initial hyperpolarization (light red box) followed by a depolarization (green box). The blue bar marks the duration of 5-HT application. The amplitudes of the depolarizing and hyperpolarizing components were measured relative to the baseline recording (Gray box). Soma, dendrites and axon are color-coded black, purple and violet, respectively. (C) Gray circles represent the baseline, light red circles represent transient hyperpolarizing component and green circles represent the persistent depolarizing component. Wilcoxon signed-rank test was performed to explore whether the 5-HT effect was statistically different from control. Absolute P-values are given above the bar graphs.

Morphological and electrophysiological properties of AS-depolarizing PNs and AS-hyperpolarizing PNs were analyzed for comparison (Fig. 3.16): AS-depolarizing PNs displayed a higher R_{in} (196.6 ± 52.2 vs 114.1 ± 49.7 M Ω) and a longer τ_{Mem} (25.6 ± 6.0 vs 19.3 ± 5.8 ms) but a lower rheobase (110.7 ± 30.5 vs 147.1 ± 32.5 pA). The number of basal dendrites were more in AS-hyperpolarizing PNs (9.5 ± 2.8) than in AS-depolarizing PNs (7.3 ± 1.8). The electrophysiological and morphological parameters including their statistical differences responding to the 5-HT application are summarized in Table 5.

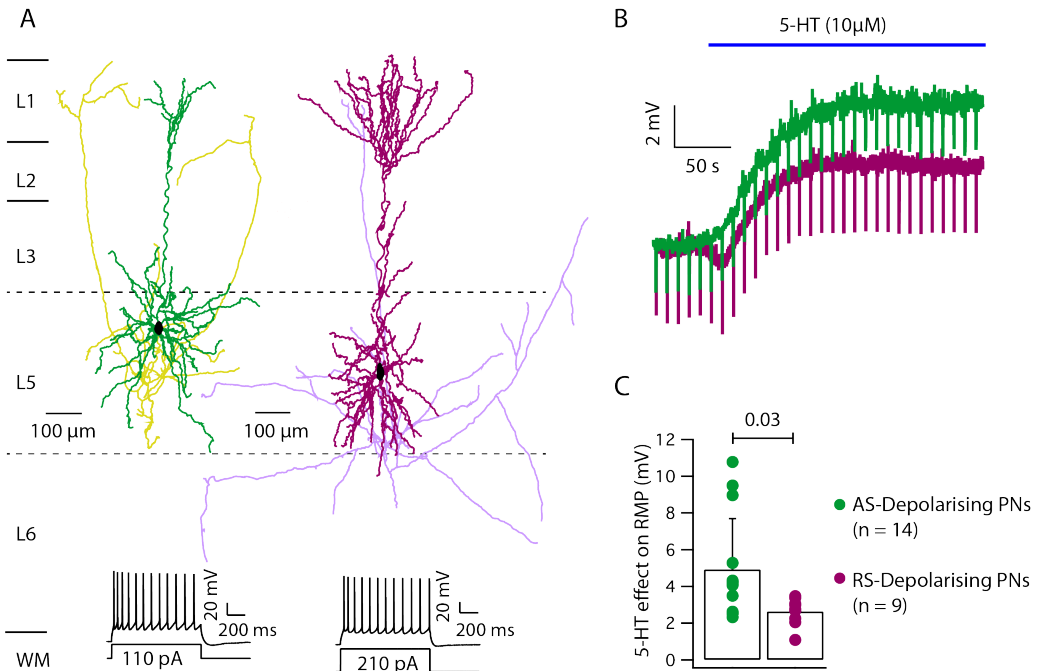


Fig. 3.15: Comparison of the 5-HT depolarizing effect between L5 AS PN and RS PN in mPFC. (A) Example reconstructions of an AS PN and RS PN. The corresponding firing patterns and rheobase currents of AS and RS PNs are given at the bottom of the panel. 5-HT induced a larger depolarization of the RMP (B, C) in SI-tufted AS PNs than in Bd-tufted RS PNs and AS PNs show no transient hyperpolarization component in response to 5-HT. The blue bar marks the duration of the 5-HT application. PN cell bodies are color-coded in black, dendrites and axon of AS PNs are color-coded green and yellow, respectively, and purple and violet, respectively, for RS PNs. Green and purple circles in (C) represent depolarizing AS and RS PNs, respectively. Tukey's test was performed to explore differences among the two groups. Absolute P-values are given above the bar graphs.

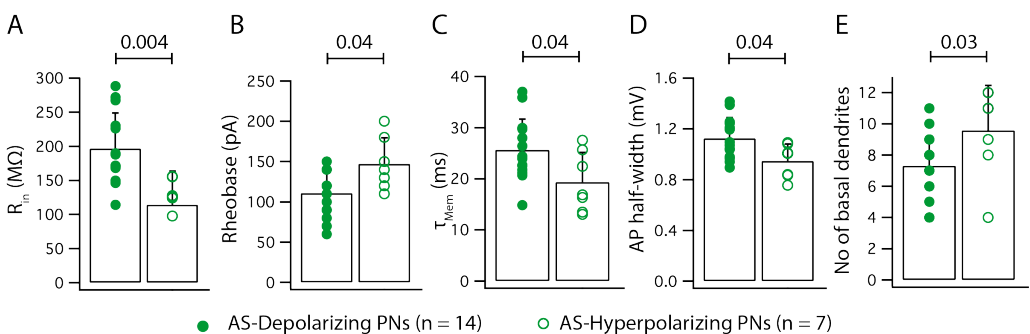


Fig. 3.16: Quantification of electro-morphic properties among 5-HT responding L5 AS PNs in mPFC. Active, passive and morphological properties of AS-depolarizing and AS-hyperpolarizing PNs in L5 of mPFC are compared (A-E). Dark green circles represent depolarizing AS, while open green circles represent hyperpolarizing AS PNs. Tukey's test was performed to explore differences among the two types of 5-HT responding AS PNs. Absolute P-values are given above the bar graphs.

PARAMETERS	AS-D (n = 14)	AS-H (n = 7)	RS-D (n = 9)	AS-D vs AS-H	AS-D vs RS-D	AS-H vs RS-D
Passive properties						
R_{in} (MΩ)	196.5 ± 52.2	114.1 ± 49.6	105.0 ± 29.6	**0.004	***4.47e-05	0.4
RMP (mV)	69.3 ± 4.6	68.2 ± 2.5	68.8 ± 4.0	0.8	0.94	0.9
τ_{Mem} (ms)	25.6 ± 6.0	19.3 ± 5.8	15.0 ± 3.2	*0.04	***0.0002	0.2
AP properties						
Rheobase (pA)	110.7 ± 30.4	147.1 ± 32.5	190 ± 39.0	*0.03	1.1E-05	*0.04
AP threshold (mV)	34.6 ± 5.7	35.3 ± 2.1	37.3 ± 2.8	0.9	0.33	0.6
AP amplitude (mV)	86.3 ± 6.8	92.5 ± 3.8	96.1 ± 9.1	0.1	**0.009	0.5
AP half-width (ms)	1.1 ± 0.1	0.9 ± 0.1	0.9 ± 0.1	*0.04	**0.009	0.9
Delay until 1st AP (ms)	260.4 ± 66.1	246.7 ± 65.0	173.4 ± 33.9	0.8	**0.002	*0.04
AHP amplitude (mV)	17 ± 3.6	17.6 ± 2.1	15.1 ± 2.4	0.8	0.3	0.2
Firing properties						
Adaptation ratio (ISI₃/ISI₁₀)	0.7 ± 0.1	0.7 ± 0.1	0.9 ± 0.1	0.7	***2.3e-05	**0.001
Firing frequency (Hz/100 pA)	8.1 ± 2.7	6.7 ± 2.1	7.6 ± 1.7	0.4	0.8	0.7
ISI average (ms)	86.8 ± 7.0	87.0 ± 7.2	90.1 ± 9.4	0.9	0.6	0.7
ISI SD (ms)	26.7 ± 7.5	23.5 ± 5.4	18.2 ± 5.2	0.5	*0.01	0.2
Morphology						
Field span of apical dendrites (μm)	297.2 ± 79.4	277 ± 37.5	442.6 ± 89.4	0.8	***0.0002	***0.0003
Number of basal dendrites	7.3 ± 1.8	9.5 ± 2.8	7.7 ± 1.9	*0.03	0.7	0.08
Soma to pia (μm)	687.5 ± 79.3	689.2 ± 73.7	720.5 ± 72.6	0.9	0.5	0.6

Table 5: Statistical comparison of the electro-morphic parameters between AS-Depolarizing (AS-D), AS-Hyperpolarizing (AS-H) and RS-Depolarizing (RS-D) L5 PN upon 5-HT application. All the electro-morphic properties are shown as average ± SD. *P < 0.05, **P < 0.01, ***P < 0.001, Tukey's test.

Further, to test whether the 5-HT induced hyperpolarization in RS PNs was mediated by SK channels, the SK channel blocker apamin was applied. Bath application of apamin (300 nM) together with the 5-HT, blocked SK channels thus preventing the occurrence of the transient hyperpolarization (-64.6 ± 0.9 vs -64.2 ± 1.0 mV) without affecting the monophasic depolarization (-63.9 ± 2.3 vs -62.3 ± 3.2 mV) of the RMP in RS PNs (Fig. 3.17).

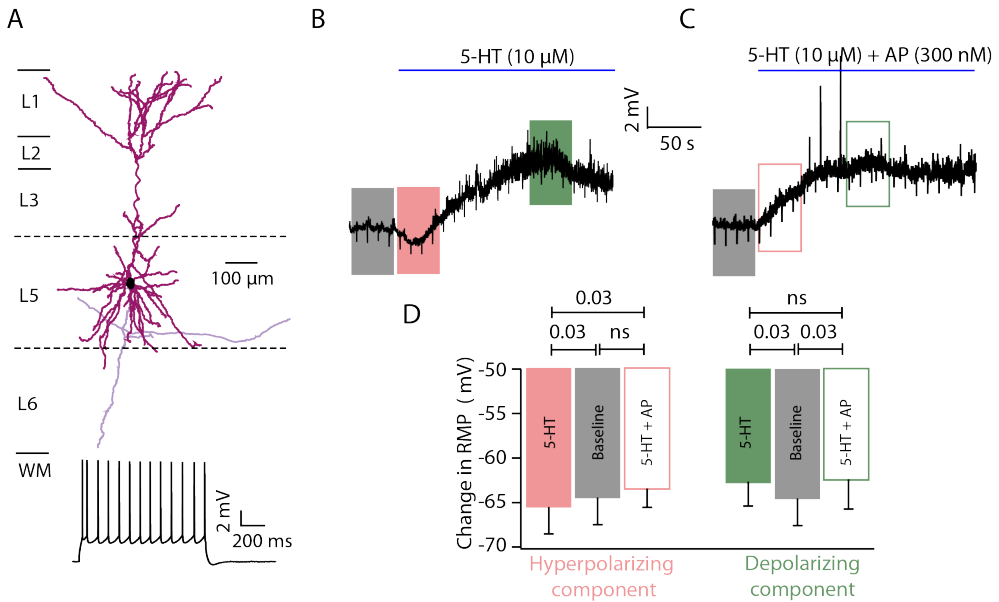


Fig. 3.17: Blockade of SK channels with apamin in L5 RS PNs in mPFC. Example reconstruction of RS (A) PN. Bottom, the corresponding firing pattern is given. (B) In RS PNs, 5-HT induced a transient initial hyperpolarization (light red box) followed by a depolarization (green box). (C) Application of 5-HT together with the SK channel blocker apamin (AP) blocked the transient hyperpolarization (open red box) without affecting depolarizing component (open green box). Changes in transient hyperpolarization and depolarization in control, 5-HT and 5-HT plus apamin conditions are shown in D. The blue bar marks the duration of drug application. Soma, dendrites and axon are color-coded black, purple and violet, respectively, for RS PNs. Gray boxes represents baseline while light red and green boxes represent hyperpolarizing and depolarizing components, respectively. Wilcoxon signed-rank test was performed to explore significant effect in different drug application conditions. n = 6, absolute P-values are given above the bar graphs.

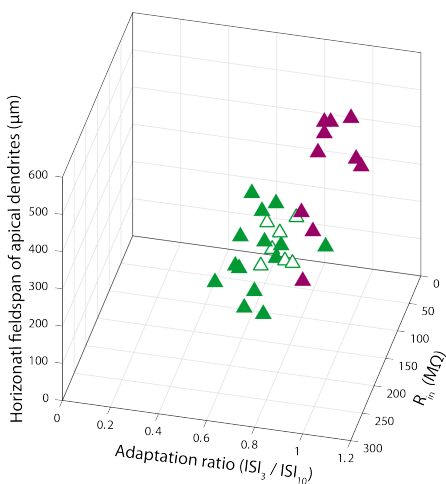


Fig. 3.18: 3D scatter plot of 5-HT responding L5 PNs in mPFC. In the scatter plot, each triangle represents one neuron. Adaptation ratio, R_m and horizontal field-span of apical dendrites of PNs are plotted in 3D. Green triangles represent AS PNs that showed depolarization upon 5-HT application, open green triangles represents AS PNs showing a 5-HT induced hyperpolarization. Purple triangles represent RS PNs that showed initial transient hyperpolarization followed by persistent depolarization upon 5-HT application.

The 3D scatter plot using adaptation ratio, R_{in} and horizontal field span of the apical dendrites (Fig. 3.18) showed two separate clusters, one corresponding to AS neurons (filled green triangles) and the other to RS neurons (filled purple triangles). The AS-hyperpolarizing PNs (open green triangles) lie within the AS-depolarizing PNs.

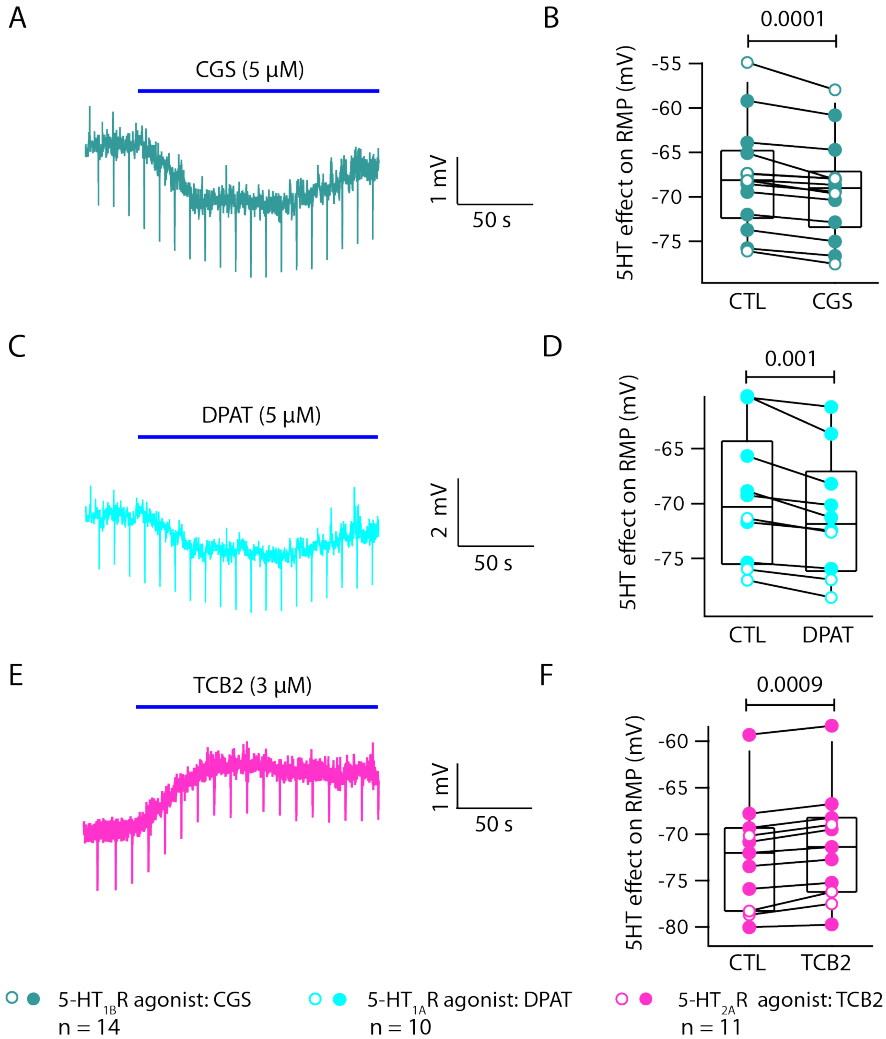


Fig. 3.19: Effect of 5-HT receptor agonists in L5 PNs in mPFC. The 5-HT_{1B}R agonist, CGS (bluish green, A,B) and the 5-HT_{1A}R agonist DPAT (cyan blue, C,D) induced a hyperpolarization of the RMP while the 5-HT_{2A}R agonist, TCB2 (pink, E,F) induced a depolarization of RMP. Desensitization of receptors was observed in presence of 5-HT_{1A}R and 5-HT_{1B}R agonist application. Open circles are AS and filled circles are RS L5 PNs. The blue bar marks the duration of drug application. For statistical comparisons between control and agonist response the Wilcoxon signed-rank test was performed. Absolute P-values are given above the box plots.

3.3. Effect of 5-HT receptor agonists on the AS and RS PNs in L5 of mPFC

To investigate the 5-HT receptor subtypes through which 5-HT modulates the neuronal activity of L5 neurons, specific 5-HT receptor agonists were bath-applied and membrane potentials were recorded (Fig. 3.19). The application of the 5-HT_{1B}R agonist, CGS (5 μ M) or the 5-HT_{1A}R agonist, DPAT (5 μ M) to mPFC L5 PNs induced both a hyperpolarization (CGS: -67.8 ± 5.8 vs -69.1 ± 5.5 mV; DPAT: -69.5 ± 6.0 vs -71.0 ± 5.5 mV). Bath application of the 5-HT_{2A}R agonist, TCB2 (3 μ M) induced depolarization in mPFC L5 PNs (-72.3 ± 5.9 vs -71.3 ± 5.9 mV). For all drug applications, recordings were made in both AS type and RS type PNs. Although the 5-HT effect differed between the AS and RS PNs, the application of specific 5-HT agonists had no significant effect. Therefore, the effect of 5-HT agonists on AS and RS PNs were combined and plotted together.

3.4. Effect of 5-HT on INs in L5 of mPFC

To investigate the effect of 5-HT in INs of L5 of PFC, INs were identified by their soma morphology and recorded in whole-cell mode. Neurons with a series resistance $<40\text{M}\Omega$ or that did not change by more than 25% during the experiment were used for analysis. After attaining the whole-cell configuration, passive and active membrane properties of single neurons were measured. Later, TTX was applied via bath application to prevent the generation of APs during recording. The TTX-containing perfusion solution serves as a control in all phases of experiments. 5-HT at a concentration of 10 μ M was applied to all the neurons via the bath. The resting membrane potential (RMP) was measured before, during and after 5-HT application. 5-HT application did not affect the RMP (-69.2 ± 8.8 vs -69.0 ± 9.2 mV) of nFS INs (Fig. 3.20, B, C) but induced a depolarization (-68.6 ± 6.0 vs -61.9 ± 9.9 mV) in all rFS INs (Fig. 3.20, E, F). In a subset (4 of 6) of bFS INs, a 5-HT induced a weak hyperpolarization (-68.5 ± 6.1 vs -70 ± 5.7 mV; Fig. 3.20, H (upper panel), I (left)). In another subset (2 of 6) of bFS INs, a 5-HT induced depolarization of the RMP was observed (-73.2 ± 6.1 vs -70.0 ± 5.7 mV; Fig. 3.20, H (lower panel), I (right)). However, no differences in morphology were observed among the two subsets of bFS INs.

3.5. Synaptic transmission in the L5 of mPFC

To study the neuronal microcircuitry in L5 of the mPFC, functional and morphological properties of L5 synaptic connections were recorded from synaptically coupled neurons. Dual whole-cell patching with the prior ‘loose seal’ searching protocol was used to find excitatory and inhibitory

neuron pairs. To characterise synaptic properties in monosynaptically coupled pairs of L5 neurons, the amplitude of the PSP, the paired pulse ratio (PPR), latency, 20-80% rise time, decay time, CV and failure rate were measured and analysed as shown in Fig. 2.6. A total of 43 neuron pairs (19 E-

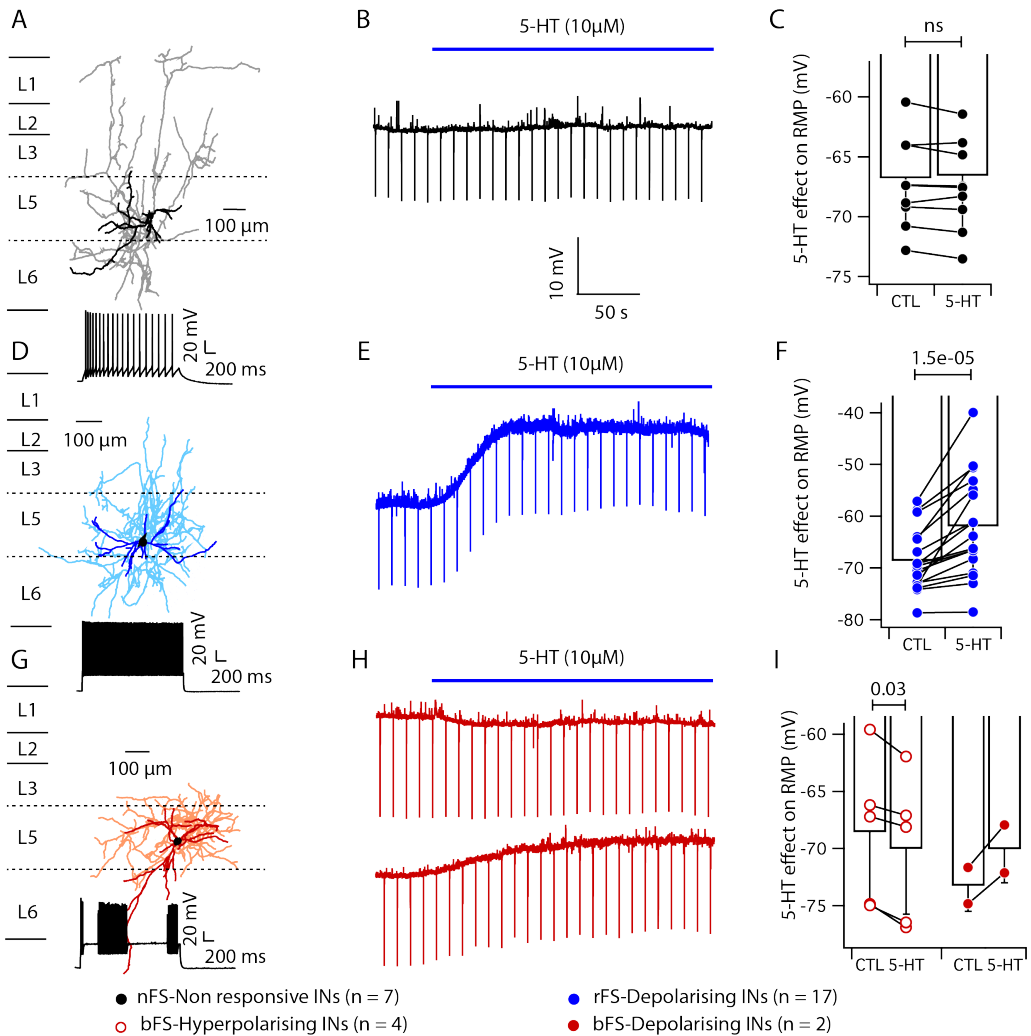


Fig. 3.20: Effect of 5-HT on L5 INs in mPFC. Example reconstructions of a nFS (A), rFS (D) and bFS (G) IN. The corresponding firing patterns of all the three IN types are given at the bottom of each panel. 5-HT had no significant effect on the RMP of nFS INs (B,C). 5-HT induced a depolarization of the RMP in almost all rFS INs (E, F). In addition, a fraction of bFS INs showed a depolarization while another showed a hyperpolarization upon 5-HT application (H, I). All somas are color-coded black, dendrites and axon are color-coded black and gray, respectively, for nFS INs, dark blue and light blue, respectively, for rFS INs and dark red and light red, respectively, for bFS INs. To evaluate significant differences between control and 5-HT response, a Wilcoxon signed-rank test was performed. Absolute P-values are given above the bar graphs.

E, 16 E-I and 8 I-E) were found to be synaptically coupled and their PSPs were recorded. All E-I and I-E pair recordings were performed using a modified paired-recording technique with a searching protocol. Within E-E pairs, 4 were recorded using the modified paired-recording technique while the rest of the 15 E-E pairs were recorded in a ‘loose-seal’ configuration because of the extremely low connectivity among the PNs. The synaptic connectivity was determined with reference to the pre- and postsynaptic neuron types.

3.5.1. Synaptic connectivity between E-E pairs in L5 of mPFC

Based on the morphological and electrophysiological classification, there are two types of excitatory PNs in L5 of PFC. The probability to find a connection for AS-RS PN pairs was 2.4% (10 connections out of 409 pairs tested) and 2.0% (8 connections out of 409 pairs tested) for RS-RS pairs. However, these connectivity ratios might be a major underestimate because of the major axonal truncations in PNs of mPFC. A total of 19 E-E pairs (Fig. 3.21) was recorded of which 10 were AS-RS PN pairs, 8 were RS-RS PN pairs and 1 AS-AS PN pair. There were some strong

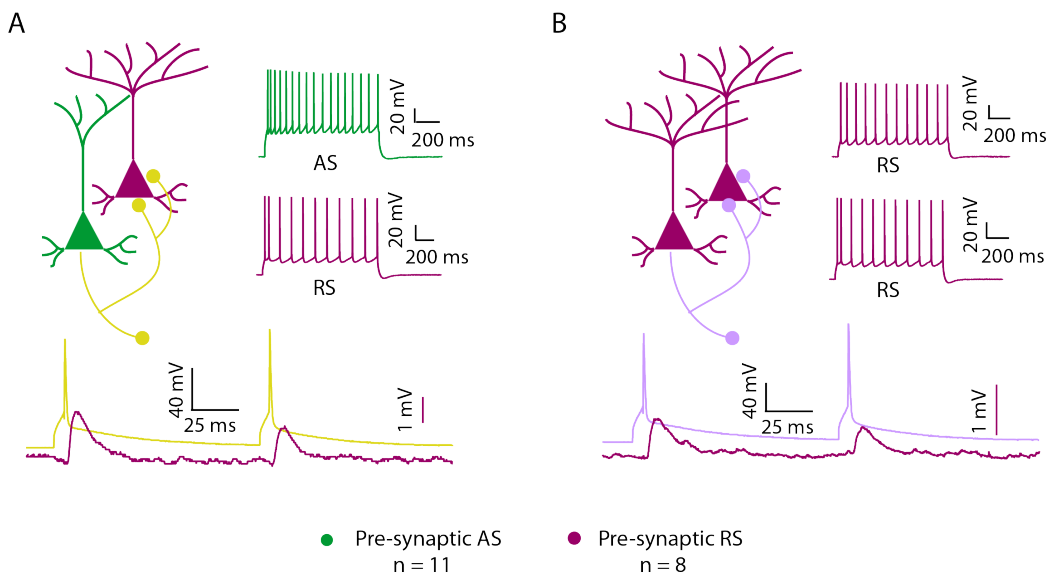


Fig. 3.21: Comparison of synaptic properties between E-E connections in L5 of mPFC. (A) Top, schematic representation and firing pattern of a synaptic connection with a presynaptic AS PN and a postsynaptic RS PN. Bottom, postsynaptic EPSPs (purple) elicited by two presynaptic APs (yellow) at a 100 ms interval. (B) Top, schematic representation and firing pattern of a synaptic connection with a presynaptic RS PN and a postsynaptic RS PN. Below, postsynaptic EPSPs (purple) elicited by two presynaptic APs (violet) at a 100 ms interval. 10 E-E pairs are AS-RS PN connections, 8 are RS-RS PN connections and 1 AS-AS PN connection.

connections with a mean unitary EPSP amplitude >2 mV and some weak connections with a unitary EPSP amplitude <0.5 mV; EPSPs displayed short-term depression (PPR: ≤ 1). The average EPSP amplitude, PPR, and CV were compared between AS-RS and RS-RS PN pairs. For RS-RS PN pairs and AS-RS PN pairs, the difference in EPSP amplitude (1.1 ± 0.6 vs 0.7 ± 0.5 mV), PPR (1.0 ± 0.2 vs 0.9 ± 0.3) and CV (0.4 ± 0.2 vs 0.5 ± 0.2) and failure rate (16.3 ± 15.4 vs 11.8 ± 10.7 %) were statistically not significant.

3.5.2. Synaptic connectivity between E-I pairs in L5 of mPFC

Because of their axonal projection pattern, nFS INs are likely to inhibit neurons (or apical tufts) located either predominately in L1 or L5/L6, rFS INs those in L5 and L6, and bFS INs almost exclusively L5 neurons. A total of 18 E-I neuron pairs (Fig. 3.22) were recorded of which 7 were AS-bFS neuron pairs, 9 were RS-rFS neuron pairs, 1 AS-nFS pair and 1 RS-bFS pair. The probability to find a connection was 8.4% for AS-bFS pairs (7 connections out of 83 pairs tested) and 10.8% for RS-rFS pairs (9 connections out of 83 pairs tested). There were some strong

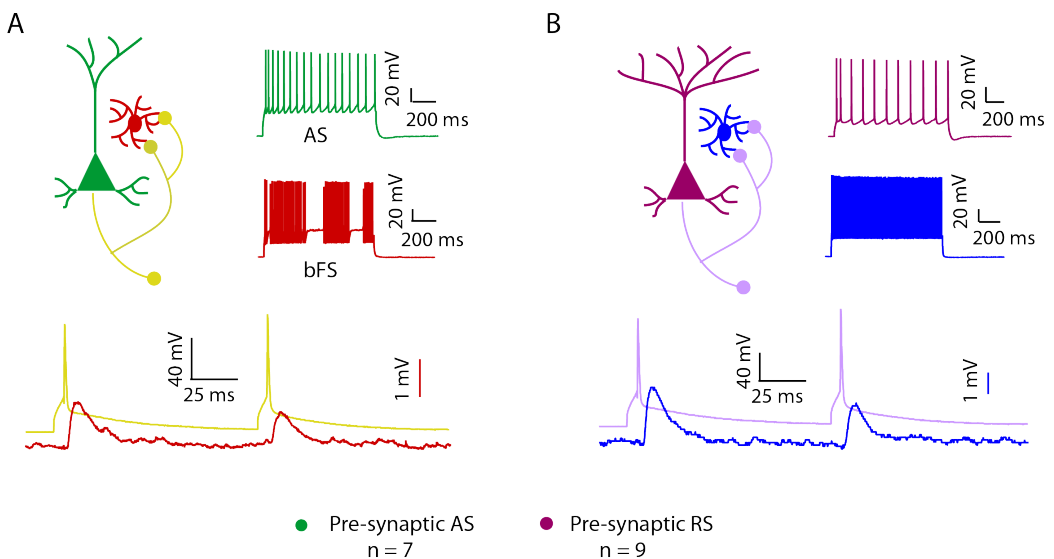


Fig. 3.22: Comparison of synaptic properties among E-I connections in L5 of mPFC. (A) Top, schematic representation and firing pattern of a synaptic connection with a presynaptic AS PN and a postsynaptic bFS IN. Below, postsynaptic EPSPs (dark red) elicited by two presynaptic APs (yellow) at a 100 ms interval. (B) Top, schematic representation and firing pattern of a synaptic connection with a presynaptic RS PN and a postsynaptic rFS IN. Below, postsynaptic EPSPs (dark blue) elicited by two presynaptic APs (violet) at a 100 ms interval. 8 E-I pairs are RS-rFS E-I connections, 6 AS-bFS E-I connections, 1 RS-bFS E-I connection, and another one AS-nFS E-I connection.

connections with a unitary EPSP amplitude >8 mV and some weak connections for which the unitary EPSP amplitude was <0.5 mV. EPSPs displayed short-term depression (PPR: ≤ 0.8). The average EPSP amplitude, PPR, and CV were compared between AS-bFS and RS-rFS pairs. For AS-bFS pairs and RS-rFS pairs the differences in EPSP amplitude (3.5 ± 3.6 vs 1.9 ± 1.5 mV), PPR (0.8 ± 0.2 vs 0.8 ± 0.04), CV (0.7 ± 0.5 vs 0.4 ± 0.2) and failure rate (10 ± 20 vs 20 ± 20 %) were not statistically significant.

3.5.3. Synaptic connectivity between I-E pairs in L5 of mPFC

A total of 8 I-E pairs (Fig. 3.23) were recorded and the probability to find a connection between bFS-AS neuron pairs was 7.2% (6 connections out of 83 pairs tested) and 2.4% between rFS-RS neuron pairs (2 connections out of 83 pairs tested). There were some strong connections with a mean unitary IPSP amplitude >1.5 mV and some weak connections with a mean unitary EPSP amplitude <0.4 mV. The postsynaptic EPSPs displayed short-term depression (PPR: ≤ 1). The average EPSP amplitude, PPR, and CV were compared between bFS-AS and rFS-RS neuron pairs

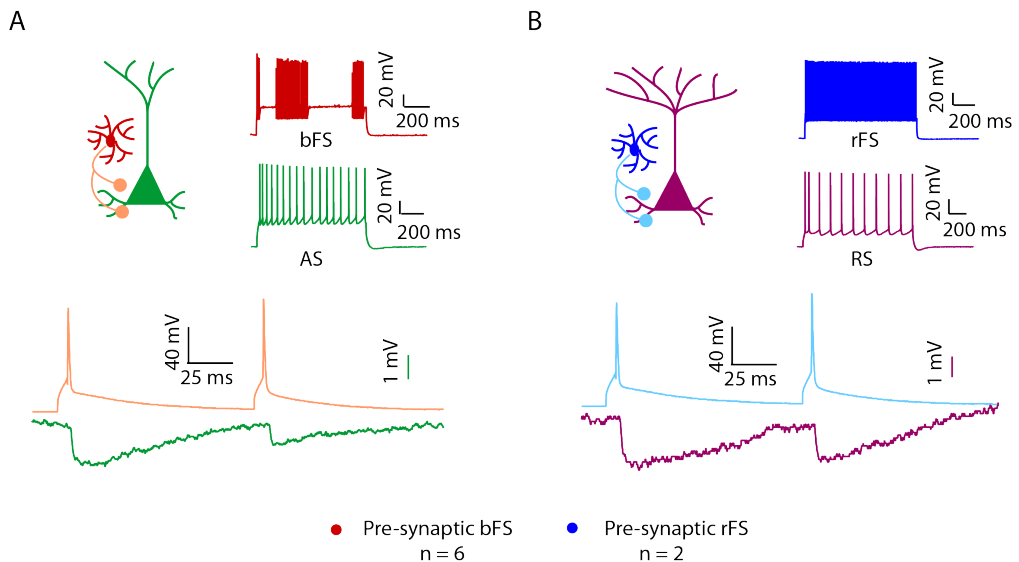


Fig. 3.23: Comparison of synaptic properties among I-E connections in L5 of mPFC. (A) Top, schematic representation and firing pattern of a synaptic connection with a presynaptic bFS IN and a postsynaptic AS PN. Bottom, postsynaptic IPSPs (dark green) elicited by two presynaptic APs (light red) at a 100 ms interval. (B) Top, schematic representation and firing pattern of a synaptic connection with a presynaptic rFS and postsynaptic RS PN. Bottom, postsynaptic EPSPs (purple) elicited by two presynaptic APs (light blue) at a 100 ms interval. 6 of these I-E pairs are bFS-AS neuron connections and two are rFS-RS neuron connections.

(Fig. 3.23). EPSP properties of different subtypes of excitatory and inhibitory connections and their statistical differences are summarized in [Table 6](#).

PSP PROPERTIES	Amplitude (mV)	PPR	Rise time (ms)	Decay time (ms)	Latency (ms)	CV	Failure rate (%)
AS-RS (n = 10)	1.1 ± 0.6	1.0 ± 0.2	1.6 ± 1.4	70.2 ± 2.4	-	0.4 ± 0.2	11.8 ± 10.7
RS-RS (n = 8)	0.7 ± 0.5	0.9 ± 0.3	1.8 ± 1.1	71.8 ± 2.5	-	0.5 ± 0.2	16.3 ± 15.4
AS-bFS (n = 6)	3.5 ± 3.6	0.8 ± 0.2	0.7 ± 0.4	67.3 ± 3.7	1.0 ± 0.4	0.7 ± 0.5	10 ± 20
RS-rFS (n = 8)	1.9 ± 1.5	0.8 ± 0.04	0.8 ± 0.3	65.7 ± 7.1	1.4 ± 1.4	0.4 ± 0.2	20 ± 20
bFS-AS (n = 6)	0.7 ± 0.5	0.8 ± 0.2	1.4 ± 0.2	64.1 ± 8.5	0.9 ± 0.2	0.5 ± 0.1	10.9 ± 13.7

Table 6: Unitary EPSP characteristics of different subtypes of L5 excitatory and inhibitory connections. The postsynaptic properties are shown as average ± SD. For pairs recorded in the ‘loose-seal’ configuration, the latency was not calculated.

3.5.4. Serotonergic suppression of E-E connections in L5 of mPFC

To understand whether 5-HT acted via pre- or postsynaptic receptors, paired recordings were made from synaptically coupled L5 neurons in mPFC. 5-HT was added to the mPFC slices via bath application for about 100-200 s. Electrophysiological and synaptic properties were measured before, during and after 5-HT application. In 7 E-E connections with a presynaptic AS PN and a postsynaptic neuron RS PN, the mean EPSP amplitude (1.1 ± 1.0 vs 0.7 ± 0.7 mV) decreased while PPR (1.1 ± 0.2 vs 1.5 ± 0.3) increased significantly following 5-HT application; no significant changes in other synaptic properties like 20-80% rise time, decay time, latency, CV and failure rate were observed. A representative 3D reconstruction and a pharmacological profile of a synaptically coupled AS-RS PN pair is shown in [Fig. 3.24](#).

3.5.5. 5-HT suppresses synaptic transmission of E-E microcircuitry in L5 of mPFC through 5-HT_{1B}Rs.

Previous studies have shown that 5-HT suppresses glutamate release from presynaptic terminals of PNs through the activation of 5-HT_{1B}Rs (Li and Bayliss 1998, Ruf and Bhagwagar 2009, Guo and Rainnie 2010, Puig and Gullledge 2011, Tian, Yamanaka et al. 2017). To test whether the 5-HT induced suppression of synaptic transmission is mediated by 5-HT_{1B}Rs, SB (5 μM, a selective 5-HT_{1B}R antagonist) was co-applied with 5-HT (10 μM) following bath application of 5-HT alone.

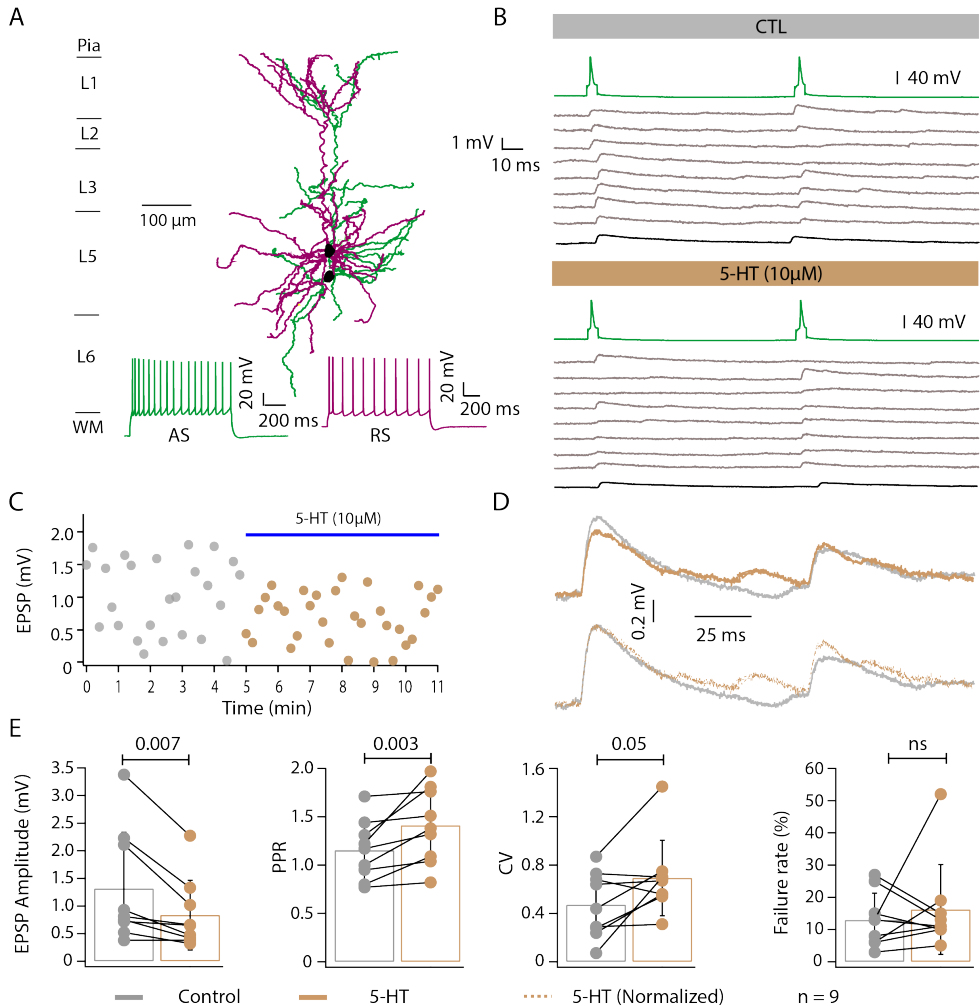


Fig. 3.24: 5-HT suppresses synaptic transmission of E-E connections in L5 of mPFC. (A-D) Example recordings from an E-E connection under control and in the presence of 5-HT (10 μ M). (A) Morphological reconstruction of the recorded AS-RS PN pair. All cell bodies are in black. Pre- and postsynaptic dendrites are shown in green and purple, respectively. Bottom, firing patterns of the pre- and postsynaptic neurons. (B) Eight consecutive EPSP doublets elicited by a train of two presynaptic APs (green) at an inter-stimulus interval of 100 ms are given in gray. The black trace at the bottom represents the average of all EPSPs. (C) Time course of the first EPSP amplitude before (gray) and during the application of 5-HT (light brown). The blue bar marks the duration of the 5-HT application. (D) Top, overlay of the average EPSP waveforms under control and during 5-HT application. Bottom, superimposed mean EPSPs in control and during 5-HT application normalized to the amplitude of the 1st EPSP in control showing the increase of the PPR. (E) Summary data (n = 9) of 5-HT induced changes in EPSP amplitude, PPR, CV and failure rate. Wilcoxon signed-rank test was used for statistical comparison between control and 5-HT effect. Absolute P-values are given above the bar graphs.

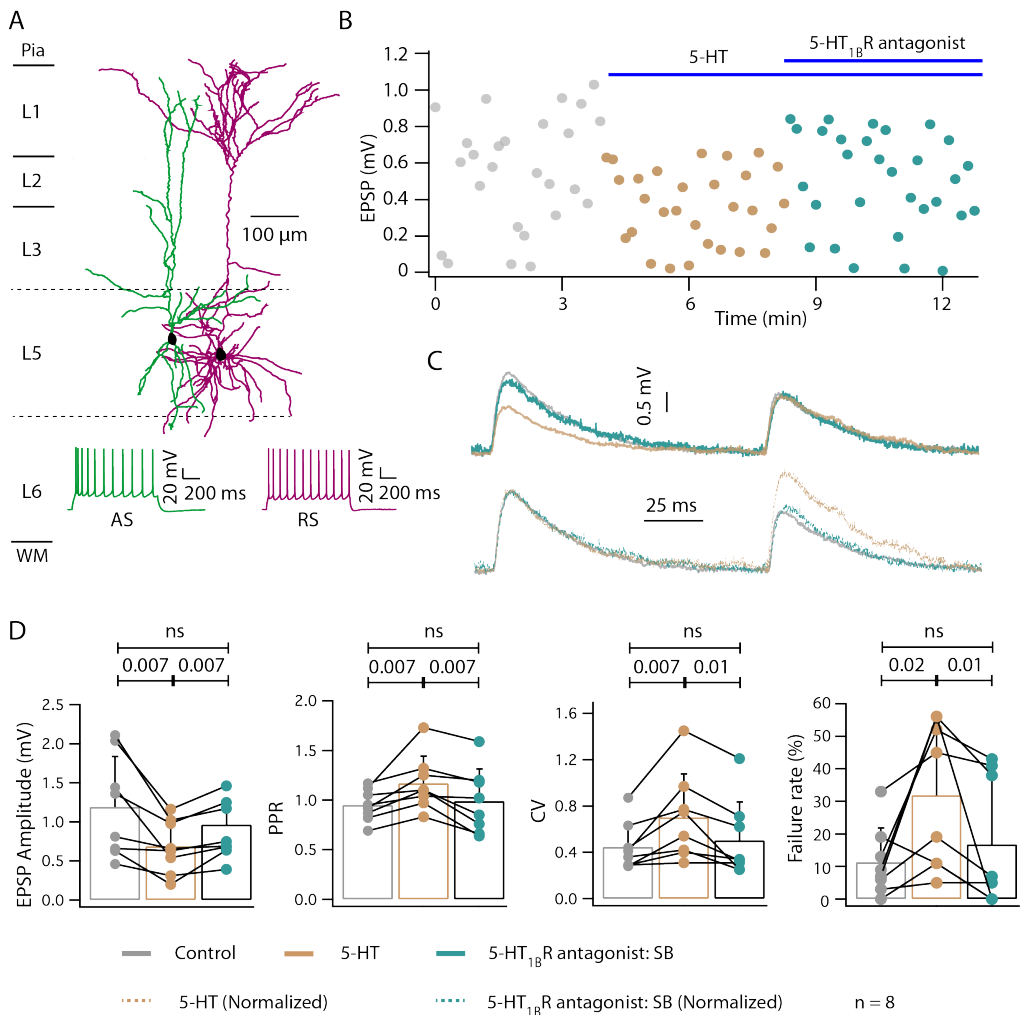


Fig. 3.25: 5-HT-induced decrease in presynaptic release probability at AS PN - RS PN pairs in L5 of mPFC. (A) Morphological reconstructions of the recorded AS-RS PN pair; color code as in Fig. 3.24; firing patterns of both neurons are depicted at the bottom of the panel. (B) Time course of the first EPSP before (gray) and during the application of 5-HT (light brown) and the 5-HT_{1B}R antagonist SB (cyan green). Blue bars indicate the duration of the drug application. (C) Top left, overlay of average EPSPs under control, 5-HT and SB application. Bottom left, overlay of mean EPSPs in control, 5-HT and in SB normalized to the amplitude of the 1st EPSP in control showing the change of PPR. (D) Summary data (n = 8) of 5-HT and SB induced changes in EPSP amplitude, PPR, CV and failure rate. Wilcoxon signed-rank test was used for statistical comparisons. Absolute P-values are given above the bar graphs.

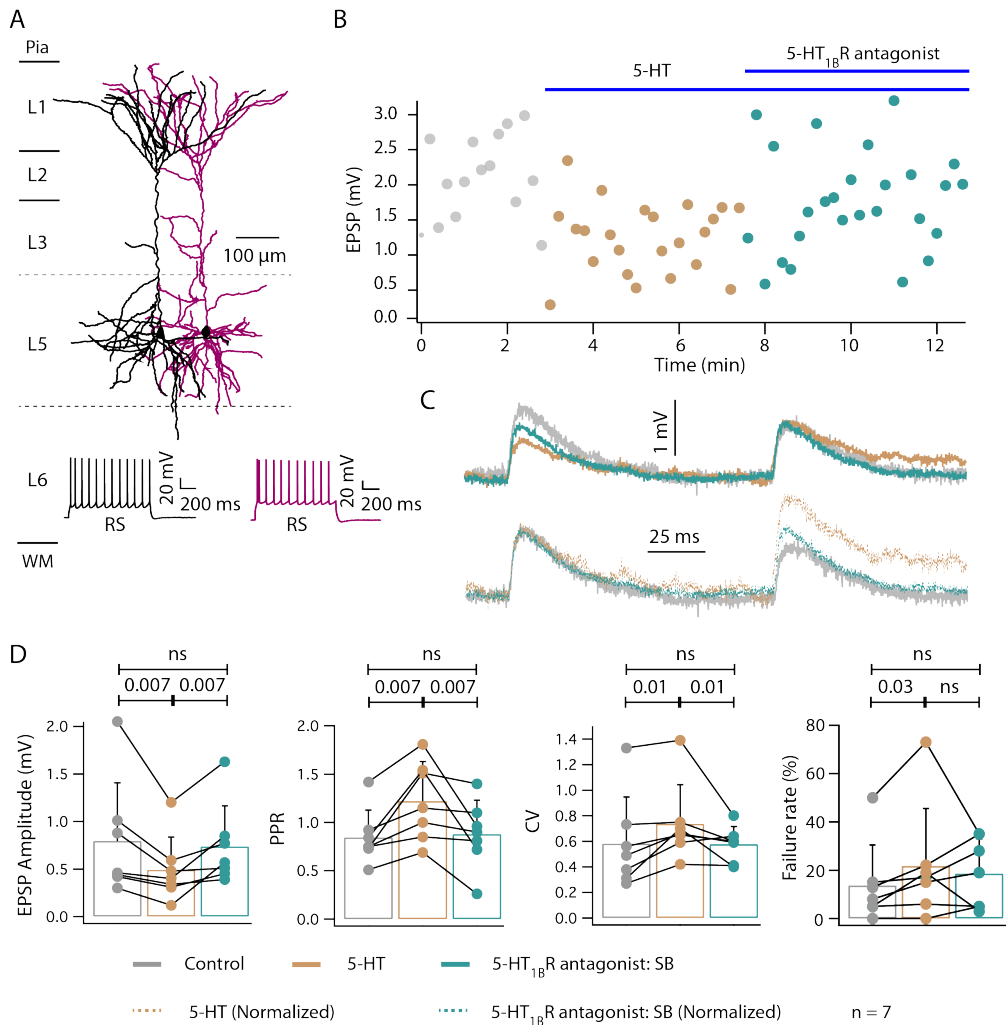


Fig. 3.26: 5-HT-induced decrease in presynaptic release probability at RS PN - RS PN pairs in L5 of mPFC. (A) Morphological reconstructions of the recorded RS-RS PN pair; all cell bodies are in black. Presynaptic and postsynaptic dendrites are shown in black and purple, respectively; Firing patterns of both neurons are given at the bottom of panel A. (B) Time course of the first EPSP amplitude before (gray) and during the application of 5-HT (light brown) and the 5-HT_{1B}R antagonist SB (bluish green). Blue bars indicate the duration of the drug application. (C) Top left, overlay of average EPSPs under control, 5-HT and SB application. Bottom left, overlay of mean EPSPs in control, 5-HT and in SB normalized to the amplitude of the 1st EPSP in control showing the change of PPR. (D) Summary data (n = 7) of 5-HT and SB induced changes in EPSP amplitude, PPR and CV. Wilcoxon signed-rank test was used for statistical comparisons. Absolute P-values are given above the bar graphs.

Application of the 5-HT_{1B}R antagonist SB (5 μM) blocked the effect of 5-HT in both AS-RS and RS-RS pairs. In the presence of 5-HT alone, the EPSP amplitude was reduced in AS-RS (1.2 ± 0.7 vs 0.8 ± 0.3 mV) and RS-RS pairs (0.7 ± 0.6 vs 0.4 ± 0.3 mV). Co-application of 5-HT and SB resulted in the recovery of the EPSP amplitude in AS-RS (0.9 ± 0.4 mV) and RS-RS (0.7 ± 0.4 mV) PN pairs. In addition, SB blocked the 5-HT effects on the PPR and CV in these synaptic connections. These results suggest that 5-HT reduces the release probability of excitatory connections (E-E) through the activation of 5-HT_{1B}Rs in presynaptic terminals of AS and RS PNs in L5 of mPFC. A representative 3D reconstruction and pharmacological profile of a synaptically coupled AS-RS pair is shown in Fig. 3.25 and an RS-RS pair is shown in Fig. 3.26. The EPSP properties of different subtypes of E-E connections and their statistical differences are summarized in Table 7.

EPSP PROPERTIES	AS-RS (n = 8)	RS-RS (n = 7)
Control		
EPSP amplitude (mV)	1.2 ± 0.7	0.7 ± 0.6
PPR	1.0 ± 0.2	0.8 ± 0.2
CV	0.3 ± 0.2	0.6 ± 0.4
Failure rate (%)	11.2 ± 10.5	13.7 ± 16.7
5-HT (10 μM)		
EPSP amplitude (mV)	0.8 ± 0.37 *0.03	0.4 ± 0.3 *0.01
PPR	1.1 ± 0.2 **0.007	1.1 ± 0.3 *0.01
CV	0.5 ± 0.2 **0.007	0.7 ± 0.3 *0.03
Failure rate (%)	31.8 ± 22.3 *0.02	21.7 ± 23.8 *0.01
5-HT_{1B}R antagonist: SB (5 μM)		
EPSP amplitude (mV)	0.9 ± 0.4 *0.01	0.7 ± 0.4 *0.01
PPR	0.9 ± 0.2 **0.007	0.8 ± 0.3 0.07
CV	0.4 ± 0.2 *0.03	0.5 ± 0.1 *0.01
Failure rate (%)	16.7 ± 20.0 *0.01	18.5 ± 14.3 1.06

Table 7: Unitary EPSP characteristics of L5 E-E connections under control, 10 μM 5-HT alone and 10 μM 5-HT + 5 μM 5-HT_{1B}R antagonist SB. The average and ± SD of various uEPSP properties for excitatory (AS-RS and RS-rFS) pairs are shown. Bold font indicates significant differences to control; *P < 0.05, **P < 0.01, ***P < 0.001 for Wilcoxon signed rank test.

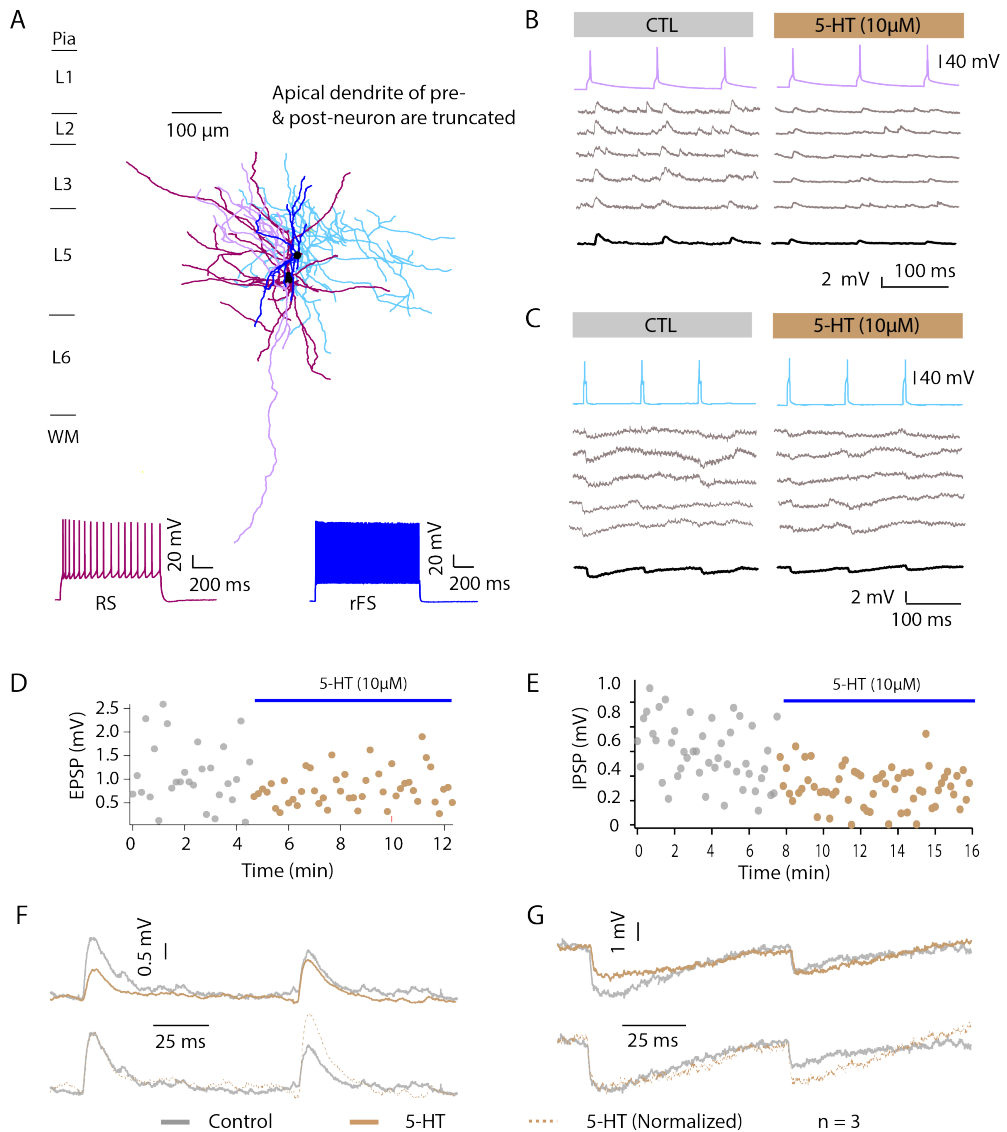


Fig. 3.27: 5-HT-induced suppression of synaptic transmission at reciprocal E-I pairs in L5 of mPFC. (A-G) Example recordings from 1 of the 3 reciprocally connected E-I/I-E pair under control and 5-HT (10 μ M) condition. (A) Morphological reconstruction of the E-I reciprocal pair. All cell bodies are in black. Dendrites and axon of the RS PN are shown in purple and violet, respectively; dendrites and axon of the rFS IN in dark blue and light blue, respectively. The firing pattern of both neurons are shown at the bottom of the panel. (B) Two EPSPs and IPSPs elicited by two consecutive APs in the RS PN (violet) and the rFS IN (light blue), respectively, are shown. Bottom black traces represent average of all PSPs. Time course of the 1st EPSP (D) and IPSP (E) amplitude before (gray) and during the 5-HT application (light brown); Blue bars indicate the duration of the 5-HT application. (F, G) Top, overlay of average EPSPs and IPSPs under control and during 5-HT application. Bottom, PSPs recorded in the presence of 5-HT are normalized to the peak PSP in control and superimposed revealing the change of PPR.

3.5.6. Serotonergic suppression in reciprocal E-I and I-E connections in L5 of mPFC

I found 3 reciprocal E-I/I-E connections of which two were RS-rFS pairs and one AS-bFS pair. A representative 3D reconstruction and a pharmacological profile of a synaptically coupled RS-rFS pair is shown in Fig. 3.27. In the presence of 5-HT, the mean unitary EPSP and IPSP amplitudes at these connections were significantly reduced (0.6 ± 0.1 vs 0.4 ± 0.1 mV) and the PPR increased (0.5 ± 0.09 vs 0.8 ± 0.05 ; Fig. 3.27, B-G). There were no significant changes in other synaptic properties. The decrease in EPSP amplitude could be due to a pre- or postsynaptic effect or a combination thereof. The increase in PPR in E-E connections suggests that 5-HT acts primarily presynaptically by reducing the neurotransmitter release probability. Because of the low sample size in E-I/I-E connections ($n = 3$), statistical comparisons were not performed.

3.5.7. 5-HT suppresses synaptic transmission of E-I microcircuitry in L5 of PFC through 5-HT_{1B}Rs.

To investigate the pure presynaptic effect of 5-HT acting via the 5-HT_{1B}R, the specific 5-HT_{1B}R agonist CGS ($5 \mu\text{M}$) was bath applied to E-I pairs with a presynaptic AS PN and postsynaptic bFS IN and in E-I pairs with a presynaptic RS PN and postsynaptic rFS IN. The 6 AS-bFS and one AS-rFS pair were pooled for analysis because they all have a presynaptic AS PN; similarly, the 6 RS-rFS and one RS-bFS neuron pair were also pooled because the presynaptic neuron was always an RS PN. The application of CGS alone significantly reduced the EPSP amplitude (1.6 ± 1.6 vs 1.0 ± 1.0 mV) and increased the PPR (1.0 ± 0.5 vs 1.7 ± 1.0) and CV (0.7 ± 0.6 vs 1.4 ± 1.8) in pairs with a presynaptic AS PN. In RS PN formed pairs, application of CGS alone reduced the EPSP amplitude (2.2 ± 3.2 vs 1.7 ± 2.7 mV) and increased the PPR (0.8 ± 0.2 vs 1.5 ± 0.8) and failure rate (0.2 ± 0.2 vs 0.3 ± 0.2). These results suggest that the suppression of synaptic transmission in E-I connections results from a reduction of the neurotransmitter release probability in presynaptic AS and presynaptic RS PNs in L5 of mPFC. This suppression is caused by the activation of presynaptic 5-HT_{1B}Rs. A representative 3D-reconstruction and a pharmacological profile of a synaptically coupled AS-bFS pair is shown in Fig. 3.28 and the RS-rFS pair is shown in Fig. 3.29. The EPSP properties of different subtypes of E-I and their statistical differences are summarized in Table 8.

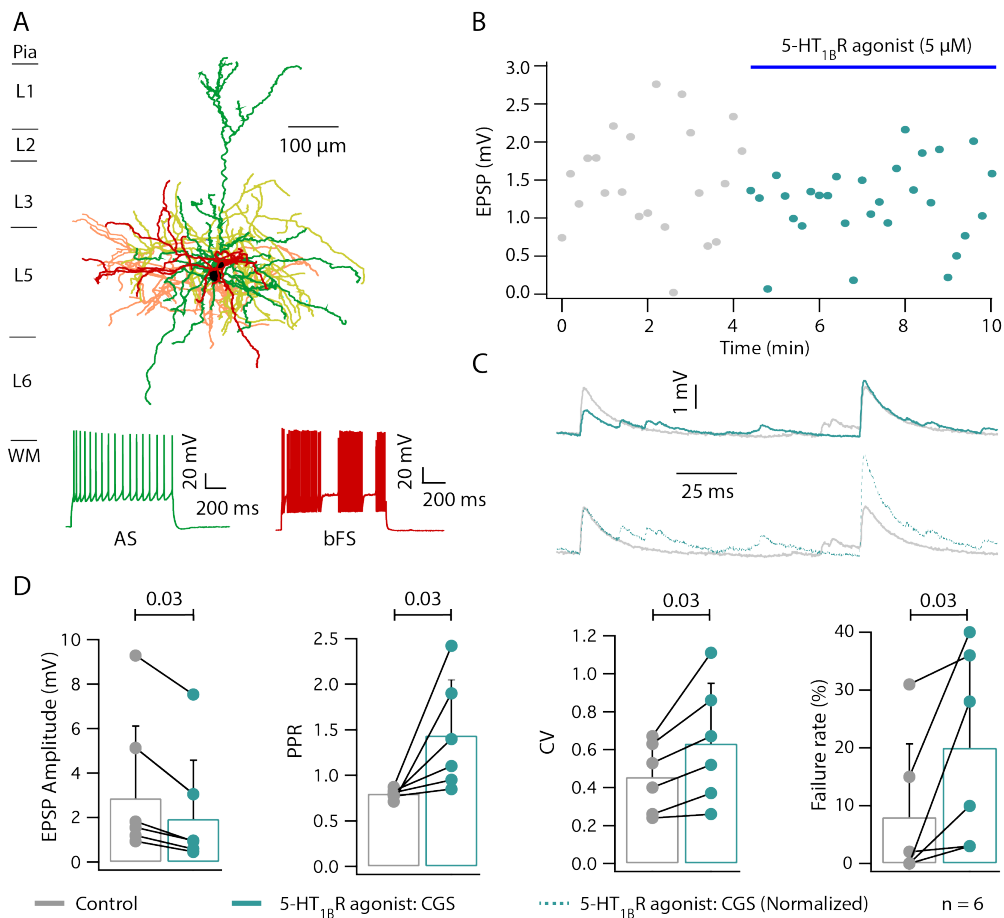


Fig. 3.28: Effect of CGS on synaptic transmission of excitatory AS PN - bFS IN synaptic connections in L5 of mPFC. (A) Morphological reconstructions of the recorded E-I pair (AS PN-bFS IN). All cell bodies are in black. Presynaptic dendrites and axon are shown in green and yellow, respectively; postsynaptic dendrites and axon are shown in dark red and light red, respectively. Firing patterns of the pre- and postsynaptic neurons are shown at the bottom of panel A. (B) Time course of the 1st EPSP before (gray) and during application of the 5-HT_{1B}R agonist CGS (5 μ M) (bluish green). The blue bar indicates the duration of the CGS application. (C) Top left, overlay of average unitary EPSPs under control and CGS application. Bottom left, EPSPs recorded in the presence of CGS are normalized to the peak EPSP in control are superimposed revealing marked changes in short-term synaptic plasticity. (D) Summary data (AS, n = 6) of CGS induced changes in EPSP amplitude, PPR, CV and failure rate. Wilcoxon signed-rank test was used for statistical comparisons. Absolute P-values are given above the bar graphs.

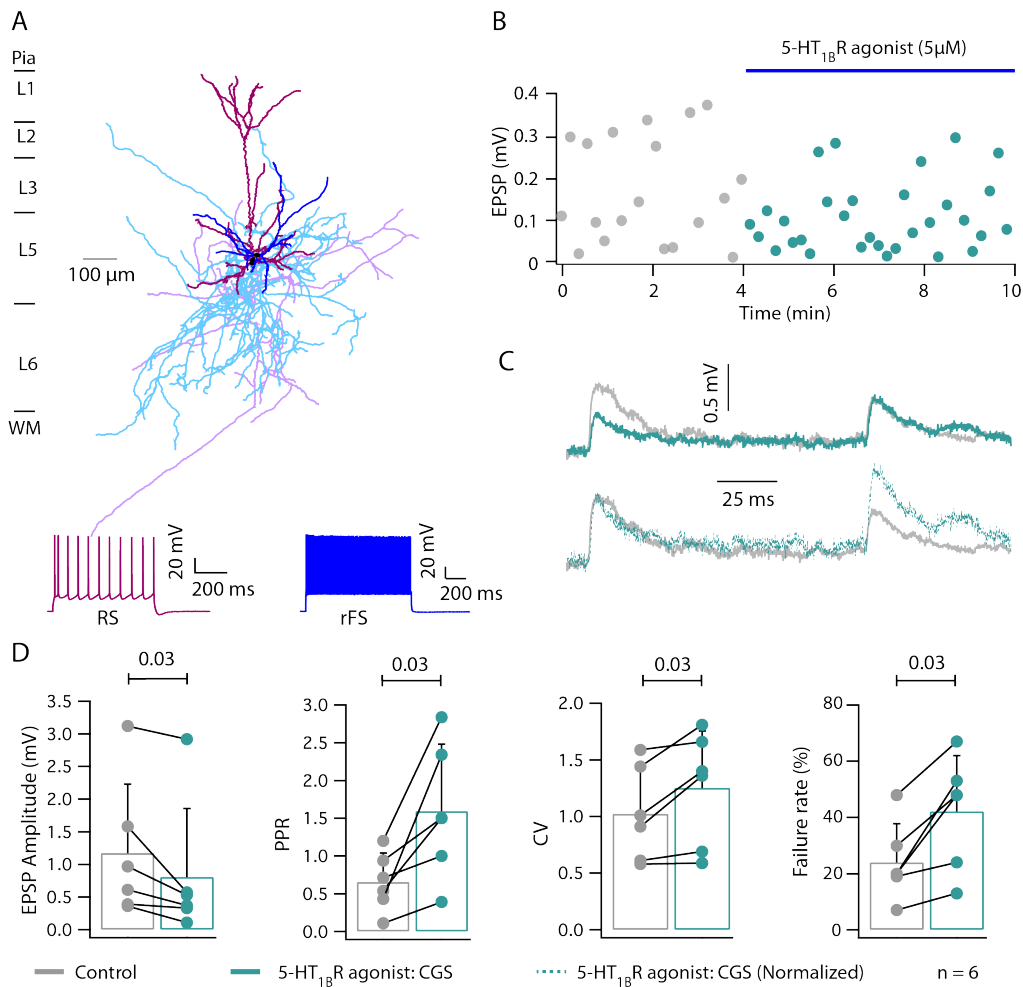


Fig. 3.29: Effect of the CGS on synaptic transmission at RS PN - rFS IN connections in L5 of mPFC. Morphological reconstructions of the recorded E-I pair (RS PN-rFS IN) (A). All cell bodies are in black. Presynaptic dendrites and axon in purple and violet, respectively. Postsynaptic dendrites and axon are shown in dark blue and light blue, respectively; the firing patterns of both neurons are shown at the bottom of the panel. (B) Time course of the 1st EPSP before (gray) and during the application of the 5-HT_{1B}R receptor agonist CGS (5 μ M) (bluish green). The blue bar indicates the duration of the CGS application. (C) Top left, overlay of average EPSPs under control conditions and in the presence of CGS application. Bottom left, EPSPs recorded in the presence of CGS are normalized to the peak EPSP in control are superimposed revealing changes in short-term synaptic plasticity. (D) Summary data (n = 6) of CGS induced changes in EPSP amplitude, PPR, CV and failure rate. Wilcoxon signed-rank test was used for statistical comparisons. Absolute P-values are given above the bar graphs.

PSP PROPERTIES	AS-bFS (n = 6)	RS-rFS (n = 6)
Control		
EPSP amplitude (mV)	2.86 ± 3.24	1.17 ± 1.05
PPR	0.79 ± 0.05	0.65 ± 0.38
CV	0.45 ± 0.18	1.02 ± 0.41
Failure rate (%)	8 ± 12	24 ± 13
5-HT_{1B}R agonist: CGS (5 μM)		
EPSP amplitude (mV)	1.93 ± 2.64 *0.03	0.8 ± 1.04 *0.03
PPR	1.43 ± 0.61 *0.03	1.59 ± 0.88 *0.03
CV	0.63 ± 0.31 *0.03	1.25 ± 0.5 *0.03
Failure rate (%)	25 ± 16 *0.03	42 ± 19 *0.01

Table 8: Unitary EPSP characteristics of L5 E-I connections under control and 5 μM 5-HT_{1B}R agonist CGS. The average and ± SD of various uEPSP properties for E-I pairs (AS-RS and RS-rFS) are shown. Bold font indicates significant differences to control; *P < 0.05, **P < 0.01, ***P < 0.001 for Wilcoxon signed rank test.

3.5.8. 5-HT facilitates synaptic transmission of the I-E microcircuitry in L5 of PFC through 5-HT_{3A}Rs.

The expression pattern of 5-HT receptor subtypes in GABAergic INs is quite diverse. INs in the cortex either express 5-HT_{1A}R or 5-HT_{2A}R or 5-HT_{3A}R. In contrast to the other 5-HT receptors, 5-HT_{3A}Rs are ligand-gated cation channels expressed on presynaptic terminals of ~30% of neocortical INs (Koyama, Matsumoto et al. 2000, Ferezou, Cauli et al. 2002). To test the presence and effect of 5-HT_{3A}R activation in I-E pairs, the 5-HT_{3A}R agonist mCPG (30 μM) was bath applied. In 6 bFS-AS pairs application of mCPG significantly increased the IPSP amplitude (0.7 ± 0.6 vs 1.1 ± 0.9 mV) and reduced the PPR (0.9 ± 0.1 vs 0.8 ± 0.1) and CV (0.5 ± 0.1 vs 0.3 ± 0.1). A representative 3D-reconstruction and pharmacological profile of a synaptically couple bFS-AS pair is shown in [Fig. 3.30](#). The IPSP properties of different subtypes of I-E connections and their statistical differences are summarized in [Table 9](#)

In summary, 5-HT through the activation of presynaptic 5-HT_{1B}Rs reduced presynaptic neurotransmitter release in L5 excitatory connection (E-E and E-I) and through the activation of presynaptic 5-HT_{3A}Rs enhanced the synaptic efficiency in L5 inhibitory connections (I-E).

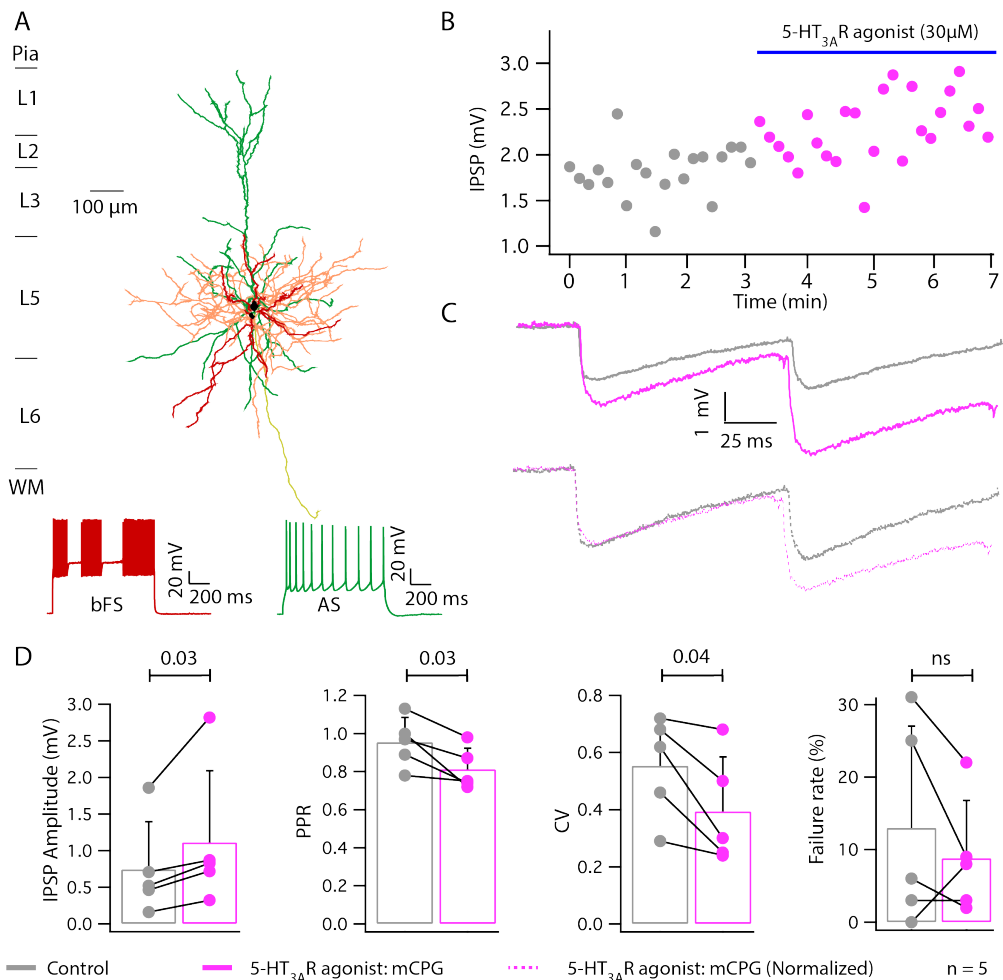


Fig. 3.30: Effect of the mCPG on synaptic transmission at bFS IN - RS PN connections in L5 of mPFC. (A) Morphological reconstruction of the recorded I-E pair (bFS IN-RS PN). All cell bodies are in black. Presynaptic dendrites and axon are shown in dark red and light red, respectively; postsynaptic dendrites and axon in green and yellow, respectively. Firing patterns of the pre- and postsynaptic neurons are depicted at the bottom of panel A. (B) Time course of the 1st IPSP before (gray) and during the application of the 5-HT_{3A}R agonist mCPG (30 μ M) (magenta). The blue bar indicates the duration of the mCPG application. (C) Top, overlay of average IPSPs under control and during mCPG application. Bottom, IPSPs recorded in the presence of mCPG are normalized to the peak IPSP in control and superimposed to determine changes in short-term synaptic plasticity. (D) Summary data (n = 5) of mCPG induced changes in IPSP amplitude, PPR, CV and failure rate. Wilcoxon signed-rank test was used for statistical comparisons. Absolute P-values are given above the bar graphs.

PSP PROPERTIES	bFS-AS (n = 5)	
	Control	5-HT _{3A} R agonist: mCPG (30 μM)
EPSP amplitude (mV)	0.7 ± 0.6	1.1 ± 0.9 *0.03
PPR	0.9 ± 0.1	0.8 ± 0.1 *0.03
CV	0.5 ± 0.1	0.3 ± 0.1 *0.03
Failure rate (%)	0.1 ± 0.1	8 ± 7

Table 9: Unitary IPSP characteristics of L5 I-E connections in control and the presence of the 5-HT_{3A}R agonist mCPG. The average and ± SD of various uIPSP properties for inhibitory (bFS-AS) pairs are shown. Bold font indicates significant differences to control; *P < 0.05, **P < 0.01, ***P < 0.001 for Wilcoxon signed rank test.

4. Discussion

4.1. Classification of PNs in L5 of mPFC

PNs in L5 of mPFC integrate input from several brain regions and distribute its output to cortical and subcortical regions. Several studies have classified PFC L5 PNs into two main groups (Dembrow, Chitwood et al. 2010, Kawaguchi 2017, Baker, Kalmbach et al. 2018, Collins, Anastasiades et al. 2018). Here, two types of PNs were identified in L5 of PFC. One group comprises PNs projecting within the telencephalic region including the cerebral cortex, the limbic forebrain structures and the basal ganglia (commissural or callosal/cortico-cortical/IT neurons). To the second group belong PNs projecting out of the telencephalic region (corticopontine/long-range corticofugal/PT/ET neurons).

A previous study (Degenetais, Thierry et al. 2002) classified PNs in the mPFC based on the intrinsic properties, while another study (Wang, Markram et al. 2006) used morphological features to classify L5 PNs in mPFC. In the present work, both intrinsic and morphological properties were used to distinguish and better understand distinct PN groups in L5 of mPFC. Initially, PNs were classified into two groups based on the adaptation ratio of the AP firing patterns evoked in response to depolarizing current pulses. Later, the morphology of these two PN groups were correlated with the firing patterns. PNs whose adaptation ratio was less than 0.8 were categorized as AS type while those with an adaptation ratio greater than 0.8 were categorized as RS PNs. AS and RS PNs are two distinct groups of L5 excitatory neurons in mPFC that differ in intrinsic electrophysiological properties and morphological features. In addition to adaptation ratio, RMP, R_{in} , τ_{Mem} , rheobase, AP amplitude and half-width were significantly different between AS and RS type PNs. The unique intrinsic electrophysiological properties across different neuronal populations are due to a differential expression of ion channels. Voltage-insensitive leak potassium (K^+) channels (K_{leak}) are involved in the regulation of neuronal excitability and thus determine the RMP and R_{in} . Activation of K_{leak} channels results in hyperpolarization of the RMP, suppression of AP firing and neuronal transmission. Therefore, neurotransmitters like 5-HT that act via G-proteins mainly inhibit K_{leak} channels (e.g., TREK 1) that would result in the induction of membrane depolarization and an increase in AP discharge (Lesage F 2003). In addition to K_{leak} channels, neuronal excitability is also controlled by voltage-dependent ion channels. Since K^+ ions are highly membrane-permeant, the typical RMP of neurons is close to the K^+ equilibrium potential.

The RMP in PNs, as well as INs, is mainly maintained by the dynamic equilibrium between Na⁺ channels (Na_vX (voltage-gated): leads to membrane depolarization), K⁺ channels (K_vX, K_{leak} and K_{ir2}: leads to membrane repolarization) and hyperpolarization-activated cyclic nucleotide-gated (HCN) channels (Day, Carr et al. 2005, Hu and Bean 2018). In L5 of the neocortex, AP initiation and propagation require the critical involvement of Na⁺ (Na_v1.1, Na_v1.2, Na_v1.3 and Na_v1.6) and K⁺ (K_v1, K_v2, K_v3 and K_v4) conductances. PNs were depolarized by the activation/deactivation of Na_v1.2, Na_v1.3 and Na_v1.6 channels (Tai, Abe et al. 2014, Frederiksen, Lu et al. 2017). The firing pattern in PNs was specifically regulated by the expression of fast-inactivating transient and slow-inactivating persistent Na_v channels (Vervaeke, Hu et al. 2006, Ramaswamy and Markram 2015, Shvartsman, Kotler et al. 2021). On the other hand, repolarization of PNs were dependent primarily on K_v4 channels. Further K_v1 mediated repolarization was specifically observed in AS PNs but not in RS PNs (Pathak, Guan et al. 2016). HCN channels are voltage-gated ion channels that were permeable to both Na⁺ and K⁺ ions. HCN channels were active at voltages near RMP, and their activation leads to depolarization of membrane and initiation of AP, thus influencing the neuronal excitability, synaptic integrity and neurotransmitter release by regulating the RMP and R_{in} (Benarroch 2013, Shah 2014). The ion conduction through the HCN channel is termed I_h-current. The differences in various intrinsic properties like V_{sag} and firing frequency between AS and RS PNs were mediated by the differences in I_h-current mechanisms involving different HCN isoforms (Dembrow, Chitwood et al. 2010). HCN1 and HCN2 isoforms were shown to be predominately expressed in L5 PNs of mPFC (Dembrow, Chitwood et al. 2010, Kase and Imoto 2012). In addition to Na⁺ and K⁺ conductances, Ca²⁺ currents especially through voltage-gated Ca²⁺ channels (Ca_v) mediate various physiological events like regulation of neurotransmitter release and synaptic neurotransmission, thus regulating the excitability of neurons (Catterall 2011). Ca_v channels in CNS are primarily of two types. Low voltage activated (T- and R-type) and high voltage activated (L-, N- and P/Q-type). The soma of PNs in L5 of mPFC express 5 types of Ca_v channels (R-, L-, N- and P/Q-type) (Almog and Korngreen 2009). Further, Ca²⁺ activated K_{ca} channels are unique channels that can sense intracellular Ca²⁺ signals to changes in membrane potential. There are three subtypes in K_{ca} channels: small conductance (SK, [4-14 pS), intermediate conductance (IK, [32-39 pS) and big conductance (BK, [200-300 pS) channels. SK channels are primarily expressed in CNS and their functional role is not well studied. In dendritic spines of PNs in hippocampus and amygdala, SK channels regulate the amplitude of EPSPs and blocking of these channels enhanced LTP (Kshatri, Gonzalez-Hernandez et al. 2018). Further, Cl⁻ ions play a crucial role in regulating the membrane

excitability of PNs. Under normal physiological conditions, the GABA released from INs activate GABA_A receptors present on PNs resulting in Cl⁻ influx causing hyperpolarization until the Cl⁻ equilibrium is reached which is around -70 mV. Increased intracellular Cl⁻ levels shifts Cl⁻ flow in opposite direction, thus depolarizing the neuron. Therefore Cl⁻ homeostasis helps in stabilizing the membrane potential of the neurons in cortex and other brain areas (Martina, Royer et al. 2001, Glickfeld, Roberts et al. 2009, Sorensen, Ledri et al. 2017).

A comparison of morphological characteristics such as soma size, the pattern of apical dendrite and axonal projections revealed that the AS PNs and RS PNs were distinct in their morphological features. The PNs classification in the present study is partly consistent with previously published classification schemes in L5 of mPFC (Dembrow, Chitwood et al. 2010, van Aerde and Feldmeyer 2015, Elliott, Tanaka et al. 2018) and other cortical regions (Harris and Shepherd 2015, Kawaguchi 2017, Baker, Kalmbach et al. 2018, Anastasiades and Carter 2021). For instance, PNs in the secondary motor cortex were divided into corticostriatal (CS) cells that project to the ipsi- and contralateral striatum and corticopontine (CPN) cells that project to the ipsilateral striatum and pontine nuclei (Kawaguchi 2017). Baker and coworkers subdivided neocortical PNs into IT PNs whose axons are confined to the telencephalon and ET PNs whose axons project to other regions of the brain (Baker, Kalmbach et al. 2018). In other studies (Harris and Shepherd 2015, Anastasiades and Carter 2021), PNs across the entire neocortex were basically divided into two subgroups: IT and PT PNs. In L5 of the mPFC, IT PNs project to other cortical areas, the striatum, the amygdala or the claustrum while PT PNs target diverse subcortical regions including the thalamus, pons and the ipsilateral striatum. In the current study, based on the apical dendrite morphology and the firing pattern, CS/IT PNs correspond to AS PNs while CPN/ET/PT cells correspond to RS PNs. Although PNs across different cortical regions share common features such as firing pattern or morphology, mPFC L5 PNs have unique properties such as projection specificity or synaptic connectivity. Therefore, a deeper insight into these properties is necessary to understand cortical activity and functions.

4.2 Classification of INs in L5 of mPFC

INs are very heterogeneous but play a critical role in regulating intracortical signaling and cortical output. Many studies have classified INs in the PFC based on electrophysiological, morphological

and molecular, developmental and connectivity properties (Xiang and Prince 2003, Naka and Adesnik 2016, Chistiakova, Ilin et al. 2019, Mihaljevic, Benavides-Piccione et al. 2019, Mazuir, Fricker et al. 2021). In L5 of the neocortex, PV+ INs are the most abundant IN class and have an rFS firing pattern. The next abundant IN type in L5 are STT+ INs of which some target apical dendritic tufts of PNs (Yavorska and Wehr 2016). The most abundant STT+ IN is the Martinotti cell which has a nFS firing pattern (McGarry, Packer et al. 2010). Both FS PV+ INs and nFS SST+ Martinotti cells were depolarized by the activation/deactivation of a single subtype of Nav1.1 channels while the repolarization was dependent on K_v3 (K_v3.1 or/and K_v3.2) channels (Tai, Abe et al. 2014, Frederiksen, Lu et al. 2017). FS phenotype is predominately attributed to K_v3.1 channel kinetics. The absence of K_v3.1 and expression of K_v3.2 alone in SST+ INs resulted in nFS phenotype (Chow, Erisir et al. 1999). Another type of ion channel that mediated FS phenotype was HCN and K_{leak} channels. PNs showed significantly slower I_h-current kinetics than L5 INs in mPFC and this difference is thought to be mediated by different HCN isoforms (Yang, Li et al. 2018). Although I_h-current via HCN6 isoform was shown to be predominately mediated in PV+ INs in the hippocampus (Hughes, Boyle et al. 2013), further studies are required to identify specific HCN isoforms in INs in the cortex. The expression of K_{leak} channels TWIK1 and TASK1 in FS INs contributed to lowered R_{in} compared to nFS INs (Okaty, Miller et al. 2009).

In the neocortex, most L5 PV+ INs are either basket cells or chandelier cells (Zhu, Stornetta et al. 2004). Axons of basket cells target the somatodendritic compartment of PNs while axons of chandelier cells target the axon initial segment of PNs (Woodruff, Anderson et al. 2010, Tai, Gallo et al. 2019). The axon of L5 Martinotti cells project to superficial layers and form a dense axonal plexus in L1 where they innervate the apical dendritic tufts of L5 PNs. This vertically projecting, L1-targeting axon is a typical feature of Martinotti cells which were described previously in L5 and other cortical layers (Wang, Toledo-Rodriguez et al. 2004, Ascoli, Alonso-Nanclares et al. 2008, Nigro, Hashikawa-Yamasaki et al. 2018, Gouwens, Sorensen et al. 2019, Gouwens, Sorensen et al. 2020, Zhou, Mansori et al. 2020). Another type of STT+ INs in L5 are the one with characteristic stuttering or quasi-like firing pattern (Ma, Hu et al. 2006, Stiefel, Englitz et al. 2013). The axons of these INs target L4 of the neocortex rather than L1. VIP+ INs have a bipolar appearance; in L5, VIP+ INs were short and their axon projects to L5 upper and lower borders; Very little is known about various IN types in L5 of mPFC. Therefore the current study focused on investigating the heterogeneity of INs in L5 of mPFC with respect to electrophysiology and morphology. INs were

classified into two major groups based on the adaptation ratio of the AP firing patterns evoked in response to hyperpolarizing and depolarizing current pulses. INs whose adaptation ratio was less than 0.8 were broadly categorized as nFS type while those with an adaptation ratio greater than 0.8 were categorized as FS INs. Based on the firing frequency, FS INs were classified into two subgroups: rFS and bFS. Here, the L5 INs were shown to innervate neurons not only in their home layer but also in other cortical layers. There were 12 nFS INs, of which 8 were reconstructed; the remainder was excluded from the analysis because of extreme truncation of the axon. In my experiments, 4 L1 inhibitors (~13%) were identified in a sample of 30 nFS INs, a percentage similar (10%) to that of Martinotti cells in L5 of mouse barrel cortex (Nigro, Hashikawa-Yamasaki et al. 2018). In addition to nFS L1 inhibitors, there were nFS INs that innervated L5 and L6, referred to as nFS L5/L6 inhibitors. nFS L5/L6 inhibitors were described in mouse visual cortex as LAMP5+ and/or as SNCG+ INs (Gouwens, Sorensen et al. 2019, Gouwens, Sorensen et al. 2020). In our experiments, 4 L5/L6 inhibitors (13%) were found among 30 nFS INs. Major truncations of the axon were observed (neurons whose axon was severely truncated were excluded from the analysis) in many nFS INs. Another IN type that innervated L5 and L6 were rFS INs also referred to as rFS L5/L6 inhibitors. rFS L5/L6 inhibitors could be large basket cells which are PV+ INs as described in Gouwens et al 2020. There were 43 rFS INs, of which 18 were reconstructed and the remainder excluded from the analysis because of extreme axon truncation. bFS IN whose axon specifically innervated a large area in L5 were referred to as L5 inhibitors. bFS L5 inhibitors could be small baskets cells that were PV+ INs (Gouwens, Sorensen et al. 2020). However, only immunohistochemical staining helps in determining the precise expression of the molecular markers in INs. There were 23 bFS INs, of which 10 were reconstructed and the rest were not included in the analysis because of extreme truncation of the axon. The two major groups of PNs and the three major groups of INs in L5 of mPFC were plotted in 3D space revealing a clear separation of these groups.

In the current study, the classification of INs in L5 of mPFC was in line with previous studies in the barrel cortex and other cortical regions (Ma, Hu et al. 2006, Bartolini, Ciceri et al. 2013, Naka and Adesnik 2016, Zeng and Sanes 2017, Chistiakova, Ilin et al. 2019, Gouwens, Sorensen et al. 2020). Of the five subtypes of INs described in Gouwens et al. (2020), the two main subtypes of PV+ INs were FS basket cells and FS chandelier cells (Fish, Hoftman et al. 2013, Hu, Gan et al. 2014, Miyamae, Chen et al. 2017, Ferguson and Gao 2018). In the current study, based on the firing

pattern and the morphology of rFS INs, these INs could be identified as either large or small basket cells that showed occasionally a translaminal projection pattern. Intrinsic burst spiking or adapting nFS INs include SST+ Martinotti cells or VIP+ bipolar or double-bouquet cells. SST+ Martinotti cells were another subtype of INs with an nFS firing pattern. Some of the L5 nFS INs in the current study resemble STT+ Martinotti cells because they show an axonal projection towards L1 and the pial surface. Furthermore, in order to correlate IN firing patterns with specific molecular markers, immunostaining of these INs especially with PV and STT is helpful and important, and this needs to be done in future work. For instance, in transgenic mice named X98, STT+ INs were specifically labeled with a green fluorescent protein (GFP) in the barrel cortex (Ma, Hu et al. 2006, Sabo and Sceniak 2006). Comparing the morphology and firing pattern of SST+ INs in these transgenic mice, GFP+ INs in the lower part of L5 and L6 in X98 mice correspond to some of the L1-targeting nFS Martinotti cells identified here. In addition to L1-targeting nFS INs, there are also some nFS non-Martinotti cells in L5 of mPFC whose axonal arbor was projected to L5/L6. Some groups (Gelman and Marin 2010, Bartolini, Ciceri et al. 2013) have classified INs based on their developmental origins in the embryonic subpallium (preoptic area, medial (MGE) and caudal (CGE) ganglionic eminences). Most PV+ and SST+ INs originate from the MGE and the remainder such as VIP+, and NYP+ INs originate from the CGE. A small and diverse set of PV+, SST+ and NPY+ INs originates in the preoptic area. However, according to the recent classification of INs (Scala, Kobak et al. 2021), all PV+ and SST+ INs originate from the MGE while all VIP+, SNCG+ and LAMP+ INs originate from the CGE.

4.3. Serotonergic effect in L5 neurons in mPFC

4.3.1. Serotonergic effect in L5 PNs in mPFC

5-HT_{1A}Rs and 5-HT_{2A}Rs are localized on the somatodendritic compartment of PNs, whereas 5-HT_{1B}Rs are located on presynaptic axon terminals of PNs (Celada, Puig et al. 2004, Guiard and Di Giovanni 2015, Yohn, Gergues et al. 2017). Activation of 5-HT_{1A}Rs or 5-HT_{1B}Rs results in a hyperpolarization of PNs while that of 5-HT_{2A}Rs causes a depolarization (Puig and Gullledge 2011, Celada, Puig et al. 2013). In rat association cortex, bath application of 5-HT to PNs induced one type of response in one subset of PNs and another response in another subset of PNs. The first response is membrane hyperpolarization, which was blocked by the 5-HT_{1A}R antagonists BMY 7378 and piperone but not by the 5-HT_{2A}R antagonist ketanserin. The second response is membrane

depolarization in conjunction with rapid AP firing; this effect was reversed by the 5-HT_{2A}R antagonist ketanserin (Araneda and Andrade 1991). In later studies in which two types of PNs were distinguished, 5-HT evoked a monophasic excitatory response (enhanced AP firing) or biphasic response (inhibition of firing followed by enhanced AP firing) via activation of 5-HT_{2A}R receptors in AS PNs and an inhibitory response via activation of 5-HT_{1A}Rs in RS PNs in mouse mPFC (Avesar and Gullledge 2012). In rats, the 5-HT effect is opposite to that observed in mice. Activation of 5-HT_{2A}Rs in RS PNs results in an excitatory response (inward current) while the activation of 5-HT_{1A}Rs in AS PNs results in an inhibitory response (outward current). These effects were blocked by their respective antagonists and suggest that 5-HT exerts its effects in a PN type-specific manner (Elliott, Tanaka et al. 2018). These findings are partly in accordance with my findings. Here, bath application of 5-HT to RS PNs induced depolarization of the RMP, while in the majority of AS PNs (66.7%), 5-HT induced a depolarization while a subset of AS PNs (33.3%) showed a hyperpolarization. When electrophysiological properties between the two populations of AS PNs were compared, depolarizing AS PNs showed a larger R_{in} , τ_{Mem} , AP half-width and smaller rheobase current in comparison to hyperpolarizing AS PNs. In a previous study, an unsupervised cluster analysis combining morphological and electrophysiological properties has classified PNs in L5 of mPFC into three groups (van Aerde and Feldmeyer 2015): SI-tufted AS PNs with high R_{in} , SI-tufted AS PNs with low R_{in} and Bd-tufted RS PNs. The two subgroups of AS PNs in the current study correspond to the previously described high R_{in} AS PNs and low R_{in} AS PNs. In our recordings, high R_{in} AS PNs showed a depolarization of the RMP while low R_{in} AS PNs showed a hyperpolarization upon 5-HT application. The third group of PNs from van Aerde et al., 2015 corresponds to the broad-tufted RS PNs that showed a depolarization of RMP upon 5-HT application.

It has been suggested that 80% of neurons expressing 5-HT_{1A}Rs also co-express 5-HT_{2A}Rs in almost all PFC regions (Martin-Ruiz, Puig et al. 2001, Amargos-Bosch, Bortolozzi et al. 2004, Santana, Bortolozzi et al. 2004, Puig and Gullledge 2011, Celada, Puig et al. 2013, Carhart-Harris and Nutt 2017). Despite this abundant co-expression, it is not well understood why a subset of AS PNs shows a hyperpolarization following 5-HT application. In addition, the hyperpolarizing subset of AS PNs showed receptor desensitization which is thought to result from the over-activation of 5-HT_{1A}Rs as seen in the case of 5-HT_{1A} auto-receptors (Hervas, Vilaro et al. 2001, Yohn, Gergues et al. 2017, Turcotte-Cardin, Vahid-Ansari et al. 2019). Occasionally, desensitization was observed in

some of the depolarizing AS PNs and RS PNs and this is thought to be mediated by the hypersensitivity of 5-HT_{2A}Rs (Yamauchi, Miyara et al. 2006). Although both the inhibitory 5-HT_{1A}Rs and the excitatory 5-HT_{2A}Rs are co-expressed in individual PNs, the application of 5-HT induced a net depolarization of the RMP. The most convincing mechanism for this may be a differential distribution of the 5-HT_{2A}Rs with 5-HT_{2A}Rs being localized on the soma, proximal apical and basal dendritic compartments and 5-HT_{1A}Rs on the axon initial segment of PNs (Cruz, Eggan et al. 2004). Therefore, activation of 5-HT_{2A}Rs on the soma and apical dendritic compartments of a PN induced depolarization of RMP while activation of 5-HT_{1A}Rs on the axon initial segment of the PNs would modulate the initial generation of AP. Several studies support the idea of a differential compartmental localization of the two 5-HT receptor subtypes in mPFC PNs which would result in independent mechanisms regulating the excitability of different PN types (Jansson, Tinner et al. 2001, Martin-Ruiz, Puig et al. 2001, Czyrak, Mackowiak et al. 2003, Celada, Puig et al. 2013). The 5-HT mediated excitatory responses involve the activation of 5-HT_{2A}Rs leading to the coupling of G_q associated G-protein α subunits thus resulting in a suppression of potassium (K_{V7}) channels. Suppression of K_{V7} channels results in a depolarization of L5 PNs. In addition to the suppression of K_{V7} channels, 5-HT_{2A}Rs engage multiple ionic effectors (Ca²⁺-dependent and independent non-specific cation channels) to enhance the intrinsic excitability of PNs (Puig and Gullledge 2011, Stephens, Baker et al. 2018). 5-HT regulates membrane excitability of neurons via several ion channels. In spinal motoneurons, 5-HT inhibits K_{leak} channels (TASK 1) through either 5-HT_{1A/2A}Rs, and activates GIRK channels through 5-HT_{1A}Rs (Perrier, Rasmussen et al. 2013). In addition, 5-HT enhanced I_h current through 5-HT_{2A}Rs in spinal motoneurons (Hsiao, Trueblood et al. 1997) and reduced I_h current in axon initial segment through 5-HT_{1A}Rs in auditory brain stem nuclei (Ko, Rasband et al. 2016). 5-HT via 5-HT_{1A}Rs inhibited N- and P/Q-type Ca²⁺ currents in neocortical PNs (Foehring 1996) and serotonergic neurons in caudal raphae nucleus (Bayliss, Li et al. 1997). 5-HT via 5-HT_{2C}Rs inhibited T-type Ca²⁺ currents in PNs of subiculum hippocampus (Petersen, Jensen et al. 2017). In L5 PNs of mPFC, 5-HT inhibited P-type Ca²⁺ channels which had thus inhibited K_{v1.2} conductance resulting in enhanced glutamate release and excitation (Lambe and Aghajanian 2001). However, studies are required to identify the ion channels regulated by 5-HT in mPFC and other cortical areas.

4.3.2. Serotonergic effect on SK channels in L5 PNs in mPFC

In a recent study (Roshchin, Ierusalimsky et al. 2020), it has been demonstrated that L5 PNs can be distinguished by two genetic markers that are differentially expressed in AS and RS PNs: the transcription factor ER81/*etv1* was exclusively expressed in AS PNs while glycosyltransferase-25 (GT) was only found in RS PNs. Although both types of PNs express SK channels (Gulledge, Park et al. 2007, Faber 2010, Yi, Ling et al. 2015, Elliott, Tanaka et al. 2018), ER81-expressing AS PNs had a larger AHP amplitude following an AP than GT-expressing RS PNs. Therefore, ER81-expressing AS PNs were referred to as slow-after-hyperpolarizing (sAHP) PNs. This sAHP following an AP was shown to be mediated by an ‘intermediate-conductance’ type of K^+ channels ($K_{Ca3.1}$) but not by SK channels. GT-expressing RS PNs were referred to as non-sAHP PNs which do not possess $K_{Ca3.1}$ channels. In L5 PNs, SK channels were predominantly expressed in RS PNs than AS PNs (Guan, Armstrong et al. 2015) and therefore mediate a medium after-hyperpolarization (mAHP) after an AP in RS PNs but not the sAHP (Villalobos, Shakkottai et al. 2004).

In the present study, a transient hyperpolarization of RMP in RS PNs was observed upon 5-HT application which was hypothesized to be due to the activation of SK channels. In the CNS, three subtypes (SK1($K_{Ca2.1}$), SK2($K_{Ca2.2}$) and SK3 ($K_{Ca2.3}$)) of SK channels are present; the bee venom toxin apamin blocks all three of these SK channels (Vogalis, Storm et al. 2003). In order to test for the presence of SK channels, apamin was applied together with 5-HT. This prevented the occurrence of the transient hyperpolarization so that in RS PNs 5-HT application produced only a monophasic depolarization. In line with our findings, the apamin inhibition of the mAHP was specific for RS PNs indicating the expression of apamin-sensitive $K_{Ca2.x}$ SK channels in RS PNs (Elliott, Tanaka et al. 2018). In the same study, apamin insensitivity was observed in AS PNs indicating the absence of the $K_{Ca2.x}$ SK channels in this sub-group of PNs.

It has been shown that 5-HT modulates SK channels (expressed in *Xenopus laevis* oocytes) and that activation of 5-HT_{1A}Rs (in slices from the lumbar region of the spinal cord from adult turtle) by its agonist (8-OH-DPAT) consistently inhibited SK channels responsible for the mAHP current after an AP (Grunnet, Jespersen et al. 2004). This was the first demonstration that metabotropic 5-HT_{1A}Rs regulate SK channels. However, the underlying signaling pathway involved remains to be identified. Later, 5-HT was found to increase the excitability and AP firing frequency (Deemyad,

Maler et al. 2011, Perrier, Rasmussen et al. 2013). This phenomenon was shown to be mediated by inhibition of SK channels responsible for mAHP currents. 5-HT plays a major role in regulating anxiety and depression-like behaviors. In socially isolated mice, inhibition of SK channels through acute systemic administration of apamin these behaviors are normalized suggesting a role of 5-HT_{1A}Rs in these disorders (Sargin, Oliver et al. 2016).

Here, the extent of the 5-HT-induced depolarization of the RMP was higher in AS than in RS PNs. In addition to a smaller depolarization, RS PNs displayed a biphasic response in which an initial transient hyperpolarization of the RMP was followed by sustained depolarization. It has been shown previously that acetylcholine induced a similar biphasic responses in both types of L5 PNs of mouse mPFC and that the initial inhibition of AP firing was eliminated by the SK channel blocker, apamin (Gulledge and Stuart 2005, Baker, Kalmbach et al. 2018). Similarly, in the current study, apamin blocked the initial transient hyperpolarization in RS PNs but did not alter the 5-HT induced depolarization. Although both types of PNs express SK channels, the ‘intermediate conductance’ Ca²⁺-activated K_{Ca}3.1 channels are predominant in AS PNs as shown in a recent study (Roshchin, Ierusalimsky et al. 2020), while Ca²⁺-activated SK channels are predominant in RS PNs in accordance with our study. Therefore, our results suggest that preferential serotonergic excitation is projection-specific and depends on the intrinsic differences between AS PNs and RS PNs in L5 of rat mPFC. However, further studies are needed to determine the role of the 5-HT_{1A}R-mediated activation of SK channels in regulating the initial transient hyperpolarization.

4.3.3. Serotonergic effect in L5 INs in mPFC

In *in vitro* studies, 5-HT application resulted in the excitation of most neocortical PNs. However, in *in vivo* studies, 5-HT generally inhibited these PNs. This discrepancy is due to the predominant activation of 5-HT_{2A}Rs in GABAergic INs which establish monosynaptic inhibitory connections with PNs (Zhou and Hablitz 1999). These findings indicate that the cortical output is dependent on the IN microcircuitry and the balance between cortical excitation and inhibition. INs express either of the three G-protein coupled 5-HT receptors (5-HT_{1A}R, 5-HT_{1B}R and 5-HT_{2A}R) (Xiang and Prince 2003, Andrade 2011, Puig and Gulledge 2011). In addition to these metabotropic 5-HT receptors, some but not all neocortical INs express 5-HT_{3A}Rs which are exclusively localized on presynaptic terminals; their activation results in a depolarization of the IN (Lee, Hjerling-Leffler et

al. 2010, Corradi and Bouzat 2014, Murthy, Niquille et al. 2014). In L5 of the mPFC, 20-30% of GABAergic INs express 5-HT_{1A}Rs and/or 5-HT_{2A}R of which 30% are PV+ FS INs (Puig and Gullledge 2011, Rudy, Fishell et al. 2011, Tremblay, Lee et al. 2016). INs expressing 5-HT_{3A}Rs are rare (6-10%) in L5 of the mPFC (Naka and Adesnik 2016, Posluszny 2019). 5-HT via its receptors regulates the membrane excitability by modulating various ion channels expressed in INs. In striatal cholinergic INs, 5-HT inhibits both K_{leak} and GIRK channels to enhance the neuronal excitability (Bonsi, Cuomo et al. 2007)(Roth and Hu 2020). In mPFC, 5-HT via 5-HT_{2A}Rs suppresses GIRK channels in FS INs (Athilingam, Ben-Shalom et al. 2017). In neonatal intersegmental commissural INs, 5-HT increases membrane excitability by decreasing the Ca²⁺ current, thus indirectly reducing K⁺ conductance. Ca²⁺ currents through P/Q-type but not N-type mediate GABA release in PV+ FS INs in mPFC (Zaitsev, Povysheva et al. 2007), while the Ca²⁺ currents through T-type (Zhi, Cao et al. 2022) and N-type (Blazon, LaCarubba et al. 2021) were specifically observed in STT+ and CCK+ INs in spinal dorsal horn and hippocampus respectively. Further studies are required to identify the 5-HT regulated ion channels in mPFC.

Application of 5-HT has been shown to excite (increased AP firing) mPFC FS INs. In L5 of rat visual cortex, 79% of FS INs and 74% of nFS INs were found to be responsive to 5-HT. Of the 5-HT responsive neurons, 50% of FS INs and 15% of nFS INs displayed an inward current (excitation), 41% of FS INs and 81% of nFS INs displayed an outward current (inhibition) and 9% of FS INs and 4% of nFS INs displayed an inward current followed by an outward current (Zhong and Yan 2011, Athilingam, Ben-Shalom et al. 2017). Inward currents were blocked by a 5-HT_{3A}R antagonist while outward currents were blocked by a 5-HT_{1A}R antagonist in all of the three 5-HT responsive groups (Xiang and Prince 2003). In my study in L5 of rat mPFC, almost all nFS INs were found to be unresponsive to 5-HT. Previous reports suggest a very low (8%) expression of 5-HT_{3A}Rs (Puig, Santana et al. 2004) or no expression of 5-HT_{1A/2A}Rs (Weber and Andrade 2010, Mengod, Palacios et al. 2015) in rat L5 nFS INs. In addition, higher 5-HT concentrations (30-100 μM) are required to activate 5-HT_{3A}Rs than those used in the current study (10 μM). Therefore, the lack of 5-HT responsiveness observed here may result from a low or no expression of 5-HT receptors or the fact that the 5-HT concentration was insufficient to substantially activate 5-HT_{3A}Rs in L5 nFS INs of mPFC. All rFS INs displayed a depolarization of the RMP, while 66.7% of the bFS INs showed a hyperpolarization and 33.3% a depolarization of the RMP upon 5-HT application. The depolarizing effect could result either from the activation of either 5-HT_{2A}Rs or 5-

HT_{3A}Rs or both. Since the expression levels of 5-HT_{3A}Rs was low in L5 of mPFC (Naka and Adesnik 2016, Posluszny 2019) this depolarizing effect is likely to be mediated by the activation of 5-HT_{2A}Rs which is in accordance with previous studies (Zhou and Hablitz 1999, Puig and Gullledge 2011, Zhong and Yan 2011, Athilingam, Ben-Shalom et al. 2017). The 5-HT induced hyperpolarization in INs may result from the activation of 5-HT_{1A}Rs. 5-HT_{1A}Rs were shown to be expressed mainly by PV⁺ neocortical INs (Aznar, Qian et al. 2003, Llado-Pelfort, Santana et al. 2012) while in one recent study, SST⁺ INs were shown to express mainly 5-HT_{2A}Rs (de Filippo, Rost et al. 2021). My results demonstrate that 5-HT exerts differential effects on the excitability of the three physiologically distinct IN types in L5 of mPFC identified here.

4.4. Monosynaptic connections in L5 of mPFC

E-E connections: Connectivity patterns between PNs in different cortical layers are highly selective. Previous studies suggest that the connection probability between neocortical L5 PNs is in the range of 1-12 % (Thomson, Deuchars et al. 1993, Markram, Lubke et al. 1997, Morishima and Kawaguchi 2006, Le Be, Silberberg et al. 2007, Otsuka and Kawaguchi 2008, Brown and Hestrin 2009). In L5 of the rat frontal cortex, the connection probability between RS-AS pairs was found to be lower (~1%) than that of AS-RS pairs (~11%) and AS-AS pairs (~10-13%) and RS-RS pairs (~13%) (Morishima and Kawaguchi 2006, Morishima, Morita et al. 2011). Similar connection probabilities were observed in the mouse motor cortex where the connection probability in AS-RS pairs and AS-AS pairs was ~20% and ~11% respectively, while RS-RS pairs were very rare (~4%) and no connections were found between RS and AS PNs (Kiritani, Wickersham et al. 2012). Relatively higher connection probabilities were observed for AS-AS pairs (18%) and RS-RS pairs (7%) in mice visual cortex than in the above mentioned two reports (Brown and Hestrin 2009). These reports indicate that AS PNs have a higher connection probability with other AS PNs as well as RS PNs, while RS PNs preferentially form synaptic connections with other RS PNs. This asymmetric connectivity was demonstrated in other reports as well (Kiritani, Wickersham et al. 2012, Harris and Shepherd 2015). In summary, AS PNs form connections with RS PNs but showed only sparse connectivity with other AS PNs. On the other hand, RS PNs formed connections with RS PNs but virtually none with AS PNs. The results from the current study are partly in line with the above mentioned earlier reports in which almost no RS-AS connections were found. However,

the connectivity ratios were rather low compared to the reported studies and was dependent on the specific PN types in L5 of mPFC.

E-I and I-E connections: GABAergic INs regulate cortical activity not only by feed-forward inhibition but also through feedback inhibition of neighboring PNs. PNs form connections with INs either unidirectionally or reciprocally. However, the specificity of IN synaptic connectivity in the mPFC is not well known. A fraction of 60% of mPFC L5 INs receive larger thalamocortical inputs than the excitatory PNs (5%) in the neocortex and thus provide feed-forward inhibition from the thalamus to the cortex (Porter, Johnson et al. 2001). Thalamocortical inputs activate especially FS INs including PV+ (Tan, Hu et al. 2008, Naka and Adesnik 2016). In addition to the thalamocortical inputs, neocortical L5 INs, in particular L5 PV+ FS INs, receive input from neighboring PNs and thus provide feedback inhibition (Naka and Adesnik 2016, Yavorska and Wehr 2016, Riedemann 2019, Sempere-Ferrandez, Martinez et al. 2019). INs can also form inhibitory connections with other INs such as SST+ and VIP+ INs forming disinhibitory circuits (IN-IN-PN) (Naka and Adesnik 2016). In L5 of the rat frontal cortex, RS PNs specifically excite STT+ INs. In turn, STT+ INs were shown to non-selectively inhibit both AS and RS PNs. Both AS and RS PNs excite PV+ INs and both of these PNs were inhibited by PV+ INs (Hilscher, Leao et al. 2017, Morishima, Kobayashi et al. 2017). In L5 of mouse mPFC, PV+ INs inhibit RS PNs more strongly than AS PNs (Lee, Gee et al. 2014, Ramaswamy and Markram 2015). In another study, FS INs were shown to preferentially form reciprocal connections with AS PNs in L5 of the rat frontal cortex (Kubota, Kondo et al. 2015). Most studies suggest that PV+ FS INs are powerful regulators of PNs thus balancing the E/I ratio in PFC (Voinova, Valiullina et al. 2015, Naka and Adesnik 2016, Baker, Kalmbach et al. 2018, Ferguson and Gao 2018). Only a few studies on the synaptic connectivity between STT+ INs and PNs are currently available. For example, in mouse barrel cortex, the axons of L5 STT+ non-Marinotti cells project predominately to L4 and were shown to inhibit L4 PNs (Nigro, Hashikawa-Yamasaki et al. 2018); in turn, L4 PNs were shown to excite L5 STT+ INs (Naka, Veit et al. 2019).

In the current study, E-I synaptic connections between PNs and INs in L5 of mPFC were sometimes reciprocal (17.7%) but mostly unidirectional (82.3%). The connection probability between RS-rFS, RS-bFS, AS-bFS, AS-nFS pairs was 9.6%, 1.2%, 8.4% and 1.2%, respectively. The probability to find a connection between PNs and INs was markedly higher than between two PNs. This is the

tendency which was found in almost all the studies of synaptic connectivity across the entire neocortex, independent of the type of layer and area of interest. The current findings on connection probabilities are partly in line with a previous study reporting that the PN-FS reciprocal connectivity was 68%, while 9% showed unidirectional PN-FS connections and 23% showed unidirectional FS-PN connections in L5 of rat frontal cortex (Otsuka and Kawaguchi 2009). In the current study in L5 of mPFC, unidirectional PN-FS connectivity was higher than their reciprocal connectivity i.e., 24% (6 of 25) of PN-FS connections were reciprocal and 68% (17 of 25) of PN-FS connections were unidirectional while 8% (2 of 25) of FS-PN connections were unidirectional; RS PNs preferentially innervated rFS INs (88.9%, 8 of 9) while AS PNs preferred to innervate (87.5%, 7 of 8) bFS INs. AS-nFS (1 of 8) and RS-bFS (1 of 9) pairs were rarely found (11-12%) in L5 of mPFC.

The probability to find a synaptic connection between a PV+ IN to PN has been found to be markedly higher (~ 67%) in L5 of mice barrel cortex (Packer and Yuste 2011) and also in L4 of rat barrel cortex (Koelbl, Helmstaedter et al. 2015). The PV+ INs in the neocortex of rodents have a very dense axonal domain in a specified layer while the STT+ INs have a broad trans-laminar axonal domain. In the current study, the probability to obtain an I-E pair was considerably lower than that reported previously: rFS IN-RS PN (~ 7.2%) and bFS IN-AS PN (~ 2.4%). Like the E-I connection specificity, all rFS INs in our brain slices preferentially innervated RS PNs while all bFS INs preferred to innervate AS PNs. In summary, the findings from the connectivity patterns among E-E, E-I and I-E connections provide major insight into the L5 neuronal connectivity and reveal distinct serotonergic modulation of L5 microcircuitry in rat mPFC.

Synaptic transmission is a rapid and dynamic process resulting from a combination of events, initiated by the influx of extracellular Ca^{2+} into the presynaptic terminal, depletion of the readily-releasable neurotransmitter vesicle pool, and the diffusion or re-uptake of neurotransmitters out of the cleft causing rapid deactivation of receptors. Short-term plasticity reflects changes in synaptic strength lasting tens of milliseconds to several seconds. In short-term depression, the response to the second AP stimulus is smaller than that evoked by the first. This reduction results from a depletion of readily-releasable neurotransmitter vesicles in the presynaptic terminal or from the inactivation of Na_vX or Ca^{2+} channels. Short-term depression is commonly observed at synapses with short inter-stimulus intervals of less than 20 ms. On the other hand synapses with longer inter-

stimulus intervals (20-500 ms) show pair-pulse facilitation in which the response to the second AP stimulus is larger than that evoked by the first. This enhancement was probably due to the availability of leftover Ca^{2+} after the first AP that contributes to the enhanced neurotransmitter release upon second stimulation (Citri and Malenka 2008, Pozo and Goda 2010). Furthermore, the activation of neurotransmitter receptors present on the presynaptic terminals may also be involved in modulating the synaptic release probability (Miller 1998, Zilberter 2000, Citri and Malenka 2008).

Short-term plasticity at excitatory and inhibitory connections can be either depressing or facilitating (Markram, Wang et al. 1998, Hempel, Hartman et al. 2000, Ma, Hu et al. 2012). In short-term facilitation, the PSP in response to the second AP stimulus is larger than that evoked by the first. This enhancement is thought to be mediated by an elevation of presynaptic Ca^{2+} influx after the first AP, acting on molecular targets that enhance the release probability of neurotransmitters (Zucker 1989, Zucker and Regehr 2002, Bennett 2003, Thomson 2003, Abbott and Regehr 2004, Regehr 2012). In the current study, all E-E, E-I and I-E pairs in L5 of mPFC showed short-term depression indicative of a reduction of glutamate release at PN axon terminals or GABA release at IN axon terminals.

In dual cell recordings, the EPSP amplitude reflects presynaptic release probability as well as postsynaptic membrane properties. PPR, CV and failure rate are mainly governed by presynaptic mechanisms while latency, rise time and decay time are generally determined by the postsynaptic neuron (Feldmeyer, Egger et al. 1999, Silver, Lubke et al. 2003). For several neocortical connections, it has been shown that the PPR, CV and failure rate are - in general terms - inversely related to the amplitude of the unitary EPSP or IPSPs (Markram, Lubke et al. 1997, Feldmeyer, Egger et al. 1999, Feldmeyer, Lubke et al. 2002, Feldmeyer, Lubke et al. 2006, Qi and Feldmeyer 2016). Therefore, a small mean PSP amplitude indicates a high PPR, large CV and high failure rate which in turn could reflect a low neurotransmitter release probability (Markram, Lubke et al. 1997, Feldmeyer, Egger et al. 1999, Feldmeyer, Lubke et al. 2002, Feldmeyer, Lubke et al. 2006, Qi and Feldmeyer 2016). In the E-E / E-I / I-E pairs described here, the PSP amplitude was highly variable ranging from 0.16-0.30 (weak connection) to 1.86-9.29 (strong connection) mV. In line with studies in rat frontal cortex (Otsuka T et al., 2008, Brown SP et al., 2009), my results did not show significant differences in the EPSP amplitudes and synaptic properties like PPR, CV, failure rate,

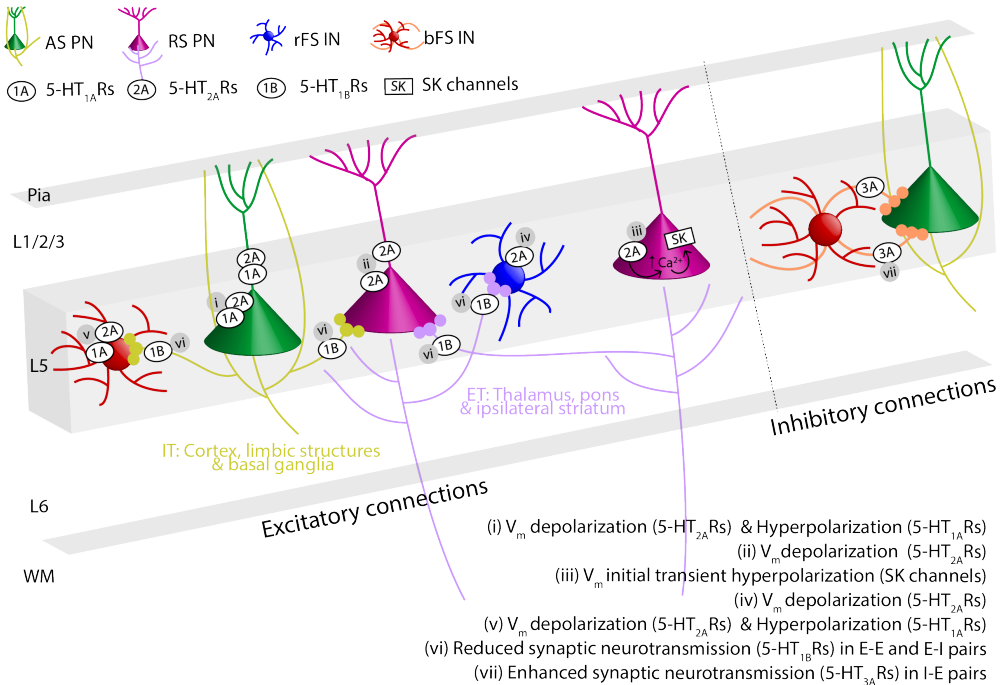
latency, rise time and decay time between AS-RS and RS-RS connections. When the EPSP amplitudes and other synaptic properties were compared between two types of E-I connections (AS PN-bFS IN and RS PN-rFS IN), no significant differences were observed either. This finding is in line with a previous study (Morishima, Kobayashi et al. 2017) reporting no significant difference in synaptic properties between AS-FS and RS-FS pairs. In most studies, rFS and bFS type INs were categorized into one group (Galarreta and Hestrin 2002, Angulo, Staiger et al. 2003, Goldberg, Jeong et al. 2011, Aracri, Banfi et al. 2015, Chistiakova, Ilin et al. 2019, Unal, Unal et al. 2020). Here, L5 FS INs in mPFC were split into two groups, the rFS and bFS INs, because of their distinct electrophysiological and morphological characteristics (see above). Although there was no difference in synaptic properties between AS-bFS and RS-rFS pairs, a preference for AS PNs to have connections with bFS type were observed while RS PNs preferred rFS type IN. In addition, similar preference patterns were observed in I-E pairs as well. In one study (Lee, Gee et al. 2014), PV+ FS INs were shown to preferentially inhibit RS PNs which is similar to the current findings in which rFS INs preferred to form connections with RS PNs. However, because there were only two rFS-RS pairs, a comparison of their synaptic properties is not possible. Taking all types of monosynaptic connections into account, the findings presented here provide novel details of the complex organization of the local neuronal microcircuitry in L5 of rat mPFC involving both excitatory PNs and inhibitory INs.

4.5. Serotonergic modulation on synaptic neurotransmission in mPFC of rats.

In addition to the postsynaptic modulatory effect of 5-HT in single neurons, the effects of 5-HT on synaptically connected neuron pairs were explored. Previous studies have reported that 5-HT produces a biphasic effect on synaptic transmission in the dorsal horn of the spinal cord (Li and Zhuo 1998) and an inhibitory effect on both excitatory and inhibitory transmission in the periaqueductal gray (Jeong, Chenu et al. 2008) and bed nucleus of the stria terminalis (Gaspar, Cases et al. 2003, Guo, Hammack et al. 2009). In another study (Tian, Yamanaka et al. 2017) 5-HT produced an inhibitory effect at excitatory synaptic connections in the anterior cingulate cortex where L5/6 PNs were stimulated extracellularly and their response was recorded in L2/3 PNs. However, the effect of 5-HT at the synaptic level within mPFC has not been studied in detail.

The concomitant increase in PPR suggests that 5-HT suppressed presynaptic neurotransmitter release at PN excitatory connections either through the activation of presynaptic 5-HT_{1A}R or 5-HT_{1B}Rs. 5-HT_{1A}R mediated suppression of synaptic transmission has been shown to describe the PNs of L2 and L3 of rat medial entorhinal cortex (Schmitz, Gloveli et al. 1998), L2 and L3 of mice anterior cingulate cortex (Tian, Yamanaka et al. 2017), in L2/3 of human mPFC (Komlosi, Molnar et al. 2012) and the dentate granule cells of rat hippocampus (Nozaki, Kubo et al. 2016). In contrast, serotonergic suppression of synaptic release via presynaptic 5-HT_{1B}R was found in L5 PNs in rat visual cortex (Murakoshi, Song et al. 2001), L4 PNs in mouse somatosensory cortex (Laurent, Goillard et al. 2002), L5 PNs of mouse mPFC (Kjaerby, Athilingam et al. 2016) and other brain regions like the corpus callosum or subcortical white matter (Tanaka and North 1993, Troca-Marin and Geijo-Barrientos 2010), the bed nucleus of the stria terminalis (Guo and Rainnie 2010), and the substantia nigra (Ding, Li et al. 2015). Here, in both types of E-E connections, 5-HT alone produced a reduction of evoked EPSP amplitudes; this reduction was abolished in the presence of a 5-HT_{1B}R antagonist (Summary Fig.). The increase in PPR, CV and failure rate in the presence of 5-HT and the reduction in the presence of the 5-HT_{1B}R antagonist indicate that serotonergic modulation of synaptic release was mediated by 5-HT_{1B}R receptors. In addition, 5-HT_{1B}R agonist, CGS induced membrane hyperpolarization in AS PNs and RS PNs during single recordings, suggesting a postsynaptic mechanism as well.

Reports on the effect of 5-HT on synaptic E-I connections in the cortex are rare. A specific study in the CA1 region of rat hippocampus demonstrated that 5-HT_{1B}Rs are responsible for presynaptic inhibition of neurotransmission in E-E and E-I connections (Mlinar, Falsini et al. 2003). The current results also demonstrate a 5-HT_{1B}R agonist-induced suppression of synaptic transmission in both of the E-I connection types. The reduction of evoked EPSP amplitude and increase in PPR, CV and failure rate in presence of a 5-HT_{1B}R agonist indicates that the presynaptic effects are mediated by 5-HT_{1B}Rs. 5-HT_{1B}Rs have different effectors at presynaptic (voltage-gated ion channels) and postsynaptic (ligand-gated ion channels) sites. At the postsynaptic site, activation of 5-HT_{1B}Rs that couple to G_{ai/o} proteins inhibits the activity of AC thereby reducing the intracellular cAMP levels and the downstream signaling events. Thus, besides being a classical neurotransmitter, 5-HT acts as a neuromodulator that regulates the balance of glutamatergic and GABAergic neurotransmission (Ciranna 2006, Celada, Puig et al. 2013, Pehrson and Sanchez 2014, Xie, Zuo et al. 2016, Tian, Yamanaka et al. 2017). For instance, activation of 5-HT_{1A/1B}Rs located at the presynaptic site of



Summary Fig.: Schematic representation of the serotonergic modulation of L5 neuronal population and microcircuits in rat mPFC. AS PNs are IT neurons projecting to cerebral cortex, limbic forebrain structures and basal ganglia, whereas RS PNs are ET neurons projecting to distal subcortical structures including thalamus, pons and ipsilateral striatum. (i) In single neuronal recordings, 5-HT through the activation of somatodendritic 5-HT_{2A}Rs and 5-HT_{1A}Rs induced a depolarization and hyperpolarization of RMP, respectively, in AS PNs. (ii) In RS PNs, 5-HT induced an initial transient hyperpolarization (via SK channels) followed by depolarization (via 5-HT_{2A}Rs). (iii) Activation of and 5-HT_{2A}Rs enhances intracellular Ca²⁺ levels that would in turn activate SK channels. (iv) In rFS INs, 5-HT induced depolarization which is thought to be mediated by the activation of 5-HT_{2A}Rs. (v) In bFS INs, 5-HT induced depolarization of RMP (via 5-HT_{2A}Rs) in a subset of INs and hyperpolarization of RMP (via 5-HT_{1A}Rs) in another subset of INs. Further, pair recordings were conducted to study the function of 5-HT_{1B}Rs expressed on axon terminals of PNs. (vi) 5-HT via activation of 5-HT_{1B}Rs, suppresses synaptic neurotransmission due to presynaptic inhibition of glutamatergic release in AS-RS, RS-RS, AS-bFS and RS-rFS excitatory pairs. (vii) 5-HT via activation of 5-HT_{3A}Rs, enhances synaptic neurotransmission in bFS-AS inhibitory pairs.

PNs and INs reduces the glutamate (Boeijinga and Boddeke 1996, Schmitz, Gloveli et al. 1998, Torres-Escalante, Barral et al. 2004) and GABA release (Mlinar, Falsini et al. 2003, Matsuoka, Hasuo et al. 2004), respectively in the cortex and other brain regions, In addition, 5-HT potentiates the inhibitory effects of GABA through the activation of 5-HT_{2A}Rs located on the INs in different brain regions (Li, Lang et al. 2000, Feng, Cai et al. 2001, Garcia-Oscos, Torres-Ramirez et al. 2015). This serotonergic potentiation of GABAergic inhibition indirectly influences the activity of

other neurons in the respective regions. Thus, GABAergic inhibition in PFC either through direct, 5-HT_{1A/1B}R-mediated or indirect, 5-HT_{2A}R-mediated mechanisms, underlie the actions of several anti-psychotic drugs such as eltoprazine and risperidone.

In I-E connections with a presynaptic rFS IN and a postsynaptic RS PN, 5-HT produced a suppression in the evoked IPSP amplitude as was found for excitatory connections. The increase in PPR suggests that this suppression was mediated by activation of presynaptic 5-HT_{1A/1B}Rs which are largely expressed in distinct populations of FS INs in L5/6 of mPFC (Puig, Watakabe et al. 2010, Athilingam, Ben-Shalom et al. 2017) and medial entorhinal cortex. However, a 5-HT_{3A}R agonist potentiated evoked IPSPs in I-E connections with a presynaptic bFS IN and postsynaptic AS PN. This effect was in agreement with a previous study (Ferezou, Cauli et al. 2002) which showed bFS INs response to the 5-HT_{3A}R agonist in different neocortical layers. In addition to the increased IPSP amplitude, a decrease in PPR, CV and failure rate is indicative of a presynaptic enhancement of neurotransmitter release. This suggests the existence of a previously not described differential 5-HT modulation of synaptic transmission at different I-E pairs, i.e., 5-HT_{1A/1B}R mediated suppression of IPSPs in rFS-RS pairs and 5-HT_{3A}R mediated potentiation in bFS-AS pairs. However, the detailed mechanism behind the enhanced synaptic neurotransmission by the 5-HT_{3A}Rs are not yet clear.

5. Bibliography

- Abbott, L. F. and W. G. Regehr (2004). "Synaptic computation." *Nature* **431**(7010): 796-803.
- Aghajanian, G. K. and G. J. Marek (1999). "Serotonin and hallucinogens." *Neuropsychopharmacology* **21**(2 Suppl): 16S-23S.
- Almog, M. and A. Korngreen (2009). "Characterization of voltage-gated Ca(2+) conductances in layer 5 neocortical pyramidal neurons from rats." *PLoS One* **4**(4): e4841.
- Amargos-Bosch, M., A. Bortolozzi, M. V. Puig, J. Serrats, A. Adell, P. Celada, M. Toth, G. Mengod and F. Artigas (2004). "Co-expression and in vivo interaction of serotonin1A and serotonin2A receptors in pyramidal neurons of prefrontal cortex." *Cereb Cortex* **14**(3): 281-299.
- Anastasiades, P. G. and A. G. Carter (2021). "Circuit organization of the rodent medial prefrontal cortex." *Trends Neurosci* **44**(7): 550-563.
- Andrade, R. (2011). "Serotonergic regulation of neuronal excitability in the prefrontal cortex." *Neuropharmacology* **61**(3): 382-386.
- Angulo, M. C., J. F. Staiger, J. Rossier and E. Audinat (2003). "Distinct local circuits between neocortical pyramidal cells and fast-spiking interneurons in young adult rats." *J Neurophysiol* **89**(2): 943-953.
- Apter, A., H. M. van Praag, R. Plutchik, S. Sevy, M. Korn and S. L. Brown (1990). "Interrelationships among anxiety, aggression, impulsivity, and mood: a serotonergically linked cluster?" *Psychiatry Res* **32**(2): 191-199.
- Aracri, P., D. Banfi, M. E. Pasini, A. Amadeo and A. Becchetti (2015). "Hypocretin (orexin) regulates glutamate input to fast-spiking interneurons in layer V of the Fr2 region of the murine prefrontal cortex." *Cereb Cortex* **25**(5): 1330-1347.
- Araneda, R. and R. Andrade (1991). "5-Hydroxytryptamine2 and 5-hydroxytryptamine 1A receptors mediate opposing responses on membrane excitability in rat association cortex." *Neuroscience* **40**(2): 399-412.
- Ascoli, G. A., L. Alonso-Nanclares, S. A. Anderson, G. Barrionuevo, R. Benavides-Piccione, A. Burkhalter, G. Buzsaki, B. Cauli, J. Defelipe, A. Fairen, D. Feldmeyer, G. Fishell, Y. Fregnac, T. F. Freund, D. Gardner, E. P. Gardner, J. H. Goldberg, M. Helmstaedter, S. Hestrin, F. Karube, Z. F. Kisvarday, B. Lambolez, D. A. Lewis, O. Marin, H. Markram, A. Munoz, A. Packer, C. C. Petersen, K. S. Rockland, J. Rossier, B. Rudy, P. Somogyi, J. F. Staiger, G. Tamas, A. M. Thomson, M. Toledo-Rodriguez, Y. Wang, D. C. West and R. Yuste (2008). "Petilla terminology: nomenclature of features of GABAergic interneurons of the cerebral cortex." *Nat Rev Neurosci* **9**(7): 557-568.
- Athilingam, J. C., R. Ben-Shalom, C. M. Keeshen, V. S. Sohal and K. J. Bender (2017). "Serotonin enhances excitability and gamma frequency temporal integration in mouse prefrontal fast-spiking interneurons." *Elife* **6**.
- Avesar, D. and A. T. Gullledge (2012). "Selective serotonergic excitation of callosal projection neurons." *Front Neural Circuits* **6**: 12.
- Aznar, S., Z. Qian, R. Shah, B. Rahbek and G. M. Knudsen (2003). "The 5-HT1A serotonin receptor is located on calbindin- and parvalbumin-containing neurons in the rat brain." *Brain Res* **959**(1): 58-67.
- Baker, A., B. Kalmbach, M. Morishima, J. Kim, A. Juavinett, N. Li and N. Dembrow (2018). "Specialized Subpopulations of Deep-Layer Pyramidal Neurons in the Neocortex: Bridging Cellular Properties to Functional Consequences." *J Neurosci* **38**(24): 5441-5455.
- Bantick, R. A., J. F. Deakin and P. M. Grasby (2001). "The 5-HT1A receptor in schizophrenia: a promising target for novel atypical neuroleptics?" *J Psychopharmacol* **15**(1): 37-46.
- Barbey, A. K., R. Colom and J. Grafman (2013). "Dorsolateral prefrontal contributions to human intelligence." *Neuropsychologia* **51**(7): 1361-1369.
- Bartolini, G., G. Ciceri and O. Marin (2013). "Integration of GABAergic interneurons into cortical cell assemblies: lessons from embryos and adults." *Neuron* **79**(5): 849-864.
- Bartos, M. and C. Elgueta (2012). "Functional characteristics of parvalbumin- and cholecystokinin-expressing basket cells." *J Physiol* **590**(4): 669-681.

- Bayliss, D. A., Y. W. Li and E. M. Talley (1997). "Effects of serotonin on caudal raphe neurons: inhibition of N- and P/Q-type calcium channels and the afterhyperpolarization." *J Neurophysiol* **77**(3): 1362-1374.
- Beebe, N. L., J. W. Young, J. G. Mellott and B. R. Schofield (2016). "Extracellular Molecular Markers and Soma Size of Inhibitory Neurons: Evidence for Four Subtypes of GABAergic Cells in the Inferior Colliculus." *J Neurosci* **36**(14): 3988-3999.
- Begre, S. and T. Koenig (2008). "Cerebral disconnectivity: an early event in schizophrenia." *Neuroscientist* **14**(1): 19-45.
- Benarroch, E. E. (2013). "HCN channels: function and clinical implications." *Neurology* **80**(3): 304-310.
- Bennett, M. R. (2003). "Obituary: Sir Bernard Katz (1911-2003)." *J Neurocytol* **32**(5-8): 431-436.
- Bizon, J. L., T. C. Foster, G. E. Alexander and E. L. Glisky (2012). "Characterizing cognitive aging of working memory and executive function in animal models." *Front Aging Neurosci* **4**: 19.
- Blanchard, D. C. and R. J. Blanchard (1990). "Behavioral correlates of chronic dominance-subordination relationships of male rats in a seminatural situation." *Neurosci Biobehav Rev* **14**(4): 455-462.
- Blanchard, R. J., D. C. Blanchard and K. J. Flannelly (1985). "Social stress, mortality and aggression in colonies and burrowing habitats." *Behav Processes* **11**(2): 209-213.
- Blanchard, R. J., K. J. Flannelly and D. C. Blanchard (1988). "Life-span studies of dominance and aggression in established colonies of laboratory rats." *Physiol Behav* **43**(1): 1-7.
- Blanchard, R. J., E. B. Yudko and D. C. Blanchard (1993). "Alcohol, aggression and the stress of subordination." *J Stud Alcohol Suppl* **11**: 146-155.
- Blazon, M., B. LaCarubba, A. Bunda, N. Czepiel, S. Mallat, L. Londrigan and A. Andrade (2021). "N-type calcium channels control GABAergic transmission in brain areas related to fear and anxiety." *OBM Neurobiol* **5**(1).
- Boeijinga, P. H. and H. W. Boddeke (1996). "Activation of 5-HT_{1B} receptors suppresses low but not high frequency synaptic transmission in the rat subicular cortex in vitro." *Brain Res* **721**(1-2): 59-65.
- Bonsi, P., D. Cuomo, J. Ding, G. Sciamanna, S. Ulrich, A. Tscherter, G. Bernardi, D. J. Surmeier and A. Pisani (2007). "Endogenous serotonin excites striatal cholinergic interneurons via the activation of 5-HT_{2C}, 5-HT₆, and 5-HT₇ serotonin receptors: implications for extrapyramidal side effects of serotonin reuptake inhibitors." *Neuropsychopharmacology* **32**(8): 1840-1854.
- Bopp, R., S. Holler-Rickauer, K. A. Martin and G. F. Schuhknecht (2017). "An Ultrastructural Study of the Thalamic Input to Layer 4 of Primary Motor and Primary Somatosensory Cortex in the Mouse." *J Neurosci* **37**(9): 2435-2448.
- Brini, M., T. Cali, D. Ottolini and E. Carafoli (2014). "Neuronal calcium signaling: function and dysfunction." *Cell Mol Life Sci* **71**(15): 2787-2814.
- Brown, S. P. and S. Hestrin (2009). "Cell-type identity: a key to unlocking the function of neocortical circuits." *Curr Opin Neurobiol* **19**(4): 415-421.
- Brown, S. P. and S. Hestrin (2009). "Intracortical circuits of pyramidal neurons reflect their long-range axonal targets." *Nature* **457**(7233): 1133-1136.
- Burnet, P. W., S. L. Eastwood and P. J. Harrison (1996). "5-HT_{1A} and 5-HT_{2A} receptor mRNAs and binding site densities are differentially altered in schizophrenia." *Neuropsychopharmacology* **15**(5): 442-455.
- Burns, J. (2006). "The social brain hypothesis of schizophrenia." *World Psychiatry* **5**(2): 77-81.
- Butler, T., D. Weisholtz, N. Isenberg, E. Harding, J. Epstein, E. Stern and D. Silbersweig (2012). "Neuroimaging of frontal-limbic dysfunction in schizophrenia and epilepsy-related psychosis: toward a convergent neurobiology." *Epilepsy Behav* **23**(2): 113-122.
- Cadena, E. J., D. M. White, N. V. Kraguljac, M. A. Reid and A. C. Lahti (2018). "Evaluation of fronto-striatal networks during cognitive control in unmedicated patients with schizophrenia and the effect of antipsychotic medication." *NPJ Schizophr* **4**(1): 8.
- Carhart-Harris, R. L. and D. J. Nutt (2017). "Serotonin and brain function: a tale of two receptors." *J Psychopharmacol* **31**(9): 1091-1120.
- Catterall, W. A. (2011). "Voltage-gated calcium channels." *Cold Spring Harb Perspect Biol* **3**(8): a003947.

- Celada, P., M. Puig, M. Amargos-Bosch, A. Adell and F. Artigas (2004). "The therapeutic role of 5-HT1A and 5-HT2A receptors in depression." *J Psychiatry Neurosci* **29**(4): 252-265.
- Celada, P., M. V. Puig and F. Artigas (2013). "Serotonin modulation of cortical neurons and networks." *Front Integr Neurosci* **7**: 25.
- Challis, C. and O. Berton (2015). "Top-Down Control of Serotonin Systems by the Prefrontal Cortex: A Path toward Restored Socioemotional Function in Depression." *ACS Chem Neurosci* **6**(7): 1040-1054.
- Chistiakova, M., V. Ilin, M. Roshchin, N. Bannon, A. Malyshev, Z. Kisvarday and M. Volgushev (2019). "Distinct Heterosynaptic Plasticity in Fast Spiking and Non-Fast-Spiking Inhibitory Neurons in Rat Visual Cortex." *J Neurosci* **39**(35): 6865-6878.
- Chow, A., A. Erisir, C. Farb, M. S. Nadal, A. Ozaita, D. Lau, E. Welker and B. Rudy (1999). "K(+) channel expression distinguishes subpopulations of parvalbumin- and somatostatin-containing neocortical interneurons." *J Neurosci* **19**(21): 9332-9345.
- Chudasama, Y. (2011). "Animal models of prefrontal-executive function." *Behav Neurosci* **125**(3): 327-343.
- Ciranna, L. (2006). "Serotonin as a modulator of glutamate- and GABA-mediated neurotransmission: implications in physiological functions and in pathology." *Curr Neuropharmacol* **4**(2): 101-114.
- Citri, A. and R. C. Malenka (2008). "Synaptic plasticity: multiple forms, functions, and mechanisms." *Neuropsychopharmacology* **33**(1): 18-41.
- Collins, D. P., P. G. Anastasiades, J. J. Marlin and A. G. Carter (2018). "Reciprocal Circuits Linking the Prefrontal Cortex with Dorsal and Ventral Thalamic Nuclei." *Neuron* **98**(2): 366-379 e364.
- Corradi, J. and C. Bouzat (2014). "Unraveling mechanisms underlying partial agonism in 5-HT3A receptors." *J Neurosci* **34**(50): 16865-16876.
- Cruz, D. A., S. M. Eggan, E. C. Azmitia and D. A. Lewis (2004). "Serotonin1A receptors at the axon initial segment of prefrontal pyramidal neurons in schizophrenia." *Am J Psychiatry* **161**(4): 739-742.
- Currie, K. P. (2010). "G protein modulation of CaV2 voltage-gated calcium channels." *Channels (Austin)* **4**(6): 497-509.
- Czyrak, A., M. Mackowiak, A. Chocyk, K. Fijal, A. Gadek-Michalska and K. Wedzony (2003). "8-OHDPAT-induced disruption of prepulse inhibition in rats is attenuated by prolonged corticosterone treatment." *Neuropsychopharmacology* **28**(7): 1300-1310.
- D'Souza, R. D. and A. Burkhalter (2017). "A Laminar Organization for Selective Cortico-Cortical Communication." *Front Neuroanat* **11**: 71.
- Dalley, J. W., R. N. Cardinal and T. W. Robbins (2004). "Prefrontal executive and cognitive functions in rodents: neural and neurochemical substrates." *Neurosci Biobehav Rev* **28**(7): 771-784.
- Day, M., D. B. Carr, S. Ulrich, E. Ilijic, T. Tkatch and D. J. Surmeier (2005). "Dendritic excitability of mouse frontal cortex pyramidal neurons is shaped by the interaction among HCN, Kir2, and K_{leak} channels." *J Neurosci* **25**(38): 8776-8787.
- de Boer, S. F. and J. M. Koolhaas (2005). "5-HT1A and 5-HT1B receptor agonists and aggression: a pharmacological challenge of the serotonin deficiency hypothesis." *Eur J Pharmacol* **526**(1-3): 125-139.
- de Filippo, R., B. R. Rost, A. Stumpf, C. Cooper, J. J. Tukker, C. Harms, P. Beed and D. Schmitz (2021). "Somatostatin interneurons activated by 5-HT2A receptor suppress slow oscillations in medial entorhinal cortex." *Elife* **10**.
- Dean, B. (2003). "The cortical serotonin2A receptor and the pathology of schizophrenia: a likely accomplice." *J Neurochem* **85**(1): 1-13.
- Deemyad, T., L. Maler and M. J. Chacron (2011). "Inhibition of SK and M channel-mediated currents by 5-HT enables parallel processing by bursts and isolated spikes." *J Neurophysiol* **105**(3): 1276-1294.
- DeFelipe, J., P. L. Lopez-Cruz, R. Benavides-Piccione, C. Bielza, P. Larranaga, S. Anderson, A. Burkhalter, B. Cauli, A. Fairen, D. Feldmeyer, G. Fishell, D. Fitzpatrick, T. F. Freund, G. Gonzalez-Burgos, S. Hestrin, S. Hill, P. R. Hof, J. Huang, E. G. Jones, Y. Kawaguchi, Z. Kisvarday, Y. Kubota, D. A. Lewis, O. Marin, H. Markram, C. J. McBain, H. S. Meyer, H. Monyer, S. B. Nelson, K. Rockland, J. Rossier, J. L. Rubenstein, B. Rudy, M. Scanziani, G. M. Shepherd, C. C. Sherwood, J. F. Staiger, G. Tamas, A.

- Thomson, Y. Wang, R. Yuste and G. A. Ascoli (2013). "New insights into the classification and nomenclature of cortical GABAergic interneurons." *Nat Rev Neurosci* **14**(3): 202-216.
- Degenetais, E., A. M. Thierry, J. Glowinski and Y. Gioanni (2002). "Electrophysiological properties of pyramidal neurons in the rat prefrontal cortex: an in vivo intracellular recording study." *Cereb Cortex* **12**(1): 1-16.
- Dembrow, N. C., R. A. Chitwood and D. Johnston (2010). "Projection-specific neuromodulation of medial prefrontal cortex neurons." *J Neurosci* **30**(50): 16922-16937.
- Ding, C., V. Emmenegger, K. Schaffrath and D. Feldmeyer (2021). "Layer-Specific Inhibitory Microcircuits of Layer 6 Interneurons in Rat Prefrontal Cortex." *Cereb Cortex* **31**(1): 32-47.
- Ding, S., L. Li and F. M. Zhou (2015). "Robust presynaptic serotonin 5-HT(1B) receptor inhibition of the striatonigral output and its sensitization by chronic fluoxetine treatment." *J Neurophysiol* **113**(9): 3397-3409.
- Eack, S. M., J. A. Wojtalik, S. M. Barb, C. E. Newhill, M. S. Keshavan and M. L. Phillips (2016). "Fronto-Limbic Brain Dysfunction during the Regulation of Emotion in Schizophrenia." *PLoS One* **11**(3): e0149297.
- Economo, M. N., N. G. Clack, L. D. Lavis, C. R. Gerfen, K. Svoboda, E. W. Myers and J. Chandrashekar (2016). "A platform for brain-wide imaging and reconstruction of individual neurons." *Elife* **5**: e10566.
- Eggermann, E. and D. Feldmeyer (2009). "Cholinergic filtering in the recurrent excitatory microcircuit of cortical layer 4." *Proc Natl Acad Sci U S A* **106**(28): 11753-11758.
- Elliott, M. C., P. M. Tanaka, R. W. Schwark and R. Andrade (2018). "Serotonin Differentially Regulates L5 Pyramidal Cell Classes of the Medial Prefrontal Cortex in Rats and Mice." *eNeuro* **5**(1).
- Elston, G. N., R. Benavides-Piccione, A. Elston, B. Zietsch, J. Defelipe, P. Manger, V. Casagrande and J. H. Kaas (2006). "Specializations of the granular prefrontal cortex of primates: implications for cognitive processing." *Anat Rec A Discov Mol Cell Evol Biol* **288**(1): 26-35.
- Faber, E. S. (2010). "Functional interplay between NMDA receptors, SK channels and voltage-gated Ca²⁺ channels regulates synaptic excitability in the medial prefrontal cortex." *J Physiol* **588**(Pt 8): 1281-1292.
- Feldmeyer, D. (2012). "Excitatory neuronal connectivity in the barrel cortex." *Front Neuroanat* **6**: 24.
- Feldmeyer, D., V. Egger, J. Lubke and B. Sakmann (1999). "Reliable synaptic connections between pairs of excitatory layer 4 neurones within a single 'barrel' of developing rat somatosensory cortex." *J Physiol* **521 Pt 1**: 169-190.
- Feldmeyer, D., J. Lubke and B. Sakmann (2006). "Efficacy and connectivity of intracolumnar pairs of layer 2/3 pyramidal cells in the barrel cortex of juvenile rats." *J Physiol* **575**(Pt 2): 583-602.
- Feldmeyer, D., J. Lubke, R. A. Silver and B. Sakmann (2002). "Synaptic connections between layer 4 spiny neurone-layer 2/3 pyramidal cell pairs in juvenile rat barrel cortex: physiology and anatomy of interlaminar signalling within a cortical column." *J Physiol* **538**(Pt 3): 803-822.
- Feldmeyer, D., G. Qi, V. Emmenegger and J. F. Staiger (2018). "Inhibitory interneurons and their circuit motifs in the many layers of the barrel cortex." *Neuroscience* **368**: 132-151.
- Feng, J., X. Cai, J. Zhao and Z. Yan (2001). "Serotonin receptors modulate GABA(A) receptor channels through activation of anchored protein kinase C in prefrontal cortical neurons." *J Neurosci* **21**(17): 6502-6511.
- Ferezou, I., B. Cauli, E. L. Hill, J. Rossier, E. Hamel and B. Lambolez (2002). "5-HT₃ receptors mediate serotonergic fast synaptic excitation of neocortical vasoactive intestinal peptide/cholecystokinin interneurons." *J Neurosci* **22**(17): 7389-7397.
- Ferguson, B. R. and W. J. Gao (2018). "PV Interneurons: Critical Regulators of E/I Balance for Prefrontal Cortex-Dependent Behavior and Psychiatric Disorders." *Front Neural Circuits* **12**: 37.
- Fish, E. W., S. Faccidomo and K. A. Miczek (1999). "Aggression heightened by alcohol or social instigation in mice: reduction by the 5-HT(1B) receptor agonist CP-94,253." *Psychopharmacology (Berl)* **146**(4): 391-399.

- Fish, K. N., G. D. Hoftman, W. Sheikh, M. Kitchens and D. A. Lewis (2013). "Parvalbumin-containing chandelier and basket cell boutons have distinctive modes of maturation in monkey prefrontal cortex." *J Neurosci* **33**(19): 8352-8358.
- Foehring, R. C. (1996). "Serotonin modulates N- and P-type calcium currents in neocortical pyramidal neurons via a membrane-delimited pathway." *J Neurophysiol* **75**(2): 648-659.
- Frederiksen, K., D. Lu, J. Yang, H. S. Jensen, J. F. Bastlund, P. H. Larsen, H. Liu, F. Crestey, K. Dekermendjian, L. Badolo, M. Laursen, C. Hougaard, C. Yang, N. Svenstrup and M. Grunnet (2017). "A small molecule activator of Nav 1.1 channels increases fast-spiking interneuron excitability and GABAergic transmission in vitro and has anti-convulsive effects in vivo." *Eur J Neurosci* **46**(3): 1887-1896.
- Frith, C. and R. Dolan (1996). "The role of the prefrontal cortex in higher cognitive functions." *Brain Res Cogn Brain Res* **5**(1-2): 175-181.
- Galarreta, M. and S. Hestrin (2002). "Electrical and chemical synapses among parvalbumin fast-spiking GABAergic interneurons in adult mouse neocortex." *Proc Natl Acad Sci U S A* **99**(19): 12438-12443.
- Garcia-Garcia, A. L., Q. Meng, S. Canetta, A. M. Gardier, B. P. Guiard, C. Kellendonk, A. Dranovsky and E. D. Leonardo (2017). "Serotonin Signaling through Prefrontal Cortex 5-HT1A Receptors during Adolescence Can Determine Baseline Mood-Related Behaviors." *Cell Rep* **18**(5): 1144-1156.
- Garcia-Oscos, F., O. Torres-Ramirez, L. Dinh, L. Galindo-Charles, E. A. Perez Padilla, J. C. Pineda, M. Atzori and H. Salgado (2015). "Activation of 5-HT receptors inhibits GABAergic transmission by pre- and post-synaptic mechanisms in layer II/III of the juvenile rat auditory cortex." *Synapse* **69**(3): 115-127.
- Gaspar, P., O. Cases and L. Maroteaux (2003). "The developmental role of serotonin: news from mouse molecular genetics." *Nat Rev Neurosci* **4**(12): 1002-1012.
- Gelman, D. M. and O. Marin (2010). "Generation of interneuron diversity in the mouse cerebral cortex." *Eur J Neurosci* **31**(12): 2136-2141.
- Gilmore, E. C. and K. Herrup (1997). "Cortical development: layers of complexity." *Curr Biol* **7**(4): R231-234.
- Goldberg, E. M., H. Y. Jeong, I. Kruglikov, R. Tremblay, R. M. Lazarenko and B. Rudy (2011). "Rapid developmental maturation of neocortical FS cell intrinsic excitability." *Cereb Cortex* **21**(3): 666-682.
- Gonchar, Y., Q. Wang and A. Burkhalter (2007). "Multiple distinct subtypes of GABAergic neurons in mouse visual cortex identified by triple immunostaining." *Front Neuroanat* **1**: 3.
- Gouwens, N. W., S. A. Sorensen, F. Baftizadeh, A. Budzillo, B. R. Lee, T. Jarsky, L. Alfiler, K. Baker, E. Barkan, K. Berry, D. Bertagnolli, K. Bickley, J. Bomben, T. Braun, K. Brouner, T. Casper, K. Crichton, T. L. Daigle, R. Dalley, R. A. de Frates, N. Dee, T. Desta, S. D. Lee, N. Dotson, T. Egdorf, L. Ellingwood, R. Enstrom, L. Esposito, C. Farrell, D. Feng, O. Fong, R. Gala, C. Gamlin, A. Gary, A. Glandon, J. Goldy, M. Gorham, L. Graybuck, H. Gu, K. Hadley, M. J. Hawrylycz, A. M. Henry, D. Hill, M. Hupp, S. Kebede, T. K. Kim, L. Kim, M. Kroll, C. Lee, K. E. Link, M. Mallory, R. Mann, M. Maxwell, M. McGraw, D. McMillen, A. Mukora, L. Ng, L. Ng, K. Ngo, P. R. Nicovich, A. Oldre, D. Park, H. Peng, O. Penn, T. Pham, A. Pom, Z. Popovic, L. Potekhina, R. Rajanbabu, S. Ransford, D. Reid, C. Rimorin, M. Robertson, K. Ronellenfitch, A. Ruiz, D. Sandman, K. Smith, J. Sulc, S. M. Sunkin, A. Szafer, M. Tieu, A. Torkelson, J. Trinh, H. Tung, W. Wakeman, K. Ward, G. Williams, Z. Zhou, J. T. Ting, A. Arkhipov, U. Sumbul, E. S. Lein, C. Koch, Z. Yao, B. Tasic, J. Berg, G. J. Murphy and H. Zeng (2020). "Integrated Morphoelectric and Transcriptomic Classification of Cortical GABAergic Cells." *Cell* **183**(4): 935-953 e919.
- Gouwens, N. W., S. A. Sorensen, J. Berg, C. Lee, T. Jarsky, J. Ting, S. M. Sunkin, D. Feng, C. A. Anastassiou, E. Barkan, K. Bickley, N. Blesie, T. Braun, K. Brouner, A. Budzillo, S. Caldejon, T. Casper, D. Castelli, P. Chong, K. Crichton, C. Cuhaciyani, T. L. Daigle, R. Dalley, N. Dee, T. Desta, S. L. Ding, S. Dingman, A. Doperalski, N. Dotson, T. Egdorf, M. Fisher, R. A. de Frates, E. Garren, M. Garwood, A. Gary, N. Gaudreault, K. Godfrey, M. Gorham, H. Gu, C. Habel, K. Hadley, J. Harrington, J. A. Harris, A. Henry, D. Hill, S. Josephsen, S. Kebede, L. Kim, M. Kroll, B. Lee, T. Lemon, K. E. Link, X. Liu, B.

- Long, R. Mann, M. McGraw, S. Mihalas, A. Mukora, G. J. Murphy, L. Ng, K. Ngo, T. N. Nguyen, P. R. Nicovich, A. Oldre, D. Park, S. Parry, J. Perkins, L. Potekhina, D. Reid, M. Robertson, D. Sandman, M. Schroedter, C. Slaughterbeck, G. Soler-Llavina, J. Sulc, A. Szafer, B. Tasic, N. Taskin, C. Teeter, N. Thatra, H. Tung, W. Wakeman, G. Williams, R. Young, Z. Zhou, C. Farrell, H. Peng, M. J. Hawrylycz, E. Lein, L. Ng, A. Arkipov, A. Bernard, J. W. Phillips, H. Zeng and C. Koch (2019). "Classification of electrophysiological and morphological neuron types in the mouse visual cortex." *Nat Neurosci* **22**(7): 1182-1195.
- Grunnet, M., T. Jespersen and J. F. Perrier (2004). "5-HT_{1A} receptors modulate small-conductance Ca²⁺-activated K⁺ channels." *J Neurosci Res* **78**(6): 845-854.
- Guan, D., W. E. Armstrong and R. C. Foehring (2015). "Electrophysiological properties of genetically identified subtypes of layer 5 neocortical pyramidal neurons: Ca²⁺(+) dependence and differential modulation by norepinephrine." *J Neurophysiol* **113**(7): 2014-2032.
- Guiard, B. P. and G. Di Giovanni (2015). "Central serotonin-2A (5-HT_{2A}) receptor dysfunction in depression and epilepsy: the missing link?" *Front Pharmacol* **6**: 46.
- Gulledge, A. T., S. B. Park, Y. Kawaguchi and G. J. Stuart (2007). "Heterogeneity of phasic cholinergic signaling in neocortical neurons." *J Neurophysiol* **97**(3): 2215-2229.
- Gulledge, A. T. and G. J. Stuart (2005). "Cholinergic inhibition of neocortical pyramidal neurons." *J Neurosci* **25**(44): 10308-10320.
- Guo, J. D., S. E. Hammack, R. Hazra, L. Levita and D. G. Rainnie (2009). "Bi-directional modulation of bed nucleus of stria terminalis neurons by 5-HT: molecular expression and functional properties of excitatory 5-HT receptor subtypes." *Neuroscience* **164**(4): 1776-1793.
- Guo, J. D. and D. G. Rainnie (2010). "Presynaptic 5-HT_{1B} receptor-mediated serotonergic inhibition of glutamate transmission in the bed nucleus of the stria terminalis." *Neuroscience* **165**(4): 1390-1401.
- Harris, K. D. and G. M. Shepherd (2015). "The neocortical circuit: themes and variations." *Nat Neurosci* **18**(2): 170-181.
- Hempel, C. M., K. H. Hartman, X. J. Wang, G. G. Turrigiano and S. B. Nelson (2000). "Multiple forms of short-term plasticity at excitatory synapses in rat medial prefrontal cortex." *J Neurophysiol* **83**(5): 3031-3041.
- Herculano-Houzel, S. (2009). "The human brain in numbers: a linearly scaled-up primate brain." *Front Hum Neurosci* **3**: 31.
- Hervas, I., M. T. Vilaro, L. Romero, M. C. Scorza, G. Mengod and F. Artigas (2001). "Desensitization of 5-HT_{1A} autoreceptors by a low chronic fluoxetine dose effect of the concurrent administration of WAY-100635." *Neuropsychopharmacology* **24**(1): 11-20.
- Hibino, H., A. Inanobe, K. Furutani, S. Murakami, I. Findlay and Y. Kurachi (2010). "Inwardly rectifying potassium channels: their structure, function, and physiological roles." *Physiol Rev* **90**(1): 291-366.
- Hilger, D., M. Masureel and B. K. Kobilka (2018). "Structure and dynamics of GPCR signaling complexes." *Nat Struct Mol Biol* **25**(1): 4-12.
- Hilscher, M. M., R. N. Leao, S. J. Edwards, K. E. Leao and K. Kullander (2017). "ChRNA2-Martinotti Cells Synchronize Layer 5 Type A Pyramidal Cells via Rebound Excitation." *PLoS Biol* **15**(2): e2001392.
- Hsiao, C. F., P. R. Trueblood, M. S. Levine and S. H. Chandler (1997). "Multiple effects of serotonin on membrane properties of trigeminal motoneurons in vitro." *J Neurophysiol* **77**(6): 2910-2924.
- Hu, H., J. Gan and P. Jonas (2014). "Interneurons. Fast-spiking, parvalbumin(+) GABAergic interneurons: from cellular design to microcircuit function." *Science* **345**(6196): 1255263.
- Hu, W. and B. P. Bean (2018). "Differential Control of Axonal and Somatic Resting Potential by Voltage-Dependent Conductances in Cortical Layer 5 Pyramidal Neurons." *Neuron* **99**(6): 1355.
- Hughes, D. I., K. A. Boyle, C. M. Kinnon, C. Bilisland, J. A. Quayle, R. J. Callister and B. A. Graham (2013). "HCN4 subunit expression in fast-spiking interneurons of the rat spinal cord and hippocampus." *Neuroscience* **237**: 7-18.

- Hurlemann, R., C. Boy, P. T. Meyer, H. Scherk, M. Wagner, H. Herzog, H. H. Coenen, K. Vogeley, P. Falkai, K. Zilles, W. Maier and A. Bauer (2005). "Decreased prefrontal 5-HT2A receptor binding in subjects at enhanced risk for schizophrenia." *Anat Embryol (Berl)* **210**(5-6): 519-523.
- Hurlemann, R., A. Matusch, K. U. Kuhn, J. Berning, D. Elmenhorst, O. Winz, H. Kolsch, K. Zilles, M. Wagner, W. Maier and A. Bauer (2008). "5-HT2A receptor density is decreased in the at-risk mental state." *Psychopharmacology (Berl)* **195**(4): 579-590.
- Isaacson, J. S. and M. Scanziani (2011). "How inhibition shapes cortical activity." *Neuron* **72**(2): 231-243.
- Jansson, A., B. Tinner, M. Bancila, D. Verge, H. W. Steinbusch, L. F. Agnati and K. Fuxe (2001). "Relationships of 5-hydroxytryptamine immunoreactive terminal-like varicosities to 5-hydroxytryptamine-2A receptor-immunoreactive neuronal processes in the rat forebrain." *J Chem Neuroanat* **22**(3): 185-203.
- Jeong, H. J., D. Chenu, E. E. Johnson, M. Connor and C. W. Vaughan (2008). "Sumatriptan inhibits synaptic transmission in the rat midbrain periaqueductal grey." *Mol Pain* **4**: 54.
- Kase, D. and K. Imoto (2012). "The Role of HCN Channels on Membrane Excitability in the Nervous System." *J Signal Transduct* **2012**: 619747.
- Kawaguchi, Y. (2017). "Pyramidal Cell Subtypes and Their Synaptic Connections in Layer 5 of Rat Frontal Cortex." *Cereb Cortex* **27**(12): 5755-5771.
- Kawaguchi, Y. and S. Kondo (2002). "Parvalbumin, somatostatin and cholecystokinin as chemical markers for specific GABAergic interneuron types in the rat frontal cortex." *J Neurocytol* **31**(3-5): 277-287.
- Kelsom, C. and W. Lu (2013). "Development and specification of GABAergic cortical interneurons." *Cell Biosci* **3**(1): 19.
- Kesner, R. P. and J. C. Churchwell (2011). "An analysis of rat prefrontal cortex in mediating executive function." *Neurobiol Learn Mem* **96**(3): 417-431.
- Kim, E. J., A. L. Juavinett, E. M. Kyubwa, M. W. Jacobs and E. M. Callaway (2015). "Three Types of Cortical Layer 5 Neurons That Differ in Brain-wide Connectivity and Function." *Neuron* **88**(6): 1253-1267.
- Kiritani, T., I. R. Wickersham, H. S. Seung and G. M. Shepherd (2012). "Hierarchical connectivity and connection-specific dynamics in the corticospinal-corticostriatal microcircuit in mouse motor cortex." *J Neurosci* **32**(14): 4992-5001.
- Kjaerby, C., J. Athilingam, S. E. Robinson, J. Iafrati and V. S. Sohal (2016). "Serotonin 1B Receptors Regulate Prefrontal Function by Gating Callosal and Hippocampal Inputs." *Cell Rep* **17**(11): 2882-2890.
- Ko, J. (2017). "Neuroanatomical Substrates of Rodent Social Behavior: The Medial Prefrontal Cortex and Its Projection Patterns." *Front Neural Circuits* **11**: 41.
- Ko, K. W., M. N. Rasband, V. Meseguer, R. H. Kramer and N. L. Golding (2016). "Serotonin modulates spike probability in the axon initial segment through HCN channels." *Nat Neurosci* **19**(6): 826-834.
- Koelbl, C., M. Helmstaedter, J. Lubke and D. Feldmeyer (2015). "A barrel-related interneuron in layer 4 of rat somatosensory cortex with a high intrabarrel connectivity." *Cereb Cortex* **25**(3): 713-725.
- Kolb B., C. J. (2004). "Organization and Plasticity of the Prefrontal Cortex of the Rat. Organization and Plasticity of the Prefrontal Cortex of the Rat." In: Otani S. (eds) *Prefrontal Cortex: From Synaptic Plasticity to Cognition*.
- Komlosi, G., G. Molnar, M. Rozsa, S. Olah, P. Barzo and G. Tamas (2012). "Fluoxetine (prozac) and serotonin act on excitatory synaptic transmission to suppress single layer 2/3 pyramidal neuron-triggered cell assemblies in the human prefrontal cortex." *J Neurosci* **32**(46): 16369-16378.
- Koyama, S., N. Matsumoto, C. Kubo and N. Akaike (2000). "Presynaptic 5-HT3 receptor-mediated modulation of synaptic GABA release in the mechanically dissociated rat amygdala neurons." *J Physiol* **529 Pt 2**: 373-383.
- Kubota, Y., S. Kondo, M. Nomura, S. Hatada, N. Yamaguchi, A. A. Mohamed, F. Karube, J. Lubke and Y. Kawaguchi (2015). "Functional effects of distinct innervation styles of pyramidal cells by fast spiking cortical interneurons." *Elife* **4**.

- Lambe, E. K. and G. K. Aghajanian (2001). "The role of Kv1.2-containing potassium channels in serotonin-induced glutamate release from thalamocortical terminals in rat frontal cortex." *J Neurosci* **21**(24): 9955-9963.
- Laurent, A., J. M. Goillard, O. Cases, C. Lebrand, P. Gaspar and N. Ropert (2002). "Activity-dependent presynaptic effect of serotonin 1B receptors on the somatosensory thalamocortical transmission in neonatal mice." *J Neurosci* **22**(3): 886-900.
- Le Be, J. V., G. Silberberg, Y. Wang and H. Markram (2007). "Morphological, electrophysiological, and synaptic properties of corticocallosal pyramidal cells in the neonatal rat neocortex." *Cereb Cortex* **17**(9): 2204-2213.
- Lee, A. T., S. M. Gee, D. Vogt, T. Patel, J. L. Rubenstein and V. S. Sohal (2014). "Pyramidal neurons in prefrontal cortex receive subtype-specific forms of excitation and inhibition." *Neuron* **81**(1): 61-68.
- Lee, S., J. Hjerling-Leffler, E. Zagha, G. Fishell and B. Rudy (2010). "The largest group of superficial neocortical GABAergic interneurons expresses ionotropic serotonin receptors." *J Neurosci* **30**(50): 16796-16808.
- Lefort, S., C. Tómm, J. C. Floyd Sarria and C. C. Petersen (2009). "The excitatory neuronal network of the C2 barrel column in mouse primary somatosensory cortex." *Neuron* **61**(2): 301-316.
- Letzkus, J. J., S. B. Wolff and A. Luthi (2015). "Disinhibition, a Circuit Mechanism for Associative Learning and Memory." *Neuron* **88**(2): 264-276.
- Li, H., B. Lang, J. F. Kang and Y. Q. Li (2000). "Serotonin potentiates the response of neurons of the superficial laminae of the rat spinal dorsal horn to gamma-aminobutyric acid." *Brain Res Bull* **52**(6): 559-565.
- Li, P. and M. Zhuo (1998). "Silent glutamatergic synapses and nociception in mammalian spinal cord." *Nature* **393**(6686): 695-698.
- Li, Y. W. and D. A. Bayliss (1998). "Presynaptic inhibition by 5-HT_{1B} receptors of glutamatergic synaptic inputs onto serotonergic caudal raphe neurons in rat." *J Physiol* **510** (Pt 1): 121-134.
- Lin, P., X. Wang, B. Zhang, B. Kirkpatrick, D. Ongur, J. J. Levitt, J. Jovicich, S. Yao and X. Wang (2018). "Functional dysconnectivity of the limbic loop of frontostriatal circuits in first-episode, treatment-naive schizophrenia." *Hum Brain Mapp* **39**(2): 747-757.
- Liu, Z., J. Zhou, Y. Li, F. Hu, Y. Lu, M. Ma, Q. Feng, J. E. Zhang, D. Wang, J. Zeng, J. Bao, J. Y. Kim, Z. F. Chen, S. El Mestikawy and M. Luo (2014). "Dorsal raphe neurons signal reward through 5-HT and glutamate." *Neuron* **81**(6): 1360-1374.
- Llado-Pelfort, L., N. Santana, V. Ghisi, F. Artigas and P. Celada (2012). "5-HT_{1A} receptor agonists enhance pyramidal cell firing in prefrontal cortex through a preferential action on GABA interneurons." *Cereb Cortex* **22**(7): 1487-1497.
- Lopez, J. F., D. M. Vazquez, D. T. Chalmers and S. J. Watson (1997). "Regulation of 5-HT receptors and the hypothalamic-pituitary-adrenal axis. Implications for the neurobiology of suicide." *Ann N Y Acad Sci* **836**: 106-134.
- Lubke, J. and D. Feldmeyer (2007). "Excitatory signal flow and connectivity in a cortical column: focus on barrel cortex." *Brain Struct Funct* **212**(1): 3-17.
- Ma, Y., H. Hu and A. Agmon (2012). "Short-term plasticity of unitary inhibitory-to-inhibitory synapses depends on the presynaptic interneuron subtype." *J Neurosci* **32**(3): 983-988.
- Ma, Y., H. Hu, A. S. Berrebi, P. H. Mathers and A. Agmon (2006). "Distinct subtypes of somatostatin-containing neocortical interneurons revealed in transgenic mice." *J Neurosci* **26**(19): 5069-5082.
- Maier, S. F. (2015). "Behavioral control blunts reactions to contemporaneous and future adverse events: medial prefrontal cortex plasticity and a corticostriatal network." *Neurobiol Stress* **1**: 12-22.
- Maier, S. F., J. Amat, M. V. Baratta, E. Paul and L. R. Watkins (2006). "Behavioral control, the medial prefrontal cortex, and resilience." *Dialogues Clin Neurosci* **8**(4): 397-406.

- Markram, H., J. Lubke, M. Frotscher, A. Roth and B. Sakmann (1997). "Physiology and anatomy of synaptic connections between thick tufted pyramidal neurones in the developing rat neocortex." *J Physiol* **500** (Pt 2): 409-440.
- Markram, H., M. Toledo-Rodriguez, Y. Wang, A. Gupta, G. Silberberg and C. Wu (2004). "Interneurons of the neocortical inhibitory system." *Nat Rev Neurosci* **5**(10): 793-807.
- Markram, H., Y. Wang and M. Tsodyks (1998). "Differential signaling via the same axon of neocortical pyramidal neurons." *Proc Natl Acad Sci U S A* **95**(9): 5323-5328.
- Martin-Ruiz, R., M. V. Puig, P. Celada, D. A. Shapiro, B. L. Roth, G. Mengod and F. Artigas (2001). "Control of serotonergic function in medial prefrontal cortex by serotonin-2A receptors through a glutamate-dependent mechanism." *J Neurosci* **21**(24): 9856-9866.
- Marx, M. and D. Feldmeyer (2013). "Morphology and physiology of excitatory neurons in layer 6b of the somatosensory rat barrel cortex." *Cereb Cortex* **23**(12): 2803-2817.
- Masson, M. B. E., Michel Hamon and a. M. Darmon (2012). "Serotonergic signaling: multiple effectors and pleiotropic effects." *WIREs Member Transp Signal*.
- Matsuoka, T., H. Hasuo and T. Akasu (2004). "5-Hydroxytryptamine 1B receptors mediate presynaptic inhibition of monosynaptic IPSC in the rat dorsolateral septal nucleus." *Neurosci Res* **48**(3): 229-238.
- Mazuir, E., D. Fricker and N. Sol-Foulon (2021). "Neuron-Oligodendrocyte Communication in Myelination of Cortical GABAergic Cells." *Life (Basel)* **11**(3).
- McCorvy, J. D. and B. L. Roth (2015). "Structure and function of serotonin G protein-coupled receptors." *Pharmacol Ther* **150**: 129-142.
- McGarry, L. M., A. M. Packer, E. Fino, V. Nikolenko, T. Sippy and R. Yuste (2010). "Quantitative classification of somatostatin-positive neocortical interneurons identifies three interneuron subtypes." *Front Neural Circuits* **4**: 12.
- McKittrick, C. R., D. C. Blanchard, R. J. Blanchard, B. S. McEwen and R. R. Sakai (1995). "Serotonin receptor binding in a colony model of chronic social stress." *Biol Psychiatry* **37**(6): 383-393.
- Meltzer, H. Y., Z. Li, Y. Kaneda and J. Ichikawa (2003). "Serotonin receptors: their key role in drugs to treat schizophrenia." *Prog Neuropsychopharmacol Biol Psychiatry* **27**(7): 1159-1172.
- Mengod, G., J. M. Palacios and R. Cortes (2015). "Cartography of 5-HT1A and 5-HT2A Receptor Subtypes in Prefrontal Cortex and Its Projections." *ACS Chem Neurosci* **6**(7): 1089-1098.
- Meunier, C. N. J., J. M. Cancela and P. Fossier (2017). "Lack of GSK3beta activation and modulation of synaptic plasticity by dopamine in 5-HT1A-receptor KO mice." *Neuropharmacology* **113**(Pt A): 124-136.
- Meyer, H. S., D. Schwarz, V. C. Wimmer, A. C. Schmitt, J. N. Kerr, B. Sakmann and M. Helmstaedter (2011). "Inhibitory interneurons in a cortical column form hot zones of inhibition in layers 2 and 5A." *Proc Natl Acad Sci U S A* **108**(40): 16807-16812.
- Meyer, H. S., V. C. Wimmer, M. Hemberger, R. M. Bruno, C. P. de Kock, A. Frick, B. Sakmann and M. Helmstaedter (2010). "Cell type-specific thalamic innervation in a column of rat vibrissal cortex." *Cereb Cortex* **20**(10): 2287-2303.
- Meyer, H. S., V. C. Wimmer, M. Oberlaender, C. P. de Kock, B. Sakmann and M. Helmstaedter (2010). "Number and laminar distribution of neurons in a thalamocortical projection column of rat vibrissal cortex." *Cereb Cortex* **20**(10): 2277-2286.
- Miczek, K. A., R. M. de Almeida, E. A. Kravitz, E. F. Rissman, S. F. de Boer and A. Raine (2007). "Neurobiology of escalated aggression and violence." *J Neurosci* **27**(44): 11803-11806.
- Mihaljevic, B., R. Benavides-Piccione, C. Bielza, P. Larranaga and J. DeFelipe (2019). "Classification of GABAergic interneurons by leading neuroscientists." *Sci Data* **6**(1): 221.
- Millan, M. J., P. Marin, J. Bockaert and C. Mannoury la Cour (2008). "Signaling at G-protein-coupled serotonin receptors: recent advances and future research directions." *Trends Pharmacol Sci* **29**(9): 454-464.
- Miller, K. D., D. J. Pinto and D. J. Simons (2001). "Processing in layer 4 of the neocortical circuit: new insights from visual and somatosensory cortex." *Curr Opin Neurobiol* **11**(4): 488-497.

- Miller, R. J. (1998). "Presynaptic receptors." *Annu Rev Pharmacol Toxicol* **38**: 201-227.
- Miyamae, T., K. Chen, D. A. Lewis and G. Gonzalez-Burgos (2017). "Distinct Physiological Maturation of Parvalbumin-Positive Neuron Subtypes in Mouse Prefrontal Cortex." *J Neurosci* **37**(19): 4883-4902.
- Mlinar, B., C. Falsini and R. Corradetti (2003). "Pharmacological characterization of 5-HT_{1B} receptor-mediated inhibition of local excitatory synaptic transmission in the CA1 region of rat hippocampus." *Br J Pharmacol* **138**(1): 71-80.
- Mohler, H. (2002). "Pathophysiological aspects of diversity in neuronal inhibition: a new benzodiazepine pharmacology." *Dialogues Clin Neurosci* **4**(3): 261-269.
- Moriguchi, Y. (2014). "The early development of executive function and its relation to social interaction: a brief review." *Front Psychol* **5**: 388.
- Morishima, M. and Y. Kawaguchi (2006). "Recurrent connection patterns of corticostriatal pyramidal cells in frontal cortex." *J Neurosci* **26**(16): 4394-4405.
- Morishima, M., K. Kobayashi, S. Kato, K. Kobayashi and Y. Kawaguchi (2017). "Segregated Excitatory-Inhibitory Recurrent Subnetworks in Layer 5 of the Rat Frontal Cortex." *Cereb Cortex* **27**(12): 5846-5857.
- Morishima, M., K. Morita, Y. Kubota and Y. Kawaguchi (2011). "Highly differentiated projection-specific cortical subnetworks." *J Neurosci* **31**(28): 10380-10391.
- Mos, J., B. Olivier, M. Poth and H. van Aken (1992). "The effects of intraventricular administration of eltopazine, 1-(3-trifluoromethylphenyl)piperazine hydrochloride and 8-hydroxy-2-(di-n-propylamino)tetralin on resident intruder aggression in the rat." *Eur J Pharmacol* **212**(2-3): 295-298.
- Muehlenkamp, F., A. Lucion and W. H. Vogel (1995). "Effects of selective serotonergic agonists on aggressive behavior in rats." *Pharmacol Biochem Behav* **50**(4): 671-674.
- Murakoshi, T., S. Y. Song, S. Konishi and T. Tanabe (2001). "Multiple G-protein-coupled receptors mediate presynaptic inhibition at single excitatory synapses in the rat visual cortex." *Neurosci Lett* **309**(2): 117-120.
- Murthy, S., M. Niquille, N. Hurni, G. Limoni, S. Frazer, P. Chameau, J. A. van Hooft, T. Vitalis and A. Dayer (2014). "Serotonin receptor 3A controls interneuron migration into the neocortex." *Nat Commun* **5**: 5524.
- Naka, A. and H. Adesnik (2016). "Inhibitory Circuits in Cortical Layer 5." *Front Neural Circuits* **10**: 35.
- Naka, A., J. Veit, B. Shababo, R. K. Chance, D. Risso, D. Stafford, B. Snyder, A. Egladyous, D. Chu, S. Sridharan, D. P. Mossing, L. Paninski, J. Ngai and H. Adesnik (2019). "Complementary networks of cortical somatostatin interneurons enforce layer specific control." *Elife* **8**.
- Nakajima, M. (2021). "Neuronal identity and cognitive control dynamics in the PFC." *Semin Cell Dev Biol*.
- Nakamura, K. (2013). "The role of the dorsal raphe nucleus in reward-seeking behavior." *Front Integr Neurosci* **7**: 60.
- Narayanan, R. T., R. Egger, A. S. Johnson, H. D. Mansvelder, B. Sakmann, C. P. de Kock and M. Oberlaender (2015). "Beyond Columnar Organization: Cell Type- and Target Layer-Specific Principles of Horizontal Axon Projection Patterns in Rat Vibrissal Cortex." *Cereb Cortex* **25**(11): 4450-4468.
- Nestler, E. J. and R. C. Malenka (2004). "The addicted brain." *Sci Am* **290**(3): 78-85.
- Nichols, D. E. and C. D. Nichols (2008). "Serotonin receptors." *Chem Rev* **108**(5): 1614-1641.
- Nigro, M. J., Y. Hashikawa-Yamasaki and B. Rudy (2018). "Diversity and Connectivity of Layer 5 Somatostatin-Expressing Interneurons in the Mouse Barrel Cortex." *J Neurosci* **38**(7): 1622-1633.
- Nozaki, K., R. Kubo and Y. Furukawa (2016). "Serotonin modulates the excitatory synaptic transmission in the dentate granule cells." *J Neurophysiol* **115**(6): 2997-3007.
- Oberlaender, M., Z. S. Boudewijns, T. Kleele, H. D. Mansvelder, B. Sakmann and C. P. de Kock (2011). "Three-dimensional axon morphologies of individual layer 5 neurons indicate cell type-specific intracortical pathways for whisker motion and touch." *Proc Natl Acad Sci U S A* **108**(10): 4188-4193.
- Ohno, Y., S. Shimizu, K. Tokudome, N. Kunisawa and M. Sasa (2015). "New insight into the therapeutic role of the serotonergic system in Parkinson's disease." *Prog Neurobiol* **134**: 104-121.

- Okaty, B. W., M. N. Miller, K. Sugino, C. M. Hempel and S. B. Nelson (2009). "Transcriptional and electrophysiological maturation of neocortical fast-spiking GABAergic interneurons." *J Neurosci* **29**(21): 7040-7052.
- Olivier, B., J. Mos and R. van Oorschot (1985). "Maternal aggression in rats: effects of chlordiazepoxide and fluprazine." *Psychopharmacology (Berl)* **86**(1-2): 68-76.
- Olivier, B. and R. van Oorschot (2005). "5-HT_{1B} receptors and aggression: a review." *Eur J Pharmacol* **526**(1-3): 207-217.
- Oquendo, M. A., S. A. Russo, M. D. Underwood, S. A. Kassir, S. P. Ellis, J. J. Mann and V. Arango (2006). "Higher postmortem prefrontal 5-HT_{2A} receptor binding correlates with lifetime aggression in suicide." *Biol Psychiatry* **59**(3): 235-243.
- Ostinelli, E. G., M. Hussein, U. Ahmed, F. U. Rehman, K. Miramontes and C. E. Adams (2018). "Risperidone for psychosis-induced aggression or agitation (rapid tranquillisation)." *Cochrane Database Syst Rev* **4**: CD009412.
- Otsuka, T. and Y. Kawaguchi (2008). "Firing-pattern-dependent specificity of cortical excitatory feed-forward subnetworks." *J Neurosci* **28**(44): 11186-11195.
- Otsuka, T. and Y. Kawaguchi (2009). "Cortical inhibitory cell types differentially form intralaminar and interlaminar subnetworks with excitatory neurons." *J Neurosci* **29**(34): 10533-10540.
- Packer, A. M. and R. Yuste (2011). "Dense, unspecific connectivity of neocortical parvalbumin-positive interneurons: a canonical microcircuit for inhibition?" *J Neurosci* **31**(37): 13260-13271.
- Pandey, G. N., Y. Dwivedi, H. S. Rizavi, X. Ren, S. C. Pandey, C. Pesold, R. C. Roberts, R. R. Conley and C. A. Tamminga (2002). "Higher expression of serotonin 5-HT_{2A} receptors in the postmortem brains of teenage suicide victims." *Am J Psychiatry* **159**(3): 419-429.
- Pathak, D., D. Guan and R. C. Foehring (2016). "Roles of specific Kv channel types in repolarization of the action potential in genetically identified subclasses of pyramidal neurons in mouse neocortex." *J Neurophysiol* **115**(5): 2317-2329.
- Pehrson, A. L. and C. Sanchez (2014). "Serotonergic modulation of glutamate neurotransmission as a strategy for treating depression and cognitive dysfunction." *CNS Spectr* **19**(2): 121-133.
- Perrier, J. F., H. B. Rasmussen, R. K. Christensen and A. V. Petersen (2013). "Modulation of the intrinsic properties of motoneurons by serotonin." *Curr Pharm Des* **19**(24): 4371-4384.
- Petersen, A. V., C. S. Jensen, V. Crepel, M. Falkerslev and J. F. Perrier (2017). "Serotonin Regulates the Firing of Principal Cells of the Subiculum by Inhibiting a T-type Ca²⁺ Current." *Front Cell Neurosci* **11**: 60.
- Petilla Interneuron Nomenclature, G., G. A. Ascoli, L. Alonso-Nanclares, S. A. Anderson, G. Barrionuevo, R. Benavides-Piccione, A. Burkhalter, G. Buzsaki, B. Cauli, J. Defelipe, A. Fairen, D. Feldmeyer, G. Fishell, Y. Fregnac, T. F. Freund, D. Gardner, E. P. Gardner, J. H. Goldberg, M. Helmstaedter, S. Hestrin, F. Karube, Z. F. Kisvarday, B. Lambollez, D. A. Lewis, O. Marin, H. Markram, A. Munoz, A. Packer, C. C. Petersen, K. S. Rockland, J. Rossier, B. Rudy, P. Somogyi, J. F. Staiger, G. Tamas, A. M. Thomson, M. Toledo-Rodriguez, Y. Wang, D. C. West and R. Yuste (2008). "Petilla terminology: nomenclature of features of GABAergic interneurons of the cerebral cortex." *Nat Rev Neurosci* **9**(7): 557-568.
- Pi, H. J., B. Hangya, D. Kvitsiani, J. I. Sanders, Z. J. Huang and A. Kepecs (2013). "Cortical interneurons that specialize in disinhibitory control." *Nature* **503**(7477): 521-524.
- Pitychoutis, P. M., C. Dalla, A. C. Sideris, P. A. Tsonis and Z. Papadopoulou-Daifoti (2012). "5-HT_{1A}, 5-HT_{2A}, and 5-HT_{2C} receptor mRNA modulation by antidepressant treatment in the chronic mild stress model of depression: sex differences exposed." *Neuroscience* **210**: 152-167.
- Porter, J. T., C. K. Johnson and A. Agmon (2001). "Diverse types of interneurons generate thalamus-evoked feedforward inhibition in the mouse barrel cortex." *J Neurosci* **21**(8): 2699-2710.
- Posluszny, A. (2019). "Updating the picture of layer 2/3 VIP-expressing interneuron function in the mouse cerebral cortex." *Acta Neurobiol Exp (Wars)* **79**(4): 328-337.

- Pozo, K. and Y. Goda (2010). "Unraveling mechanisms of homeostatic synaptic plasticity." *Neuron* **66**(3): 337-351.
- Puig, M. V., P. Celada and F. Artigas (2004). "[Serotonergic control of prefrontal cortex]." *Rev Neurol* **39**(6): 539-547.
- Puig, M. V. and A. T. Gullledge (2011). "Serotonin and prefrontal cortex function: neurons, networks, and circuits." *Mol Neurobiol* **44**(3): 449-464.
- Puig, M. V., N. Santana, P. Celada, G. Mengod and F. Artigas (2004). "In vivo excitation of GABA interneurons in the medial prefrontal cortex through 5-HT3 receptors." *Cereb Cortex* **14**(12): 1365-1375.
- Puig, M. V., A. Watakabe, M. Ushimaru, T. Yamamori and Y. Kawaguchi (2010). "Serotonin modulates fast-spiking interneuron and synchronous activity in the rat prefrontal cortex through 5-HT1A and 5-HT2A receptors." *J Neurosci* **30**(6): 2211-2222.
- Qi, G. and D. Feldmeyer (2016). "Dendritic Target Region-Specific Formation of Synapses Between Excitatory Layer 4 Neurons and Layer 6 Pyramidal Cells." *Cereb Cortex* **26**(4): 1569-1579.
- Radnikow, G. and D. Feldmeyer (2018). "Layer- and Cell Type-Specific Modulation of Excitatory Neuronal Activity in the Neocortex." *Front Neuroanat* **12**: 1.
- Ramaswamy, S. and H. Markram (2015). "Anatomy and physiology of the thick-tufted layer 5 pyramidal neuron." *Front Cell Neurosci* **9**: 233.
- Rao, M. S. and H. Mizuno (2021). "Elucidating mechanisms of neuronal circuit formation in layer 4 of the somatosensory cortex via intravital imaging." *Neurosci Res* **167**: 47-53.
- Regehr, W. G. (2012). "Short-term presynaptic plasticity." *Cold Spring Harb Perspect Biol* **4**(7): a005702.
- Riedemann, T. (2019). "Diversity and Function of Somatostatin-Expressing Interneurons in the Cerebral Cortex." *Int J Mol Sci* **20**(12).
- Riga, D., M. R. Matos, A. Glas, A. B. Smit, S. Spijker and M. C. Van den Oever (2014). "Optogenetic dissection of medial prefrontal cortex circuitry." *Front Syst Neurosci* **8**: 230.
- Roberts, A. C. (1996). "Comparison of cognitive function in human and non-human primates." *Brain Res Cogn Brain Res* **3**(3-4): 319-327.
- Rodriguez-Arias, M., J. Minarro, M. A. Aguilar, J. Pinazo and V. M. Simon (1998). "Effects of risperidone and SCH 23390 on isolation-induced aggression in male mice." *Eur Neuropsychopharmacol* **8**(2): 95-103.
- Rosell, D. R. and L. J. Siever (2015). "The neurobiology of aggression and violence." *CNS Spectr* **20**(3): 254-279.
- Rosell, D. R., J. L. Thompson, M. Slifstein, X. Xu, W. G. Frankle, A. S. New, M. Goodman, S. R. Weinstein, M. Laruelle, A. Abi-Dargham and L. J. Siever (2010). "Increased serotonin 2A receptor availability in the orbitofrontal cortex of physically aggressive personality disordered patients." *Biol Psychiatry* **67**(12): 1154-1162.
- Roshchin, M. V., V. N. Ierusalimsky, P. M. Balaban and E. S. Nikitin (2020). "Ca(2+)-activated KCa3.1 potassium channels contribute to the slow afterhyperpolarization in L5 neocortical pyramidal neurons." *Sci Rep* **10**(1): 14484.
- Roth, F. C. and H. Hu (2020). "An axon-specific expression of HCN channels catalyzes fast action potential signaling in GABAergic interneurons." *Nat Commun* **11**(1): 2248.
- Rudy, B., G. Fishell, S. Lee and J. Hjerling-Leffler (2011). "Three groups of interneurons account for nearly 100% of neocortical GABAergic neurons." *Dev Neurobiol* **71**(1): 45-61.
- Ruf, B. M. and Z. Bhagwagar (2009). "The 5-HT1B receptor: a novel target for the pathophysiology of depression." *Curr Drug Targets* **10**(11): 1118-1138.
- Russo, S. J., D. M. Dietz, D. Dumitriu, J. H. Morrison, R. C. Malenka and E. J. Nestler (2010). "The addicted synapse: mechanisms of synaptic and structural plasticity in nucleus accumbens." *Trends Neurosci* **33**(6): 267-276.
- Ryglewski, S., H. J. Pflueger and C. Duch (2007). "Expanding the neuron's calcium signaling repertoire: intracellular calcium release via voltage-induced PLC and IP3R activation." *PLoS Biol* **5**(4): e66.

- Sabo, S. L. and M. P. Sceniak (2006). "Somatostatin diversity in the inhibitory population." *J Neurosci* **26**(29): 7545-7546.
- Sakaue, M., Y. Ago, C. Sowa, Y. Sakamoto, B. Nishihara, Y. Koyama, A. Baba and T. Matsuda (2002). "Modulation by 5-hT2A receptors of aggressive behavior in isolated mice." *Jpn J Pharmacol* **89**(1): 89-92.
- Sakurai, T. and N. J. Gamo (2019). "Cognitive functions associated with developing prefrontal cortex during adolescence and developmental neuropsychiatric disorders." *Neurobiol Dis* **131**: 104322.
- Santana, N. and F. Artigas (2017). "Laminar and Cellular Distribution of Monoamine Receptors in Rat Medial Prefrontal Cortex." *Front Neuroanat* **11**: 87.
- Santana, N., A. Bortolozzi, J. Serrats, G. Mengod and F. Artigas (2004). "Expression of serotonin1A and serotonin2A receptors in pyramidal and GABAergic neurons of the rat prefrontal cortex." *Cereb Cortex* **14**(10): 1100-1109.
- Sargin, D., D. K. Oliver and E. K. Lambe (2016). "Chronic social isolation reduces 5-HT neuronal activity via upregulated SK3 calcium-activated potassium channels." *Elife* **5**.
- Scala, F., D. Kobak, M. Bernabucci, Y. Bernaerts, C. R. Cadwell, J. R. Castro, L. Hartmanis, X. Jiang, S. Laternus, E. Miranda, S. Mulherkar, Z. H. Tan, Z. Yao, H. Zeng, R. Sandberg, P. Berens and A. S. Tolias (2021). "Phenotypic variation of transcriptomic cell types in mouse motor cortex." *Nature* **598**(7879): 144-150.
- Schmitz, D., T. Gloveli, R. M. Empson, A. Draguhn and U. Heinemann (1998). "Serotonin reduces synaptic excitation in the superficial medial entorhinal cortex of the rat via a presynaptic mechanism." *J Physiol* **508** (Pt 1): 119-129.
- Sempere-Ferrandez, A., S. Martinez and E. Geijo-Barrientos (2019). "Synaptic mechanisms underlying the intense firing of neocortical layer 5B pyramidal neurons in response to cortico-cortical inputs." *Brain Struct Funct* **224**(4): 1403-1416.
- Shah, M. M. (2014). "Cortical HCN channels: function, trafficking and plasticity." *J Physiol* **592**(13): 2711-2719.
- Sharp, T., L. Boothman, J. Raley and P. Queree (2007). "Important messages in the 'post': recent discoveries in 5-HT neurone feedback control." *Trends Pharmacol Sci* **28**(12): 629-636.
- Shvartsman, A., O. Kotler, O. Stoler, Y. Khrapunsky, I. Melamed and I. A. Fleidervish (2021). "Subcellular distribution of persistent sodium conductance in cortical pyramidal neurons." *J Neurosci*.
- Siever, L. J. (2008). "Neurobiology of aggression and violence." *Am J Psychiatry* **165**(4): 429-442.
- Silver, R. A., J. Lubke, B. Sakmann and D. Feldmeyer (2003). "High-probability unquantal transmission at excitatory synapses in barrel cortex." *Science* **302**(5652): 1981-1984.
- Soloff, P. H., J. C. Price, C. C. Meltzer, A. Fabio, G. K. Frank and W. H. Kaye (2007). "5HT2A receptor binding is increased in borderline personality disorder." *Biol Psychiatry* **62**(6): 580-587.
- Soyka, M. (2011). "Neurobiology of aggression and violence in schizophrenia." *Schizophr Bull* **37**(5): 913-920.
- Spruston, N. (2008). "Pyramidal neurons: dendritic structure and synaptic integration." *Nat Rev Neurosci* **9**(3): 206-221.
- Stahl, S. M. (2008). "Personalized medicine, pharmacogenomics, and the practice of psychiatry: on the threshold of predictive therapeutics in psychopharmacology?" *CNS Spectr* **13**(2): 115-118.
- Steinbeis, N., B. C. Bernhardt and T. Singer (2012). "Impulse control and underlying functions of the left DLPFC mediate age-related and age-independent individual differences in strategic social behavior." *Neuron* **73**(5): 1040-1051.
- Stephens, E. K., A. L. Baker and A. T. Gullledge (2018). "Mechanisms Underlying Serotonergic Excitation of Callosal Projection Neurons in the Mouse Medial Prefrontal Cortex." *Front Neural Circuits* **12**: 2.
- Stiefel, K. M., B. Englitz and T. J. Sejnowski (2013). "Origin of intrinsic irregular firing in cortical interneurons." *Proc Natl Acad Sci U S A* **110**(19): 7886-7891.
- Strominger, N. L. D., R. J.; Laemle, L. B. (2012). "Cerebral Cortex. In: Noback's Human Nervous System, Seventh Edition." *Humana Press, Totowa, NJ*.

- Swanson, O. K. and A. Maffei (2019). "From Hiring to Firing: Activation of Inhibitory Neurons and Their Recruitment in Behavior." Front Mol Neurosci **12**: 168.
- Tai, C., Y. Abe, R. E. Westenbroek, T. Scheuer and W. A. Catterall (2014). "Impaired excitability of somatostatin- and parvalbumin-expressing cortical interneurons in a mouse model of Dravet syndrome." Proc Natl Acad Sci U S A **111**(30): E3139-3148.
- Tai, Y., N. B. Gallo, M. Wang, J. R. Yu and L. Van Aelst (2019). "Axo-axonic Innervation of Neocortical Pyramidal Neurons by GABAergic Chandelier Cells Requires AnkyrinG-Associated L1CAM." Neuron **102**(2): 358-372 e359.
- Tan, Z., H. Hu, Z. J. Huang and A. Agmon (2008). "Robust but delayed thalamocortical activation of dendritic-targeting inhibitory interneurons." Proc Natl Acad Sci U S A **105**(6): 2187-2192.
- Tanaka, E. and R. A. North (1993). "Actions of 5-hydroxytryptamine on neurons of the rat cingulate cortex." J Neurophysiol **69**(5): 1749-1757.
- Thomson, A. M. (2003). "Presynaptic frequency- and pattern-dependent filtering." J Comput Neurosci **15**(2): 159-202.
- Thomson, A. M. (2010). "Neocortical layer 6, a review." Front Neuroanat **4**: 13.
- Thomson, A. M., J. Deuchars and D. C. West (1993). "Large, deep layer pyramid-pyramid single axon EPSPs in slices of rat motor cortex display paired pulse and frequency-dependent depression, mediated presynaptically and self-facilitation, mediated postsynaptically." J Neurophysiol **70**(6): 2354-2369.
- Tian, Z., M. Yamanaka, M. Bernabucci, M. G. Zhao and M. Zhuo (2017). "Characterization of serotonin-induced inhibition of excitatory synaptic transmission in the anterior cingulate cortex." Mol Brain **10**(1): 21.
- Torres-Escalante, J. L., J. A. Barral, M. D. Ibarra-Villa, A. Perez-Burgos, J. L. Gongora-Alfaro and J. C. Pineda (2004). "5-HT_{1A}, 5-HT₂, and GABAB receptors interact to modulate neurotransmitter release probability in layer 2/3 somatosensory rat cortex as evaluated by the paired pulse protocol." J Neurosci Res **78**(2): 268-278.
- Tremblay, R., S. Lee and B. Rudy (2016). "GABAergic Interneurons in the Neocortex: From Cellular Properties to Circuits." Neuron **91**(2): 260-292.
- Troca-Marin, J. A. and E. Geijo-Barrientos (2010). "Inhibition by 5-HT of the synaptic responses evoked by callosal fibers on cortical neurons in the mouse." Pflugers Arch **460**(6): 1073-1085.
- Turcotte-Cardin, V., F. Vahid-Ansari, C. Luckhart, M. Daigle, S. D. Geddes, K. F. Tanaka, R. Hen, J. James, Z. Merali, J. C. Beique and P. R. Albert (2019). "Loss of Adult 5-HT_{1A} Autoreceptors Results in a Paradoxical Anxiogenic Response to Antidepressant Treatment." J Neurosci **39**(8): 1334-1346.
- Unal, C. T., B. Unal and M. M. Bolton (2020). "Low-threshold spiking interneurons perform feedback inhibition in the lateral amygdala." Brain Struct Funct **225**(3): 909-923.
- van Aerde, K. I. and D. Feldmeyer (2015). "Morphological and physiological characterization of pyramidal neuron subtypes in rat medial prefrontal cortex." Cereb Cortex **25**(3): 788-805.
- van Aerde, K. I., G. Qi and D. Feldmeyer (2015). "Cell type-specific effects of adenosine on cortical neurons." Cereb Cortex **25**(3): 772-787.
- Vazquez, D. M., R. Eskandari, C. A. Zimmer, S. Levine and J. F. Lopez (2002). "Brain 5-HT receptor system in the stressed infant rat: implications for vulnerability to substance abuse." Psychoneuroendocrinology **27**(1-2): 245-272.
- Vervaeke, K., H. Hu, L. J. Graham and J. F. Storm (2006). "Contrasting effects of the persistent Na⁺ current on neuronal excitability and spike timing." Neuron **49**(2): 257-270.
- Villalobos, C., V. G. Shakkottai, K. G. Chandry, S. K. Michelhaugh and R. Andrade (2004). "SKCa channels mediate the medium but not the slow calcium-activated afterhyperpolarization in cortical neurons." J Neurosci **24**(14): 3537-3542.
- Vogalis, F., J. F. Storm and B. Lancaster (2003). "SK channels and the varieties of slow after-hyperpolarizations in neurons." Eur J Neurosci **18**(12): 3155-3166.

- Voinova, O., F. Valiullina, Y. Zakharova, M. Mukhtarov, A. Draguhn and A. Rozov (2015). "Layer Specific Development of Neocortical Pyramidal to Fast Spiking Cell Synapses." *Front Cell Neurosci* **9**: 518.
- Wagstyl, K., S. Larocque, G. Cucurull, C. Lepage, J. P. Cohen, S. Bludau, N. Palomero-Gallagher, L. B. Lewis, T. Funck, H. Spitzer, T. Dickscheid, P. C. Fletcher, A. Romero, K. Zilles, K. Amunts, Y. Bengio and A. C. Evans (2020). "BigBrain 3D atlas of cortical layers: Cortical and laminar thickness gradients diverge in sensory and motor cortices." *PLoS Biol* **18**(4): e3000678.
- Wang, D. H. and K. Wong-Lin (2013). "Comodulation of dopamine and serotonin on prefrontal cortical rhythms: a theoretical study." *Front Integr Neurosci* **7**: 54.
- Wang, Y., H. Markram, P. H. Goodman, T. K. Berger, J. Ma and P. S. Goldman-Rakic (2006). "Heterogeneity in the pyramidal network of the medial prefrontal cortex." *Nat Neurosci* **9**(4): 534-542.
- Wang, Y., M. Toledo-Rodriguez, A. Gupta, C. Wu, G. Silberberg, J. Luo and H. Markram (2004). "Anatomical, physiological and molecular properties of Martinotti cells in the somatosensory cortex of the juvenile rat." *J Physiol* **561**(Pt 1): 65-90.
- Wang, Y., M. Ye, X. Kuang, Y. Li and S. Hu (2018). "A simplified morphological classification scheme for pyramidal cells in six layers of primary somatosensory cortex of juvenile rats." *IBRO Rep* **5**: 74-90.
- Weber, E. T. and R. Andrade (2010). "Htr2a Gene and 5-HT(2A) Receptor Expression in the Cerebral Cortex Studied Using Genetically Modified Mice." *Front Neurosci* **4**.
- White, T., M. Schmidt and C. Karatekin (2009). "White matter 'potholes' in early-onset schizophrenia: a new approach to evaluate white matter microstructure using diffusion tensor imaging." *Psychiatry Res* **174**(2): 110-115.
- Wierenga, C. J., F. E. Mullner, I. Rinke, T. Keck, V. Stein and T. Bonhoeffer (2010). "Molecular and electrophysiological characterization of GFP-expressing CA1 interneurons in GAD65-GFP mice." *PLoS One* **5**(12): e15915.
- Woodruff, A. R., S. A. Anderson and R. Yuste (2010). "The enigmatic function of chandelier cells." *Front Neurosci* **4**: 201.
- Xiang, Z. and D. A. Prince (2003). "Heterogeneous actions of serotonin on interneurons in rat visual cortex." *J Neurophysiol* **89**(3): 1278-1287.
- Xie, G., W. Zuo, L. Wu, W. Li, W. Wu, A. Bekker and J. H. Ye (2016). "Serotonin modulates glutamatergic transmission to neurons in the lateral habenula." *Sci Rep* **6**: 23798.
- Yaman, B. and R. Bal (2020). "Serotonin hyperpolarizes the dorsal raphe nucleus neurons of mice by activating G protein-coupled inward rectifier potassium channels." *Neuroreport* **31**(12): 928-935.
- Yamauchi, M., T. Miyara, T. Matsushima and T. Imanishi (2006). "Desensitization of 5-HT2A receptor function by chronic administration of selective serotonin reuptake inhibitors." *Brain Res* **1067**(1): 164-169.
- Yang, G. R., J. D. Murray and X. J. Wang (2016). "A dendritic disinhibitory circuit mechanism for pathway-specific gating." *Nat Commun* **7**: 12815.
- Yang, S. S., Y. C. Li, A. A. Coley, L. A. Chamberlin, P. Yu and W. J. Gao (2018). "Cell-Type Specific Development of the Hyperpolarization-Activated Current, Ih, in Prefrontal Cortical Neurons." *Front Synaptic Neurosci* **10**: 7.
- Yavorska, I. and M. Wehr (2016). "Somatostatin-Expressing Inhibitory Interneurons in Cortical Circuits." *Front Neural Circuits* **10**: 76.
- Yi, F., T. Y. Ling, T. Lu, X. L. Wang, J. Li, W. C. Claycomb, W. K. Shen and H. C. Lee (2015). "Down-regulation of the small conductance calcium-activated potassium channels in diabetic mouse atria." *J Biol Chem* **290**(11): 7016-7026.
- Yohn, C. N., M. M. Gergues and B. A. Samuels (2017). "The role of 5-HT receptors in depression." *Mol Brain* **10**(1): 28.
- Yuan, P. and N. Raz (2014). "Prefrontal cortex and executive functions in healthy adults: a meta-analysis of structural neuroimaging studies." *Neurosci Biobehav Rev* **42**: 180-192.

- Yuste, R., M. Hawrylycz, N. Aalling, A. Aguilar-Valles, D. Arendt, R. Armananzas, G. A. Ascoli, C. Bielza, V. Bokharaie, T. B. Bergmann, I. Bystron, M. Capogna, Y. Chang, A. Clemens, C. P. J. de Kock, J. DeFelipe, S. E. Dos Santos, K. Dunville, D. Feldmeyer, R. Fiath, G. J. Fishell, A. Foggetti, X. Gao, P. Ghaderi, N. A. Goriounova, O. Gunturkun, K. Hagihara, V. J. Hall, M. Helmstaedter, S. Herculano-Houzel, M. M. Hilscher, H. Hirase, J. Hjerling-Leffler, R. Hodge, J. Huang, R. Huda, K. Khodosevich, O. Kiehn, H. Koch, E. S. Kuebler, M. Kuhnemund, P. Larranaga, B. Lelieveldt, E. L. Louth, J. H. Lui, H. D. Mansvelder, O. Marin, J. Martinez-Trujillo, H. M. Chameh, A. N. Mohapatra, H. Munguba, M. Nedergaard, P. Nemeč, N. Ofer, U. G. Pfisterer, S. Pontes, W. Redmond, J. Rossier, J. R. Sanes, R. H. Scheuermann, E. Serrano-Saiz, J. F. Staiger, P. Somogyi, G. Tamas, A. S. Tolias, M. A. Tosches, M. T. Garcia, C. Wozny, T. V. Wuttke, Y. Liu, J. Yuan, H. Zeng and E. Lein (2020). "A community-based transcriptomics classification and nomenclature of neocortical cell types." *Nat Neurosci* **23**(12): 1456-1468.
- Zaitsev, A. V., N. V. Povysheva, D. A. Lewis and L. S. Krimer (2007). "P/Q-type, but not N-type, calcium channels mediate GABA release from fast-spiking interneurons to pyramidal cells in rat prefrontal cortex." *J Neurophysiol* **97**(5): 3567-3573.
- Zamponi, G. W. and K. P. Currie (2013). "Regulation of Ca(V)2 calcium channels by G protein coupled receptors." *Biochim Biophys Acta* **1828**(7): 1629-1643.
- Zeng, H. and J. R. Sanes (2017). "Neuronal cell-type classification: challenges, opportunities and the path forward." *Nat Rev Neurosci* **18**(9): 530-546.
- Zhi, Y. R., F. Cao, X. J. Su, S. W. Gao, H. N. Zheng, J. Y. Jiang, L. Su, J. Liu, Y. Wang, Y. Zhang and Y. Zhang (2022). "The T-Type Calcium Channel Cav3.2 in Somatostatin Interneurons in Spinal Dorsal Horn Participates in Mechanosensation and Mechanical Allodynia in Mice." *Front Cell Neurosci* **16**: 875726.
- Zhong, P. and Z. Yan (2011). "Differential regulation of the excitability of prefrontal cortical fast-spiking interneurons and pyramidal neurons by serotonin and fluoxetine." *PLoS One* **6**(2): e16970.
- Zhou, F. M. and J. J. Hablitz (1999). "Activation of serotonin receptors modulates synaptic transmission in rat cerebral cortex." *J Neurophysiol* **82**(6): 2989-2999.
- Zhou, X., I. Mansori, T. Fischer, M. Witte and J. F. Staiger (2020). "Characterizing the morphology of somatostatin-expressing interneurons and their synaptic innervation pattern in the barrel cortex of the GFP-expressing inhibitory neurons mouse." *J Comp Neurol* **528**(2): 244-260.
- Zhu, Y., R. L. Stornetta and J. J. Zhu (2004). "Chandelier cells control excessive cortical excitation: characteristics of whisker-evoked synaptic responses of layer 2/3 nonpyramidal and pyramidal neurons." *J Neurosci* **24**(22): 5101-5108.
- Zilberter, Y. (2000). "Dendritic release of glutamate suppresses synaptic inhibition of pyramidal neurons in rat neocortex." *J Physiol* **528**(Pt 3): 489-496.
- Zucker, R. S. (1989). "Short-term synaptic plasticity." *Annu Rev Neurosci* **12**: 13-31.
- Zucker, R. S. and W. G. Regehr (2002). "Short-term synaptic plasticity." *Annu Rev Physiol* **64**: 355-405.

Abbreviations

3D	three dimensions
ACg	anterior cingulate cortex
ADHD	attention deficit hyperactivity disorder
AHP	after-hyperpolarization
AP	action potential
AS	adaptive-spiking
Bd	broad-tufted
bFS INs	intermittent burst-like FS INs
cAMP	cyclic adenosine monophosphate
Ca _v	voltage-gated Ca ²⁺
CCK	cholecystokinin
CGS	5-HT _{1B} R agonist
CREB	cAMP response element binding protein
CT PNs	corticothalamic PNs
CV	coefficient of variation
DAG	diacyl-glycerol
dIPFC	dorsolateral PFC
DRN	dorsal raphe nucleus
E/I	excitation and inhibition ratio
EPSP)	excitatory postsynaptic potential
ET PNs	extratelencephalic PNs
FS INs.	fast spiking INs.
GABA	γ-aminobutyric acid
GDP	guanosine diphosphate
GIRK	G-protein-coupled inwardly-rectifying K ⁺ channels
GPCRs	G protein-coupled receptors
HCN	hyperpolarization-activated, cyclic-nucleotide gated channels
HPA axis	hypothalamic-pituitary-adrenal axis
IL	infralimbic cortex
INs	interneurons

IP ₃	inositol trisphosphate
ISI	inter-spike interval
IT PNs	intratelencephalic PNs
K _{ir}	inwardly-rectifying K ⁺ channels
LAMP5	lysosomal-associated membrane protein 5
mCPG	5-HT _{3A} R agonist
MO	medial orbital cortex
mPFC	medial prefrontal cortex
nFS INs.	non-fast spiking INs.
NPY	neuropeptide Y
PFC	prefrontal cortex
PKA	protein kinase A
PLC	phospholipase C
PNs	pyramidal neurons
PPR	paired pulse ratio
PrL	prelimbic cortex
PSP	postsynaptic potential
PV	parvalbumin
rFS INs	regular FS INs
R _{in}	input resistance
RS	regular-spiking
SB	5-HT _{1B} R antagonist
SI	slender-tufted
SD	standard deviation
SK channels	Ca ²⁺ -activated potassium channels
STT	somatostatin
TTX	Tetrodotoxin
VIP	vasoactive intestinal peptide
V _{sag}	voltage sag
τ _{Mem}	time constant

List of Figures

Fig. 1.1: Functional and neuroanatomical homology between human and rodent PFC.....	12
Fig. 1.2: Types of PNs and INs across different layers in rat neocortex.....	14
Fig. 1.3: 3D-reconstruction of a single PN spanning different regions of brain.....	15
Fig. 1.4: Neuronal classification based on transcriptomic and morphoelectric characteristics.....	17
Fig. 1.5: Serotonergic pathways in human and rodent brain.....	19
Fig. 1.6: Signaling mechanisms associated with 5-HT receptors in mPFC.....	20
Fig. 2.1: Preparation of coronal brain sections in rat prelimbic region of mPFC.....	25
Fig. 2.2: Representation of cortical layers and identification of neurons in rat mPFC.....	27
Fig. 2.3: Whole-cell patch-clamp technique.....	28
Fig. 2.4: Patch-clamp recording from and biocytin labeling of a synaptically coupled neuron pair.....	30
Fig. 2.5: Analysis of passive properties of L5 neurons in mPFC.....	33
Fig. 2.6: Analysis of active properties of L5 neurons in mPFC.....	34
Fig. 2.7: Analysis of synaptic properties of synaptically coupled L5 neurons in mPFC.....	35
Fig. 2.8: Reconstruction of an excitatory L5 PN in mPFC.....	37
Fig. 2.9: Schematic representation of a box-plot.....	38
Fig. 3.1: Electrophysiological classification of L5 PNs in mPFC.....	40
Fig. 3.2: Quantification of electrophysiological properties of L5 PNs in mPFC.....	41
Fig. 3.3: Morphological reconstructions of L5 PNs in mPFC.....	43
Fig. 3.4: Quantification of morphological properties of L5 PNs in mPFC.....	44
Fig. 3.5: 3D scatter plot of the adaptation ratio, R_{in} and horizontal field-span of apical dendrites of AS PNs and RS PNs.....	45
Fig. 3.6: Axon-carrying dendrite in few of the Bd-tufted RS PNs in L5 of mPFC.....	45
Fig. 3.7: Electrophysiological classification of L5 INs in mPFC.....	47
Fig. 3.8: Quantification of electrophysiological properties of L5 INs in mPFC.....	48
Fig. 3.9: Morphological reconstructions of L5 INs in mPFC.....	49
Fig. 3.10: Quantification of morphological properties of L5 INs in mPFC.....	50
Fig. 3.11: Comparison of single AP properties among L5 PNs and INs in mPFC.....	51
Fig. 3.12: 3D scatter plot using intrinsic properties of L5 INs in mPFC.....	52
Fig. 3.13: Effect of 5-HT on L5 AS PNs in mPFC.....	53
Fig. 3.14: Effect of 5-HT on L5 RS PNs in mPFC.....	54

Fig. 3.15: Comparison of the 5-HT depolarizing effect between L5 AS PNs and RS PNs in mPFC.....	55
Fig. 3.16: Quantification of electro-morphia properties among 5-HT responding L5 AS PNs in mPFC.....	55
Fig. 3.17: Blockade of SK channels with apamin in L5 RS PNs in mPFC.....	57
Fig. 3.18: 3D scatter plot of 5-HT responding L5 PNs in mPFC.....	57
Fig. 3.19: Effect of 5-HT receptor agonists in L5 PNs in mPFC.....	58
Fig. 3.20: Effect of 5-HT on L5 INs in mPFC.....	60
Fig. 3.21: Comparison of synaptic properties between E-E connections in L5 of mPFC.....	61
Fig. 3.22: Comparison of synaptic properties among E-I connections in L5 of mPFC.....	62
Fig. 3.23: Comparison of synaptic properties among I-E connections in L5 of mPFC.....	63
Fig. 3.24: 5-HT suppresses synaptic transmission of E-E connection in L5 of mPFC.....	65
Fig. 3.25: 5-HT-induced decrease in presynaptic release probability at AS PN-RS PN pairs in L5 of mPFC.....	66
Fig. 3.26: 5-HT-induced decrease in presynaptic release probability at RS PN - RS PN pairs in L5 of mPFC....	67
Fig. 3.27: 5-HT-induced suppression of synaptic transmission at a reciprocal E-I pair in L5 of mPFC.....	69
Fig. 3.28: Effect of CGS on synaptic transmission at AS PN - bFS IN connections in L5 of mPFC.....	71
Fig. 3.29: Effect of CGS on synaptic transmission at RS PN - rFS IN connections in L5 of mPFC.....	72
Fig. 3.30: Effect of mCPG on synaptic transmission at bFS IN - RS PN connection in L5 of mPFC.....	74
Summary Fig.: Schematic representation of serotonergic modulation of L5 neuronal population and microcircuits in rat mPFC.....	93

List of Tables

Table 1: Statistical comparison of the electrophysiological parameters between L5 AS and RS PNs.....	42
Table 2: Statistical comparison of the morphological parameters between L5 AS and RS PNs.....	44
Table 3: Statistical comparison of the electrophysiological parameters among L5 nFS, rFS and bFS INs in mPFC	47
Table 4: Statistical comparison of the morphological parameters among L5 nFS, rFS and bFS INs.....	50
Table 5: Statistical comparison of the electro-morphic parameters among AS-Depolarizing (AS-D), AS-Hyperpolarizing (AS-H) and RS-Depolarizing (RS-D) L5 PNs upon 5-HT application.....	56
Table 6: Unitary EPSP characteristics of different subtypes of L5 excitatory and inhibitory connections.....	64
Table 7: Unitary EPSP characteristics of L5 E-E connections under control, 10 μ M 5-HT alone and 10 μ M 5-HT + 5 μ M 5-HT _{1B} R antagonist SB	68
Table 8: Unitary EPSP characteristics of L5 E-I connections under control and 5 μ M 5-HT _{1B} R agonist CGS.....	73
Table 9: Unitary IPSP characteristics of L5 I-E connections in control and the presence of 5-HT _{3A} R agonist mCPG.....	75

Curriculum Vitae

Personal information	
Name:	Ramya Rama
Gender:	Female
Date of birth:	1 st November, 1988
Nationality:	Indian
Email:	r.rama@fz-juelich.de , r.ramya.987@gmail.com
University Education	
Since June 2016	PhD student, Institute of Neuroscience and Medicine 10 (INM-10), Research Centre Jülich (FZJ), Germany.
2015 - 2016	Visiting Scholar, Institute for Biochemistry, Friedrich–Alexander University (FAU) Erlangen–Nürnberg, Germany.
2012 - 2015	M.Sc. in Integrative Neuroscience, Otto von Guericke University (OVGU), Magdeburg.
2009 - 2011	M.Sc. in Environmental Biotechnology, Jawaharlal Nehru Technological University (JNTU), Hyderabad.
2006 - 2009	B.Sc. in Biotechnology, Microbiology, Chemistry Osmania University (OU), Hyderabad.
Conferences	
2019	Jordan Research Conference (JRC) ‘Modulation of neural circuits and behaviour’, Switzerland. Poster: Role of serotonin in regulating the excitatory and inhibitory balance of prefrontal cortex.
2018	Society for Neuroscience (SFN), San Diego. Poster: Differential serotonergic modulation of layer 5 neuronal activity in rat prefrontal cortex.
2018	11 th FENS Forum of Neuroscience, Berlin.
2015	11 th Göttingen meeting of the German Neuroscience Society, Göttingen. Poster: Neuroplastins interact with TRAF6 to initiate cell signaling.
Publications	
2022	R. Rama , K. Derlig, N. Viessmann, R. Gossmann, F. Oriold, A. Giessl, J. H. Brandstatter, R. Enz and R. Dahlhaus. "Simiate and the focal adhesion kinase FAK1 cooperate in the regulation of dendritogenesis." <i>Sci Rep</i> 12 (1): 11274.
2020	S. K. Vemula, A. Malci, L. Junge, A. C. Lehmann, R. Rama , J. Hradsky, R. A. Matute, A. Weber, M. Prigge, M. Naumann, M. R. Kreutz, C. I. Seidenbecher, E. D. Gundelfinger and R. Herrera-Molina. "The Interaction of TRAF6 With Neuroplastin Promotes Spinogenesis During Early Neuronal Development." <i>Front Cell Dev Biol</i> 8 : 579513.

Band / Volume 257

**High-Performance Computing Approach to Hybrid Functionals
in the All-Electron DFT Code FLEUR**

M. Redies (2022), xi, 109 pp

ISBN: 978-3-95806-639-7

Band / Volume 258

**Establishing regulatable expression systems in the acetic acid bacterium
Gluconobacter oxydans 621H**

P. M. Fricke (2022), VIII, 187 pp

ISBN: 978-3-95806-642-7

Band / Volume 259

**Density-Functional Perturbation Theory within the All-Electron Full-
Potential Linearized Augmented Plane-Wave Method: Application to
Phonons**

C.-R. Gerhorst (2022), xvi, 317 pp

ISBN: 978-3-95806-649-6

Band / Volume 260

Crystal and Magnetic Structure of CrAs under Extreme Conditions

A. Eich (2022), viii, 235 pp

ISBN: 978-3-95806-655-7

Band / Volume 261

**Applications of transcription factor-based biosensors for strain
development and evolutionary engineering**

R. G. Stella (2022), x, 128 pp

ISBN: 978-3-95806-657-1

Band / Volume 262

**Strömungsmechanische Simulation und experimentelle Validierung
des kryogenen Wasserstoff-Moderators für die Europäische
Spallationsneutronenquelle ESS**

Y. Beßler (2022), XXIV, 154, xxxiii pp

ISBN: 978-3-95806-660-1

Band / Volume 263

**9th Georgian-German School and Workshop in Basic Science
September 12 – 16, 2022 | Kutaisi, Tbilisi | Georgia**

A. Kacharava, E. Portius, N. J. Shah, H. Ströher (2022)

ISBN: 978-3-95806-664-9

Band / Volume 264

Self-assembly of Au-Fe₃O₄ dumbbell nanoparticles

N. Nandakumaran (2022), xiv, 234 pp

ISBN: 978-3-95806-666-3

Band / Volume 265

Time-resolved and three-dimensional characterisation of magnetic states in nanoscale materials in the transmission electron microscope

T. Weißels (2023), xx, 211 pp

ISBN: 978-3-95806-685-4

Band / Volume 266

Dissecting iron and heme regulatory networks and adaptation to heme stress in *Corynebacterium glutamicum*

A. Krüger (2023), IV, 274 pp

ISBN: 978-3-95806-686-1

Band / Volume 267

Morphological and functional characterization of layer 5 neurons in rat medial prefrontal cortex, their synaptic microcircuitry and serotonin modulation

R. Rama (2023), 116 pp

ISBN: 978-3-95806-688-5

Weitere **Schriften des Verlags im Forschungszentrum Jülich** unter
<http://wwwzb1.fz-juelich.de/verlagextern1/index.asp>

Schlüsseltechnologien / Key Technologies

Band / Volume 267

ISBN 978-3-95806-688-5